Remote Sensing Series 63

Petra D'Odorico

Monitoring the Spectral Performance of the APEX Imaging Spectrometer for Inter-Calibration of Satellite Missions

Remote Sensing Laboratories
Department of Geography
University of Zurich, 2012

Remote Sensing Series 63

Petra D'Odorico

Monitoring the Spectral Performance of the APEX Imaging Spectrometer for Inter-Calibration of Satellite Missions

Remote Sensing Laboratories
Department of Geography
University of Zurich, 2012

Front page: picture of refracted rainbow (source: http://www.lightingsciences.ca/).

D'Odorico, Petra

Monitoring the Spectral Performance of the APEX Imaging Spectrometer for Inter-Calibration of Satellite Missions.

Remote Sensing Series, Vol. 63
Remote Sensing Laboratories, Department of Geography, University of Zurich
Switzerland, 2012

ISBN: 978-3-03703-029-5

Editorial board of the Remote Sensing Series: Prof. Dr. Michael E. Schaepman, Dr. Erich Meier, Dr. Mathias Kneubühler, Dr. David Small, Dr. Felix Morsdorf.

This work was approved as a PhD thesis by the Faculty of Science of the University of Zurich in the spring semester 2012. Doctorate committee: Prof. Dr. Michael E. Schaepman (chair), Dr. Mathias Kneubühler, Dr. Michael Jehle. External examiner: Dr. Nigel Fox, National Physical Laboratory (NPL), UK.

SUMMARY

Remote sensing is possibly the most valuable technique available today to quantitatively measure variables defining our Earth system and processes. However, understanding all factors influencing the measurement process is required before a correct interpretation of the measurement can take place. Ideally, the measurement of solar radiation reflected by the surface carries information exclusively about the object or phenomenon under study. This is however never the case as interaction with the atmosphere, contamination by the background, and the instrument characteristics are responsible for changing the properties of the measured radiation.

For applications relying on spectroscopy data, instrument spectral characteristics are arguably the most important piece of information required for a correct interpretation of measurement. The Spectral Response Function (SRF), associated with each detector pixel and described by a center wavelength and a Full-Width-at-Half-Maximum (FWHM), synthesizes the spectral characteristics of the instrument. Measurements required to define instrument's SRF are firstly carried out during laboratory characterization. It is however acknowledged that once the instrument becomes spaceborne or airborne, the stresses of the operational environment (e.g., vibrations, temperature and pressure variations) and the natural aging of the system lead to changes in instrument spectral characteristics and related performance. Ignoring these changes and relying on nominal spectral parameters characterized in the laboratory, can lead to errors in the final data sets and derived products.

This dissertation investigates the properties and the causes of instrument spectral performance changes in an airborne environment. A new approach has been developed and validated for monitoring in-flight instrument spectral characteristics, which has eventually been used to compensate the observed variations during spectroscopy data processing. The Airborne Prism EXperiment (APEX) imaging spectrometer is at the center of this investigation. APEX is an airborne dispersive pushbroom imaging spectrometer operating in the wavelength domain between 380 and 2500 nm. It is designed to serve as a simulation, validation and calibration sensor for current and future spaceborne missions. APEX's unique feature is the inclusion of onboard characterization equipment in the instrument design, known as the In-Flight Characterization (IFC) facility. By targeted acquisition of IFC measurements and processing via ad-hoc developed algorithms, it is possible to estimate the in-flight updated spectral parameters of the instrument. Vicarious (i.e., scene-based) calibration approaches relying on atmospheric absorption features were employed to complement and validate the estimation of instrument spectral parameters. The compensation of the in-flight wavelength position shifts has been demonstrated to produce reliable results when applied to APEX operational data. Calibrated APEX data were successfully employed for the simulation and cross-calibration of current and future satellite sensors spectral performances. A discussion of the main findings highlights advantages and limitations of the proposed techniques and suggests possible improvements as well as future perspectives for the continuation of this work.

ZUSAMMENFASSUNG

Die Fernerkundung ist heutzutage wahrscheinlich die wertvollste Methode um Parameter, die Prozesse unserer Umwelt definieren, quantitativ und global zu messen. Für eine korrekte Interpretation dieser Messungen ist das Verständnis aller Faktoren die den Messprozess beeinflussen entscheidend. Im Idealfall beinhaltet die Messung des reflektierten Sonnenlichts ausschließlich Informationen über das reflektierende Objekt oder Phänomen. Dies ist jedoch selten der Fall, da Interaktionen mit der Atmosphäre, eine Kontaminierung durch den Hintergrund und die Instrumenteigenschaften die Zusammensetzung und Ausbreitung der Sonnenstrahlung verändern.

Für spektroskopiedaten-basierte Anwendungen sind die spektralen Eigenschaften des Instruments normalerweise die wichtigsten Parameter um eine korrekte Interpretation der Messung zu gewährleisten. Das spektrale Ansprechverhalten einzelner Detektorpixel wird über deren Zentrumswellenlänge sowie der Halbwertsbreite beschrieben und definiert damit die spektralen Eigenschaften des Instruments. Um die spektralen Eigenschaften des Instruments zu bestimmen, werden entsprechend Charakterisierung Messungen im Labor durchgeführt. Das Instrument ist jedoch an Bord einer luft- oder weltraumgestützten Plattform variierenden umweltbedingten Stressfaktoren ausgesetzt (z. B. Vibrationen, Temperatur und Druckkraft Schwankungen). Diese führen, zusammen mit dem natürlichen Alterungsprozess, zur Veränderung der spektralen Eigenschaften und Performance des Instruments. Werden solche Veränderungen nicht berücksichtigt, sondern weiterhin die im Labor charakterisierten spektralen Parameter zur Verarbeitung der Daten verwendet, kann das zu signifikanten Fehlern im Datensatz und der daraus abgeleiteten Produkte führen.

Diese Dissertation untersucht die Eigenschaften und Ursachen für Änderungen der Charakteristik eines Spektrometers unter realen Bedingungen im Flugzeug. Dazu wurden neue Ansätze zum Monitoring der spektralen Eigenschaften eines flugzeuggestützten Sensors entwickelt und validiert. Die durch die Messungen beobachteten Abweichungen im Vergleich zu den Labormessungen werden genutzt um die Rohdaten vor einer Produktgenerierung entsprechend zu korrigieren. Das abbildende Spektrometer APEX (*Airborne Prism EXperiment*) steht im Fokus dieser Recherche. APEX ist ein dispersives, abbildendes pushbroom Spektrometer, das den Wellenlängenbereich zwischen 380 und 2500 nm abdeckt. APEX wurde entwickelt um gegenwärtige sowie zukünftige weltraumgestützte Missionen bei der Simulation, Kalibration und Validation zu unterstützen. Die Möglichkeit der in-flight Charakterisierung mittels eines auf APEX integrierten Charakterisierungs Equipments, bekannt als *In-Flight Characterization* (IFC) *facility*, ermöglicht die Messung der spektralen Eigenschaften des Sensors ausserhalb von Laborbedingungen. Gezielte Erfassung von IFC Messungen und Prozessierung mit Hilfe von ad-hoc entwickelten Algorithmen ermöglichte die Schätzung repräsentativer spektraler Parameter für ein luftgestütztes Instrument zu jedem Zeitpunkt. Ausserdem werden atmosphärische Absorptionsbanden aus Luftbilddaten verwendet, um die Schätzung der spektralen Parameter zusätzlich zu ergänzen und zu validieren. Dadurch konnte die Korrektur der Wellenlängenpositionen plausibel auf die APEX Datensätze angewendet werden. Die so kalibrierten APEX Daten werden erfolgreich für eine Simulation und Kalibration ausgewählter weltraumgestützter Missionen verwendet. In der Diskussion der Forschungsergebnisse werden die Vor- und Nachteile der entwickelten Ansätze besprochen und es wird auf mögliche Verbesserungen hingewiesen. Abschliessend wird ein Ausblick für weiterführende Arbeiten gegeben.

TABLE OF CONTENTS

1 INTRODUCTION

1.1 Optical remote sensing

Remote sensing is the science of obtaining information about an object, area, or phenomenon through the analysis of data acquired by a device that is not in proximity of the object, area, or phenomenon under study (Lillesand et al., 2004). The remotely collected data can be of many forms, including force distribution, acoustic wave distributions, or electromagnetic energy distributions. In remote sensing of electromagnetic (EM) energy, a wide branch is dedicated to the optical region of the EM spectrum traditionally encompassing the wavelength range from 10 nm to 1000 μm. This range includes the measurements of the reflective spectral radiances in ultraviolet, visible and infrared sub-regions (approximately from 350 to 2500 nm) commonly used for land remote sensing. In this region of the EM spectrum, the sun acts as a natural source of radiation and provides all the necessary energy for physical and chemical processes on Earth (Palmer et al., 2009).

Spectral radiance is the radiometric measure that describes the amount of electromagnetic radiation that passes through or is emitted from a particular area, and falls within a given solid angle in a specified direction at a certain wavelength (Kostkowski, 1997). It is expressed in W m^{-2} sr^{-1} nm^{-1}. It is used to characterize both emission from diffuse sources (e.g., the sun) and reflection from diffuse surfaces (e.g., the target). By integrating over the solid angle, other radiometric measures may be derived from radiance. *Irradiance* (W m^{-2}) refers to the power per unit area that is incident on a surface and *radiant exitance* (W m^{-2}) to the power per unit area leaving a source. The ratio between radiance exitance and irradiance is known as *reflectance* (Martonchik et al., 2000). Each material interacting with solar radiation reflects (or emits), transmits and absorbs energy according to its atomic structure such that it can be characterized through its reflectance profile, referred to as *spectral signature* (Price, 1994).

To fully understand the measurement of a spectral signature characterizing a certain material, we must understand the process of generation, transmission and detection of optical radiation. This process usually involves a system composed of a radiation source, a propagation medium, a target interacting with the radiation and a sensor measuring the radiation (Lillesand et al., 2004). Ideally, in such a system, the measurement of the signal by a specific sensor would result in complete and exclusive information about the target or phenomenon being observed. In reality, however, a number of factors other than the target are known to play a role in determining what is being measured (Jones et al., 2010). As both source and detector are 'remote' from the target, the characteristics of the radiation detected by the sensor are affected not only by its reflection/emission from the target but also by interactions with the intervening atmosphere (de Haan et al., 1991). Attenuation and scattering of solar radiation in the atmosphere both on its way to the surface and, after reflection back to the detector lead to a change in the radiation intercepted by the sensor as compared to the hypothetical (atmosphere-free) observation (Tanre et al., 1979). When the atmosphere is not itself the subject of investigation, its contribution is regarded as noise and has to be removed in order to isolate the useful signal from the surface target (Jones et al., 2010). This effort is referred to as atmospheric correction (Gao et al., 2009). An additional source of unwanted radiation comes from the surrounding ground pixels that may be in or in proximity of the instrumental field of view. This leads to an unwanted effect known as adjacency effect, and contributes towards the at-sensor radiance over a target pixel. The adjacency effect is low when the surface reflectance of the target ground pixel is at least as large as that of the surrounding ground pixels, but greater when the target pixel reflectance is lower than that of the surrounding (Jones et al., 2010). Apposite correction procedures are applied to correct for this effect often in combination with atmospheric correction (Kerekes, 2009; Tanre et al., 1981). Last but not least, the radiation reflected/emitted by the target is influenced by the sensor design. The limits of instrument

characteristics and associated performance can affect the accuracy, validity, consistency and inter-comparability of acquired data (Gaddis et al., 1996; Nieke et al., 2008). Technological advancements in instrument design constantly force these instrument-derived limits, opening ways for new Earth observation data products. An important advancement was the realization, beginning of the eighties, that it was technically feasible to fly imaging spectrometers from aircraft and spacecraft. This enabled the remote measurement of laboratory-like spectra allowing the quantification of earth materials based on their biogeochemical composition (Goetz et al., 1985). The increased spectral detail in the signature of a material acquired by a spectrometer, derives from measuring the reflected light in many, narrow, contiguous wavelength intervals. This however implies more stringent spectral performance requirements, as even the slightest change in instrument spectral performance would significantly impact data and product integrity (Green, 1998; Nieke et al., 2008). An accurate and frequent instrument characterization is therefore critical to guarantee an up-to-date instrument calibration and thus reliable measurements of reflectance of a target of interest. Moreover, accurately calibrated spectrometers operated in the field or from airborne platforms represent an indispensable source of data for the simulation, cross-calibration and validation of spaceborne observations (Green et al., 2003; Teillet et al., 2001; Teillet et al., 2007).

1.2 Spectral response model for imaging spectrometers

Instrument characteristics inevitably transform the physical properties of the incoming radiation. This transformation corresponds to a degradation of the signal since no instrument is able to measure a physical quantity with infinite precision (Jansson, 1997). The limit in the amount of detail the instrument can capture is referred to as the instrument's *resolution* (Schowengerdt, 1997). Understanding the nature of the signal degradation in relation to instrument's resolution is crucial for enhanced sensor and algorithm design (Kerekes et al., 2005). A correct interpretation of the resulting information further depends on it. A discussion of these aspects can be found in Teillet et al. (1997) and more recently in Damm et al. (2011).

For remote sensing systems, resolution can refer to different domains, such as spectral, spatial and temporal. Moreover, there is a radiometric resolution associated to the gain values as a function of wavelength (Schowengerdt, 1997). In this dissertation, the main focus is on the spectral characteristics of an imaging spectrometer determining its spectral resolution and overall performance. Instrument spectral performance is arguably the most critical aspect of knowledge required for reliable spectroscopy (Bender et al., 2011). The American Society for Testing and Materials (ASTM) defines spectral resolution as the ratio $\lambda/\Delta\lambda$, where λ is the wavelength of radiant energy being examined and $\Delta\lambda$ is the spectral width over which this energy is integrated expressed in wavelength units. By the *Rayleigh criterion*, which is often considered the working definition of resolution, two peaks are considered resolved when the maximum of one falls on the first minimum of the other (Jansson, 1997). Revisiting the definition of spectral resolution - and more in general the problem of instrument induced signal degradation - from an instrument point of view implies to familiarize oneself with a number of concepts, the most relevant of which are presented hereafter.

The response of the instrument as a function of wavelength is known as Spectral Response Function (SRF). Following Mouroulis et al. (2000a), we define the SRF of an instrument by a center wavelength position and a response shape (usually normalized to one). For spectrometers, acquiring radiation in many contiguous spectral bands, SRFs are commonly approximated by Gaussian shapes and the Full-Width-at-Half-Maximum (FWHM) is used to define the covered wavelength interval. The Spectral Sampling Interval (SSI) defines the spectral distance between the centers of adjacent spectral pixels (Brazile et al., 2008; Swayze et al., 2003) (Figure 1).

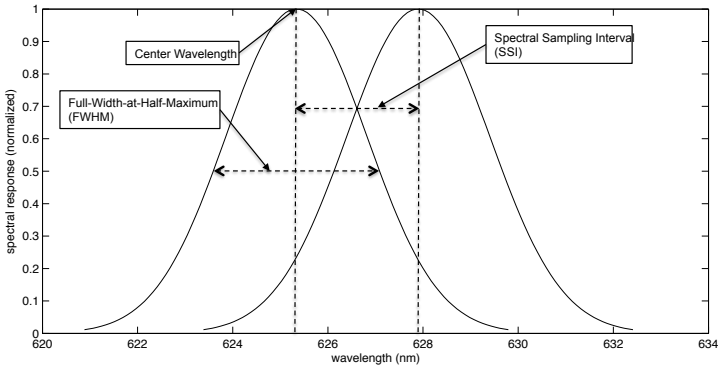

Figure 1 Spectral Response Function (SRF) and Spectral Sampling Interval (SSI).

From an instrument point of view, SRFs originate from the spectrally selective effects in the slit, the optics, the spectral selection elements and the detector spectral responsivity (Kerekes, 2009). A schematic view of the instrument components, leading to the definition of the SRF in a prism spectrometer, is shown in Figure 2.

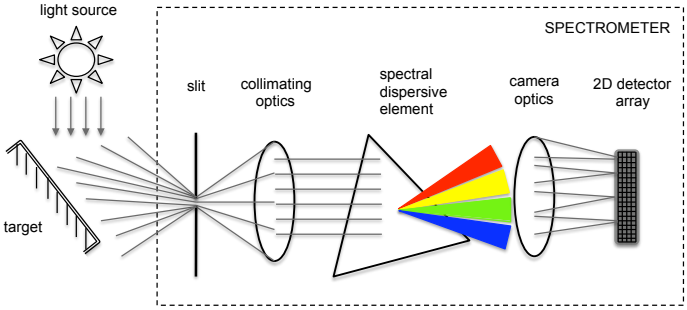

Figure 2 A simple schematic of a spectrometer. All dispersive spectrometers have a spectral selection element, either a prism (this figure) or a grating, dispersing white light into its individual wavelengths.

We can think of the SRF as originating from the convolution of the slit image with the pixel response function, where the latter is simply assumed to be a rectangular function (rect(w_2)). The slit image is itself a convolution of the slit, again a rectangular function (rect(w_1)), and the optical Line Spread Function (LSF) in the tangential direction (Mouroulis et al., 2000a). Thus we have:

$$\mathrm{SRF} = \mathrm{rect}(w_1) \otimes \mathrm{LSF}_\mathrm{T} \otimes \mathrm{rect}(w_2) \qquad (1)$$

where w_1 and w_2 represent the width of the projected slit and of the detector pixel, respectively,

while ⊗ denotes convolution. In this work we will thus use the term slit image for the response of a spectrometer to the light source up to where it reaches the array detector and the term Spectral Response Function (SRF) for the slit image convolved with the detector pixel response.

As seen in the simplified spectrometer diagram shown in Figure 2, the white light reflected by the target entering the spectrometer slit is dispersed into its individual constituent wavelengths by means of a spectral selection element. Dispersive spectral selection works by spatially spreading out the radiation spectrum before focusing by the camera lenses on a linear or area array (Schmidt, 2005). The wavelength dispersive element can be a grating (diffraction) or a prism (refraction). The collimating optics (e.g., lenses, mirrors) deployed to obtain a parallel beam toward the dispersive element, the dispersive element itself and finally the camera optics focusing the spectrum on the detector, determine the optical quality of the system as defined by the LSF. Figure 3, adapted from an illustration by Lerner (2006), visualizes this concept.

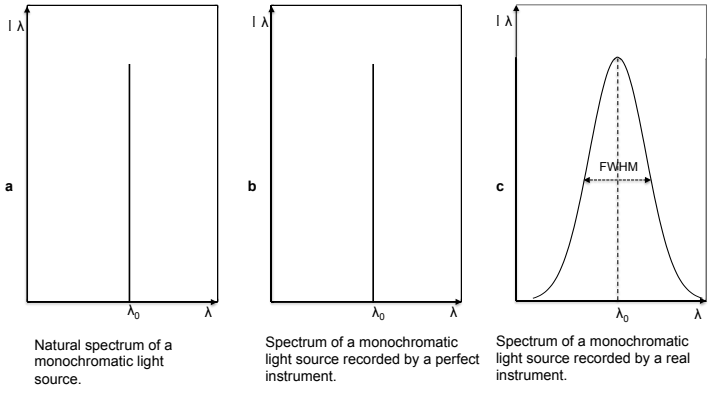

Figure 3 The natural spectrum of a monochromatic light source (a); the same light source imaged through a theoretically 'perfect' spectrometer (b); the monochromatic light imaged through a real spectrometer (c) (modified after Lerner 2006, p.719).

In Figure 3, the natural spectrum of an infinitely narrow monochromatic emission line is compared with its image on the focal plane of a 'theoretical' ideal instrument and of a real instrument. The center wavelength is defined as the peak response of the detector element to the emission line. For an ideal instrument the natural spectral width of the monochromatic light would be preserved when imaged on the focal plane, a real instrument, however, broadens it. This broadening is caused by the optical system itself and its inability to measure at infinitive precision (Lerner, 2006).

Eventually the slit image, dispersed by the dispersion element (e.g., prism) and possibly further spread by the optics, is sampled by the detector. The majority of spectrometers deploy array detectors where each detector element in the direction of the light dispersion (i.e., spectral pixel) provides a single reading, i.e., an individual measure of the amount of light incident upon it. The ratio between the width of the slit image (representing the resolution of our instrument, the FWHM in Figure 3c) and the SSI (i.e., pixel spacing on the array detector) in the same units (e.g., nm) is known as sampling ratio (Roscoe et al., 1996). The sampling ratio is what ultimately determines how well a spectrum can be reconstructed. If the resolution (FWHM) of the spectrometer is comparable or smaller than the pixel spacing, the spectrum is undersampled.

This means that a full restoration of the spectral information is not possible as spectral features are lost. The problem is reduced by increasing the instrument sampling ratio, however, as described in a study by Roscoe et al. (1996), technically this is not a straight forward step. The authors take as an example the measurement of atmospheric constituents (e.g., NO2) whose spectra are characterized by adjacent peaks separated by less than 3 nm. They claim an instrument resolution of better than ~1 nm is needed to avoid smoothing or loss of optical depth of absorption. Considering that modern array detectors usually do not exceed 1200 pixels, to achieve a sufficient sampling rate of for instance 10 samples per resolution element would mean to restrict the spectral range covered by our instrument to ~120 nm (Roscoe et al., 1996). Therefore a compromise between the sampling rate, the spectral resolution and the covered spectral range must be sought, with the limiting factor mainly resting with detector technology. It should be added here that in the real case a proper spectrum reconstruction also depends on the shape of the instrument response function and on the input signal to be sampled. Numerical experiments showed that for applications dealing with the measurement of atmospheric trace gases, sampling ratios between 4.5 and 6.5 pixels/FWHM are recommended to avoid undersampling (Chance et al., 2005). A perfect reconstruction of the spectrum is unattainable with the current range of spectrometers employed in Earth observation (Schaepman, 2009). Today, imaging spectrometers employed for land applications are commonly characterized by a spectral resolution (FWHM) comparable with the SSI as illustrated in Figure 4.

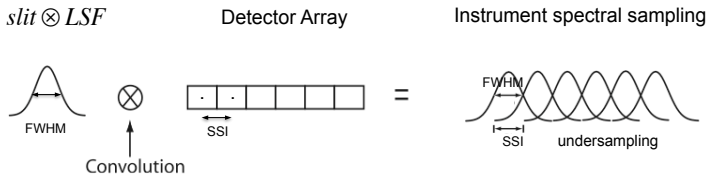

Figure 4 Instrument spectral sampling commonly used in spectrometers employed in Earth observation. The Full Width at Half Maximum (FWHM) or resolution of the spectrometer, resulting from the convolution of the geometrical slit with the optics Line Spread Function (LSF), is comparable to the Spectral Sampling Interval (SSI) provided by the array detector.

To summarize the discussion of the various concepts in this chapter and recalling Eq. (1), we emphasize that of the three factors which contribute to the SRF: i) the slit width, ii) the LSF of the optics and the dispersive element, and iii) the detector pixel size, the first two can be controlled by instrument design while the latter ultimately determines the spectral performance (Ball, 2001; Bender et al., 2011). For a detector with a given SSI and number of pixels, an optimal compromise has to be reached between the proper spectral sampling and the instantaneous spectral coverage one needs to achieve.

1.3 Calibration of spectral performance

Calibration can generally be defined as the set of operations, which establish, under specified conditions, the relationship between values indicated by a measuring instrument and the corresponding known values of a standard (NASA Earth Observing System). Calibration of instrument spectral performance refers to the procedure establishing the relationship between the instrument pixels and the wavelength scale (Hopkinson et al., 2004). Measurements to establish this relationship should be carried out within stated accuracies and should allow

traceability through an unbroken chain of comparisons to designed wavelength standards (Kostkowski, 1997; Fox, 2011). For a spectrometer, this means characterizing the SRF associated with each spectral pixel of the detector by specifying a center wavelength and a FWHM value. Both, the center wavelength of the pixel SRF and its FWHM, must be known to within a small fraction of the nominal FWHM associated with the pixel, typically less than a few percent (Green, 1998; Mouroulis et al., 2000b).

Initially, calibration foresees an instrument characterization carried out in the laboratory to determine whether a spectrometer meets its requirements as of design. In the laboratory, measurements are carried out under controlled and stable conditions employing different available spectral calibration standards (e.g., discharge gas lamps, lasers, monochromators, *etc.*) (Hopkinson et al., 2004). Typically, the SRF is measured by illuminating the spectrometer with monochromatic light and recording the response of consecutive spectral pixels. This generates a function that peaks when the monochromatic light beam coincides with the middle of the spectral pixel corresponding to the selected wavelength. It should be noted that the calibration strategy and the difficulty of the characterization task depend on the type of imaging spectrometer. *Pushbroom* scanning spectrometers employ two-dimensional arrays acquiring the across-track swath at once, as opposed to *whiskbroom* scanners featuring linear array technology and rotating mirrors to scan the Earth in across-track direction (Schaepman, 2009). This leads to possibly better geometric co-registration of spatial pixels in pushbroom systems, but also to spectral mis-registration and the associated effect in the data output, known as smile effect. Smile is the effect for which spectral response is not constant with across-track pixel position and is to a high extent intrinsic to the instrument design (Neville et al., 2003). This requires the measurement of SRFs to be performed in the spectral as well as in the spatial detector dimension, highly increasing the characterization load for pushbroom systems. As an example, a whiskbroom scanning instrument such as the Airborne Visible / Infrared Imaging Spectrometer (AVIRIS) (Green et al., 1998), with a single spatial pixel, requires only calibration of the 224 spectral pixels. A pushbroom scanning instrument such as Hyperion (Pearlman et al., 2003), with 256 spatial pixels, in the direction perpendicular to the optical dispersion, and 198 spectral pixels, requires instead over 50'000 pixels calibrations to be performed (Neville et al., 2008). The focus of this dissertation is on the monitoring and calibration of spectral performance of an airborne pushbroom spectrometer. These systems generate spectroscopic data cubes (Figure 5), where the second spatial dimension (along-track) is given by the forward motion of the aircraft or satellite platform.

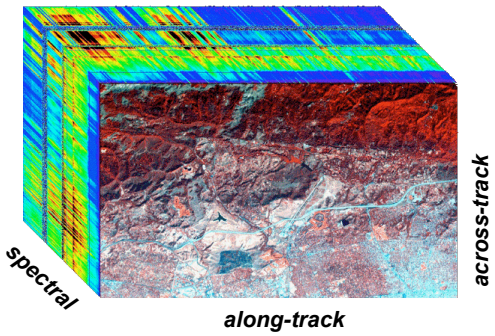

Figure 5 The spectroscopic data cube generated by a pushbroom imaging spectrometer. The across-track and spectral dimensions correspond to the dimension of the area-array detector, while the along-track dimension is obtained by forward motion of the airborne or spaceborne platform (source: http://aviris.jpl.nasa.gov).

As reported in Gege *et al.* (2009) the characterization measurements carried out in the laboratory are further processed to derive the parameters describing the instrument spectral response model. These are listed in Table 1. The FWHM parameter corresponds to what is defined as spectral resolution in earlier sections. The spectral response is usually fitted to a known curve during processing, which in the case of spectrometers is typically a Gaussian. Laboratory characterization measurements procedures are described in Gege *et al.* (2009) and Hopkinson *et al.* (2004) whereas for greater detail on the processing of these measurements to derive calibration parameters we refer to Brazile *et al.* (2003) and Hüni *et al.* (2009).

Table 1 Spectral parameters describing the instrument spectral response model.

Parameters		Description
$SRF_{i,x}(\lambda)$	Spectral Response Function of a selected spectral (*i*) and spatial (*x*) pixel	Normalized signal vs. wavelength λ
$\lambda_{i,x}$	Center wavelength of a selected spectral (*i*) and spatial (*x*) pixel	Peak maximum of $SRF_{i,x}(\lambda)$
Smile effect	Spectral smile of a selected spectral pixel	Center wavelength $\lambda_{i,x}$ vs. pixel number x
SSI	Spectral Sampling Interval of selected spectral and spatial pixels	Wavelength difference $\lvert\lambda_{i+1,x} - \lambda_{i,x}\rvert$ of adjacent spectral pixels
Spectral range	Spectral range of selected pixels	Wavelength difference $\lvert\lambda_{N,x} - \lambda_{1,x}\rvert$ of first and last spectral pixel
FWHM	Full Width at Half Maximum of a selected spectral and spatial pixel	Wavelength interval corresponding to ½ $SRF_{i,x}(\lambda)$

1.4 Monitoring of spectral performance in an operational environment

Although every attempt is made to ensure that pre-flight laboratory characteristics remain in place, once the instrument becomes airborne or spaceborne, it is acknowledged that for optical sensors this is rarely the case (Fox et al., 2011). It is therefore in the operational (air or space) environment where a re-characterization of the instrument performance needs to take place and where the real challenge of calibration sets in (Fox et al., 2003). Mechanical and environmental stresses, coupled with natural instrument aging, are known to lead to change and degradation of sensor performance (Gao et al., 2004). In the spectral domain, this change shows as modifications of the SRF with respect to the position (i.e., shift of center wavelength) and, to a much less extent, shape (i.e., change in FWHM) determined during laboratory characterization (Brazile et al., 2006; Guanter et al., 2006). In the attempt to monitor such performance changes, different post-launch (in-flight) spectral calibration approaches are being implemented for spaceborne and airborne instruments. The majority of these approaches are based on the evaluation of sharp absorption features present in the observed radiance spectra as compared to the same feature present in a well-known reference spectrum. The common baseline to these

methods is the high sensitivity of the measured spectrum to the instrument spectral performance in spectral windows where abrupt radiance changes occur (D'Odorico et al., 2011b; Guanter et al., 2009).

This section presents a brief review of a representative selection of in-orbit and in-flight spectral performance monitoring strategies implemented for spaceborne and airborne spectrometers, respectively. Perhaps the most important difference, to be taken into account when monitoring performance of spaceborne vis-à-vis airborne instruments is the respective operational environment. Space instruments have to survive the launch vibration but can count on a relatively stable environment thereafter. Airborne instruments however must maintain their characteristics in the face of constant vibration, temperature and pressure changes, and further tolerate several cold cycles as they are powered off and on (Bender et al., 2010). While spaceborne missions commonly rely on a combination of onboard and vicarious approaches, the monitoring of airborne systems is usually exclusively and critically depending on the latter.

The MEdium Resolution Imaging Spectrometer (MERIS) (Rast et al., 1999) onboard the ENVISAT platform is equipped with an erbium doped 'pink' diffuser, which illuminated by solar irradiance produces a radiance spectrum rich in absorption features. This approach is able to characterize MERIS spectral bands within the nominal mission accuracy requirements of 1 nm. It is however not suited for the near infrared due to the absence of useful erbium absorption lines in this spectral region. The use of Fraunhofer lines complements these measurements by providing the necessary reference in the violet and near infrared parts of the spectrum. Earth or 'white' diffuser observations are used to detect these lines. In Earth observations, oxygen absorption features originating in the atmosphere can additionally be exploited. MERIS spectral programmability, i.e., fifteen spectral bands selectable by ground command with a programmable width and spectral location, represent an advantage not only for Earth imaging but also for calibration. Dedicated calibration acquisitions can be performed with continuous narrow bands programmed to sample specific absorption features (Delwart et al., 2007).

The Hyperion (Pearlman et al., 2003) instrument mounted on the EO-1 spacecraft monitors spectral performance and related calibration based on data of the Earth's atmospheric limb. The atmospheric limb collection is essentially the same as a solar calibration but scheduled such that the instrument views the sun through different tangent heights of the atmosphere. The spacecraft performs a yaw maneuver to view the sun and allow the sunlight to be reflected off the solar calibration panel into the instrument aperture. The incoming radiance is uniform across the field of view and contains spectral features corresponding to solar lines, atmospheric features and absorption features originating from the paint on the instrument cover (Barry et al., 2002).

The MODerate resolution Imaging Spectroradiometer (MODIS) (Salomonson et al., 1989) system onboard the Terra and Aqua satellites exhibit a rather unconventional on-orbit spectral calibration concept. A light source, a spherical integration sphere and a grating monochromator provide the needed reference signal. Monochromators are rarely deployed in space environments, as they require regular wavelength re-calibration due to possible performance changes. For MODIS, a stable didymium glass with known transmission peaks is provided to establish the relationship between monochromator step and wavelength when the grating is located at a series of positions. The measured MODIS band responses versus grating step number are then scaled to wavelengths. A reference silicon photo-diode is used to normalize the didymium signal as well as the MODIS response signal to remove the light source spectral shape (Montgomery et al., 2000).

The Environmental Mapping and Analysis Program (EnMAP) mission (Stuffler et al., 2009) scheduled for launch in 2013 bases its in-orbit spectral performance monitoring on similar principles as those of previously reviewed missions. The proposed design foresees the use of an integrating sphere with light originating from a tungsten halogen lamp, housed outside of the sphere. The light is filtered through a didymium-doped glass, which provides a number of

spectral features across the visible and infrared range. In addition to the on-board approach EnMAP will carry out atmospheric limb observations in a similar fashion as Hyperion. Limb observations are performed through the solar port used for the direct sun imaging therefore no special maneuver is required as it is constantly pointing to the sun.

Currently, the on-orbit calibration strategies vary widely in both frequency and type of measurements as discussed in this chapter. The Committee on Earth Observation Satellites (CEOS) through its working group on calibration and validation (CalVal) is aiming to establish a consensus within the international remote sensing community so that calibration, validation and quality assurance processes are harmonized across satellite missions. Planned initiatives, such as the satellite mission TRUTHS (Fox et al., 2003) envisaged by ESA or the analogous CLARREO (Wielicki, 2011) mission planned by NASA, might aid this objective by complementing or fully replacing calibration efforts by individual missions. These satellite missions are meant to enable, for the first time, high-accuracy Système International d'unités (SI) traceability to be established in orbit. The direct use of primary standards and replication of the terrestrial traceability chain is meant to extend the SI into space and allow establishing a metrology laboratory in orbit (Fox et al., 2011).

Airborne instruments face a slightly different reality, with only very few instruments featuring onboard characterization sources. Operational since the early 90s, the AVIRIS spectrometer (Green et al., 1990) represents one such exception. Equipped with an onboard quartz halogen lamp and a set of spectral filters, AVIRIS represents the first airborne system designed to allow for in-flight spectral performance monitoring by means of targeted calibration acquisitions (Chrien et al., 1995). At the end of the 90s, the Reflective Optics System Imaging Spectrometer (ROSIS) (Kunkel et al., 1991) followed a similar path, including a mercury lamp for in-flight spectral performance monitoring in its design (Thiemann et al., 2001). However, the absence of literature reporting on the use of these airborne onboard characterization strategies leaves room only for speculations on their deployment up to the current day. A broad range of publications can instead be reviewed dealing with vicarious approaches, often referred to as scene-based approaches for they rely on the Earth observation scene itself. These methods exploit stable natural absorption features originating from atmospheric constituents (predominantly O_2 and CO_2) and, depending on instrument spectral resolution, solar Fraunhofer lines. Examples for AVIRIS, CASI, ROSIS and HyMap airborne spectrometers can be found in Guanter et al. (2007; 2006), Green et al. (2001) and Brazile et al. (2008).

The Airborne Prism EXperiment (APEX) imaging spectrometer features a unique in-flight calibration concept (Itten et al., 2008; Jehle et al., 2010). It is equipped with an In-Flight Characterization (IFC) facility allowing the characterization of radiometric, spectral, and geometric system performance, both in-flight and on ground covering the full Field Of View (FOV). The inclusion of a NIST Standard Reference Material (SRM) filter for spectral performance monitoring allows the transfer of state-of-the-art calibration standards and SI traceability methodologies into the airborne environment. The main focus of this dissertation is on the spectral performance monitoring of the APEX spectrometer.

1.5 Objective and research questions

The present dissertation contributes to the understanding of instrument-induced modifications of the measured spectral radiation. This understanding is critical for the improvement of instrument design, algorithm optimization, and for correct interpretation of remote sensing data and products. This dissertation should answer the following five research questions, grouped into two topical domains.

Monitoring in-flight spectral performance of the APEX imaging spectrometer.

Develop and validate an operational strategy aimed at the in-flight spectral performance and calibration monitoring of ESA's airborne imaging spectrometer APEX (chapters 3-4).

- Is APEX spectral performance measured during laboratory characterization still valid in an operational environment, if not, which are the causes of deviation?
- Is it feasible to monitor and characterize in-flight spectral performance based on the In-Flight Characterization (IFC) facility onboard APEX?
- What are the feasibilities and utilities of employing vicarious approaches to complement onboard methods for the purpose of spectral performance monitoring?

Exploitation of APEX calibrated data for the simulation, calibration and validation of space missions.

Investigate the potential of using APEX calibrated dataset to simulate, calibrate and validate existing and upcoming space missions for cross-sensor spectral calibration (chapter 5).

- Can APEX calibrated data be used to simulate satellite sensor radiances?
- Can APEX calibrated data be used for the spectral cross-calibration and validation of satellite observations?

1.6 Structure of the dissertation

Chapter 1 provides the framework and the definitions required for the understanding of the peer-reviewed contributions. It familiarizes the reader with the problem of imaging spectrometer spectral performance in an operational environment and briefly reviews the state-of-the-art in the field of in-flight (and in-orbit) monitoring. Research questions and outline of the present dissertation are also presented.

Chapter 2 is based on a co-authored publication (Jehle et al. 2010). It provides an overview of the APEX airborne imaging spectrometer, representing the main instrument in this dissertation. The publication is self-contained in terms of structure and content.

Chapter 3 is based on a first-authored peer-reviewed scientific publication (D'Odorico et al., 2010) addressing the first three research questions of the present dissertation. A series of experiments evaluating APEX spectral performance in function of different environmental conditions are presented. The publication is self-contained in terms of structure and content.

Chapter 4 is based on a first-authored peer-reviewed scientific publications (D'Odorico et al., 2011b) addressing the first three research questions of the present dissertation. A strategy for APEX spectral performance monitoring in-flight is proposed, based on onboard and vicarious measurements. The publication is self-contained in terms of structure and content.

Chapter 5 is based on a first-authored peer-reviewed scientific publication (D'Odorico et al., 2011a) addressing the last two research questions of the present dissertation. A study evaluating the potential of APEX to serve the simulation and spectral cross-calibration of satellite missions is presented. The publication is self-contained in terms of structure and content.

Chapter 6 summarizes the main findings from the publications presented in chapters 3-5, provides concluding remarks and an outlook.

1.7 References

Ball, D.W., 2001. The Basic of Spectroscopy SPIE - The International Society of Optical Engineering, 142 p.

Barry, P.S., Shepanski, J. and Segal, C., 2002. Hyperion on-orbit validation of spectral calibration using atmospheric lines and an on-board system. Proceedings of SPIE, 4480: 231-235.

Bender, H.A., Mouroulis, P., Eastwood, M.L., Green, R.O., Geier, S. and Hochberg, E.B., 2011. Alignment and characterization of high uniformity imaging spectrometers. Proceedings of SPIE, 81580J-11.

Bender, H.A., Mouroulis, P.Z., Green, R.O. and Wilson, D.W., 2010. Optical design, performance, and tolerancing of next-generation airborne imaging spectrometers. Proceedings of SPIE, 78120P-12.

Brazile, J., Kohler, P. and Hefti, S., 2003. A software architecture for in-flight acquisition and offline scientific post-processing of large volume hyperspectral data, Proceeding of the 10th USENIX Tcl/Tk Conference, Ann Arbor, MI.

Brazile, J., Neville, R.A., Staenz, K., Schlaepfer, D., Sun, L. and Itten, K.I., 2006. Scene-based spectral response function shape discernibility for the APEX imaging spectrometer. IEEE Geoscience and Remote Sensing Letters, 3(3): 414-418.

Brazile, J., Neville, R.A., Staenz, K., Schläpfer, D., Sun, L. and Itten, K., 2008. Towards scene-based retrieval of spectral response functions for hyperspectral imagers using Frauenhofer features. Canadian Journal of Remote Sensing, 34(1): S43-S58.

Chance, K., Kurosu, T.P. and Sioris, C.E., 2005. Undersampling correction for array detector-based satellite spectrometers. Applied Optics 44(7): 1296-1304.

Chrien, T., Eastwood, M., Green, R., Sarture, C., Johnson, H., Chovit, C. and Hajek, P., 1995. Airborne Visible/Infrared Imaging Spectrometer (AVIRIS) onboard calibration system. Fifth Annual JPL Airborne Earth Science Workshop Proceedings, Jet Propulsion Laboratory, Pasadena, CA.

D'Odorico, P., Alberti, E. and Schaepman, M.E., 2010. In-flight spectral performance monitoring of the Airborne Prism Experiment. Applied Optics 49(16): 3082-3091.

D'Odorico, P., Gonsamo, A., Damm, A. and Schaepman, M.E., 2011a. Experimental evaluation of Sentinel-2 spectral response function for NDVI time-series continuity. IEEE Transactions on Geoscience and Remote Sensing, submitted.

D'Odorico, P., Guanter, L., Schaepman, M.E. and Schläpfer, D., 2011b. Performance assessment of onboard and scene-based methods for Airborne Prism Experiment spectral characterization. Applied Optics, 50(23): 4755-4764.

Damm, A., Erler, A., Hillen, W., Meroni, M., Schaepman, M.E., Verhoef, W. and Rascher, U., 2011. Modeling the impact of spectral sensor configurations on the FLD retrieval accuracy of sun-induced chlorophyll fluorescence. Remote Sensing of Environment, 115(8): 1882-1892.

de Haan, J.F., Hovenier, J.W., Kokke, J.M.M. and van Stokkom, H.T.C., 1991. Removal of atmospheric influences on satellite-borne imagery: A radiative transfer approach. Remote Sensing of Environment, 37(1): 1-21.

Delwart, S., Preusker, R., Bourg, L., Santer, R., Ramon, D. and Fischer, J., 2007. MERIS In-flight Spectral Calibration. International Journal of Remote Sensing, 28(3): 479-496.

Fox, N., Aiken, J., Barnett, J.J., Briottet, X., Carvell, R., Frohlich, C., Groom, S.B., Hagolle, O., Haigh, J.D., Kieffer, H.H., Lean, J., Pollock, D.B., Quinn, T., Sandford, M.C.W., Schaepman, M., Shine, K.P., Schmutz, W.K., Teillet, P.M., Thome, K.J., Verstraete, M.M. and Zalewski, E., 2003. Traceable radiometry underpinning terrestrial- and helio-studies

(TRUTHS). Advances in Space Research, 32(11): 2253-2261.

Fox, N., Kaiser-Weiss, A., Schmutz, W., Thome, K., Young, D., Wielick, B., Winkler, R. and Woolliams, E., 2011. Accurate radiometry from space: an essential tool for climate studies. The Royal Society of London. Philosophical Transactions. Series A. Mathematical, Physical and Engineering Sciences, 369(1953): 4028-4063.

Gaddis, L.R., Soderblom, L.A., Kieffer, H.H., Becker, K.J., Torson, J. and Mullins, K., 1996. Decomposition of AVIRIS spectra: extraction of surface-reflectance, atmospheric, and instrumental components. IEEE Transactions on Geoscience and Remote Sensing, 34(1): 163 - 178.

Gao, B.-C., Montes, M.J., Davis, C.O. and Goetz, A.F.H., 2009. Atmospheric correction algorithms for hyperspectral remote sensing data of land and ocean. Remote Sensing of Environment, 113(1): S17-S24.

Gao, B.C., Montes, M. and Davis, C., 2004. Refinement of wavelength calibrations of hyperspectral imaging data using a spectrum-matching technique. Remote Sensing of Environment, 90(4): 424-433.

Gege, P., Fries, J., Haschberger, P., Schoetz, P., Schwarzer, H., Strobl, P., Suhr, B., Ulbrich, G. and Jan Vreeling, W., 2009. Calibration facility for airborne imaging spectrometers. ISPRS Journal of Photogrammetry and Remote Sensing, 64(4): 387-397.

Goetz, A.F.H., Vane, G., Solomon, J.E. and Rock, B.N., 1985. Imaging spectrometry for Earth remote sensing, Science, 228: 1147.

Green, R., 1998. Spectral calibration requirements for Earth-looking imaging spectrometers in the solar-reflected spectrum. Applied Optics, 37(4): 683-690.

Green, R., Eastwood, M., Sarture, C., Chrien, T., Aronsson, M., Chippendale, B., Faust, J., Pavri, B., Chovit, C., Solis, M., Olah, M. and Williams, O., 1998. Imaging spectroscopy and the Airborne Visible/Infrared Imaging Spectrometer (AVIRIS). Remote Sensing of Environment, 65(3): 227–248.

Green, R. and Pavri, B., 2001. AVIRIS inflight calibration experiment measurements, analysis and results in 2000. Proceedings of the tenth JPL airborne earth science workshop. JPL Pub., Pasadena, CA, pp. 205-219.

Green, R.O., Pavri, B. and Chrien, T., 2003. On-orbit radiometric and spectral calibration characteristics of EO-1 Hyperion derived with an underflight of AVIRIS and in situ measurements at Salar de Arizaro, Argentina. IEEE Transactions on Geoscience and Remote Sensing, 41(6): 1194 - 1203.

Green, R.O., Conel, J.E., Margolis, J.S., Carrere, V., Bruegge, C.J., Rast, M. and Hoover, G., 1990. In-flight validation and calibration of the spectral and radiometric characteristics of the Airborne Visible/Infrared Imaging Spectrometer (AVIRIS), Proceedings of SPIE. Imaging Spectroscopy of the Terrestrial Environment, pp. 18-36.

Guanter, L., Estellés, V. and Moreno, J., 2007. Spectral calibration and atmospheric correction of ultra-fine spectral and spatial resolution remote sensing data. Application to CASI-1500 data. Remote Sensing of Environment, 109(1): 54-65.

Guanter, L., Richter, R. and Moreno, J., 2006. Spectral calibration of hyperspectral imagery using atmospheric absorption features. Applied Optics, 45(10): 2360-2370.

Guanter, L., Segl, K., Sang, B., Alonso, L., Kaufmann, H. and Moreno, J., 2009. Scene-based spectral calibration assessment of high spectral resolution imaging spectrometers. Optics Express, 17(14): 11594-11606.

Hopkinson, G.R., Goodman, T.M. and Prince, S.R., 2004. A Guide to the Use and Calibration of Detector Array Equipment, PM142. SPIE Press, 234 p.

Hüni, A., Biesemans, J., Meuleman, K., Dell'Endice, F., Schläpfer, D., Adriaensen, S., Kempenaers, S., Odermatt, D., Kneubühler, M. and Nieke, J., 2009. Structure, components and interfaces of the Airborne Prism Experiment (APEX) Processing and Archiving Facility.

IEEE Transactions on Geoscience and Remote Sensing, 47(1): 1-4.

Itten, K., Dell'Endice, F., Hueni, A., Kneubuehler, M., Schlaepfer, D., Odermatt, D., Seidel, F., Huber, S., Schopfer, J., Kellenberger, T., Buehler, Y., D'Odorico, P., Nieke, J., Alberti, E. and Meuleman, K., 2008. APEX - the Hyperspectral ESA Airborne Prism Experiment. Sensors, 8(10): 6235-6259.

Jansson, P.A., 1997. Deconvolution of Images and Spectra. Academic Press, 514 p.

Jehle, M., Hueni, A., Damm, A., D'Odorico, P., Weyermann, J., Kneubühler, M., Schläpfer, D. and Schaepman, M.E., 2010. APEX - current status, performance and product generation. IEEE Sensors 2010, Waikoloa (HI), pp. 533 - 537.

Jones, H.G. and Vaughan, R.A., 2010. Remote Sensing of Vegetation: Principles, Techniques, and Applications. 1st Ed., Oxford University Press, 400 p.

Kerekes, J.P., 2009. Optical sensor technology. In: T.A. Warner, M.D. Nellis and G. Foody (Editors), The SAGE Handbook of Remote Sensing, pp. 95-107.

Kerekes, J.P. and Baum, J.E., 2005. Full-spectrum spectral imaging system analytical model. IEEE Transactions on Geoscience and Remote Sensing, 43(3): 571 - 580.

Kostkowski, H.J., 1997. Reliable Spectroradiometry. Spectroradiometry Consulting, Maryland, 605 p.

Kunkel, B., Blechinger, F., Viehmann, D., Van Der Piepen, H. and Doerffer, R., 1991. ROSIS imaging spectrometer and its potential for ocean parameter measurements (airborne and space-borne). International Journal of Remote Sensing, 12(4): 753-761.

Lerner, J.M., 2006. Imaging spectrometer fundamentals for researchers in the biosciences - A tutorial. Cytometry, Part A 69A: 712–734.

Lillesand, T., Kiefer, R.W. and Chipman, J.W., 2004. Remote Sensing and Image Interpretation. 5th Ed., J. Wiley & Sons, 720 p.

Martonchik, J.V., Bruegge, C.J. and Strahler, A., 2000. A review of reflectance nomenclature used in remote sensing. Remote Sensing Reviews, 19: 9-20.

Montgomery, H., Che, N., Parker, K. and Bowser, J., 2000. The algorithm for MODIS wavelength on-orbit calibration using the SRCA. IEEE Transactions on Geoscience and Remote Sensing, 38(2): 877-884.

Mouroulis, P., Green, R. and Chrien, T., 2000a. Design of pushbroom imaging spectrometer for optimum recovery of spectroscopic and spatial information. Applied Optics, 39(13): 2210-2220.

Mouroulis, P. and McKerns, M.M., 2000b. Pushbroom imaging spectrometer with high spectroscopic data fidelity: experimental demonstration. Optical Engineering, 39(3): 808-816.

Neville, R.A., Sun, L. and Staenz, K., 2003. Detection of spectral line curvature in imaging spectrometer data. Proceedings of SPIE, 5093: 144-154.

Neville, R.A., Sun, L. and Staenz, K., 2008. Spectral calibration of imaging spectrometers by atmospheric absorption feature matching. Canadian Journal of Remote Sensing, 34(1): S29–S42.

Nieke, J., Schlaepfer, D., Dell'Endice, F., Brazile, J. and Itten, K.I., 2008. Uniformity of imaging spectrometry data products. IEEE Transactions on Geoscience and Remote Sensing, 46(10): 3326-3336.

Palmer, J.M. and Grant, B.G., 2009. The Art of Radiometry, PM184. SPIE, 386 p.

Pearlman, J.S., Barry, P.S., Segal, C.C., Shepanski, J., Beiso, D. and Carman, S.L., 2003. Hyperion, a space-based imaging spectrometer. IEEE Transactions on Geoscience and Remote Sensing, 41(6): 1160-1173.

Price, J.C., 1994. How unique are spectral signatures? Remote Sensing of Environment, 49(3): 181-186.

Rast, M., Bezy, J.L. and Bruzzi, S., 1999. The ESA Medium Resolution Imaging Spectrometer MERIS a review of the instrument and its mission. International Journal of Remote Sensing, 20(9): 1681-1702.

Roscoe, H.K., Fish, D.J. and Jones, R.L., 1996. Interpolation errors in UV - visible spectroscopy for stratospheric sensing: implications for sensitivity, spectral resolution, and spectral range. Applied Optics, 35(3): 427-432.

Salomonson, V.V., Barnes, W.L., Maymon, P.W., Montgomery, H.E. and Ostrow, H., 1989. MODIS: advanced facility instrument for studies of the Earth as a system. IEEE Transactions on Geoscience and Remote Sensing, 27(2): 145-153.

Schaepman, M.E., 2009. Imaging spectrometers. In: T.A. Warner, M.D. Nellis and G. Foody (Editors), The SAGE Handbook of Remote Sensing, pp. 166-178.

Schmidt, W., 2005. Optical Spectroscopy in Chemistry and Life Sciences - An Introduction. Wiley, 384 p.

Schowengerdt, R.A., 1997. Remote Sensing - Model and Methods for Image Processing. 2nd Ed., Academic Press, 522 p.

Stuffler, T., Förster, K., Hofer, S., Leipold, M., Sang, B., Kaufmann, H., Penne, B., Mueller, A. and Chlebek, C., 2009. Hyperspectral imaging - An advanced instrument concept for the EnMAP mission (Environmental Mapping and Analysis Programme). Acta Astronautica, 65(7-8): 1107-1112.

Swayze, G., Clark, R., Goetz, A., Chrien, T. and Gorelick, N., 2003. Effects of spectrometer band pass, sampling, and signal-to-noise ratio on spectral identification using the Tetracorder algorithm. Journal of Geophysical Research, 108(E9 5105).

Tanre, D., Herman, M. and Deschamps, P.Y., 1981. Influence of the background contribution upon space measurements of ground reflectance. Applied Optics, 20(20): 3676-3684.

Tanre, D., Herman, M., Deschamps, P.Y. and de Leffe, A., 1979. Atmospheric modeling for space measurements of ground reflectances, including bidirectional properties. Applied Optics, 18(21): 3587-3594.

Teillet, P.M., Fedosejevs, G., Gauthier, R.P., O'Neill, N.T., Thome, K.J., Biggar, S.F., Ripley, H., Meygret, A., 2001. A generalized approach to the vicarious calibration of multiple Earth observation sensors using hyperspectral data. Remote Sensing of Environment, 77(3): 304-327.

Teillet, P.M., Fedosejevs, G., Thome, K.J. and Barker, J.L., 2007. Impacts of spectral band difference effects on radiometric cross-calibration between satellite sensors in the solar-reflective spectral domain. Remote Sensing of Environment, 110(3): 393-409.

Teillet, P.M., Staenz, K. and William, D.J., 1997. Effects of spectral, spatial, and radiometric characteristics on remote sensing vegetation indices of forested regions. Remote Sensing of Environment, 61(1): 139-149.

Thiemann, S., Strobl, P., Gege, P., Stahl, N., Mooshuber, W. and van der Piepen, H., 2001. Das abbildende Spektrometer ROSIS. Publikationen der Deutschen Gesellschaft für Photogrammetrie und Fernerkundung, 10: 147-153.

Wielicki, B.A., 2011. Climate Absolute Radiance and Refractivity Observatory (CLARREO): achieving climate change absolute accuracy in orbit. Bulletin of the American Meteorological Society, submitted.

2 APEX - CURRENT STATUS, PERFORMANCE AND PRODUCT GENERATION

This chapter has been published as: Jehle, M., Hueni, A., Damm, A., D'Odorico, P., Weyermann, J., Kneubühler, M., Schläpfer, D., and Schaepman, M.E., 2010. APEX - current status, performance and product generation. IEEE Sensors 2010, Waikoloa (HI), pp. 533 - 537.

APEX - Current Status, Performance and Validation Concept

Michael Jehle, Andreas Hueni, Alexander Damm, Petra D'Odorico, Jörg Weyermann, Mathias Kneubühler, Daniel Schläpfer, Michael E. Schaepman
Remote Sensing Laboratories
University of Zurich
Zurich, Switzerland
michael.jehle@geo.uzh.ch

Koen Meuleman
Flemish Institute for Technological Research (VITO)
Boeretang, Belgium
koen.meuleman@vito.be

***Abstract*—The Airborne Prism EXperiment (APEX) is an airborne pushbroom imaging spectrometer for Earth observation. Its products will become available in 2011. APEX is currently prepared for final acceptance configuration completing final hardware upgrades, refined calibration methodologies and test flights. APEX is composed of an airborne dispersive pushbroom imaging spectrometer, a Calibration Home Base (CHB) for instrument calibration and a data Processing and Archiving Facility (PAF) for operational product generation and delivery. A unique In-Flight Characterization (IFC) unit is integrated within the sensor optical head, providing pre- and post- data-acquisition characterization monitoring the instruments spectral and radiometric stability. This paper outlines the activities performed with a special focus on system calibration and validation procedures, as well as preliminary measurement results.**

I. INTRODUCTION

The Airborne Prism EXperiment (APEX) is an instrument being developed by a joint Swiss-Belgian consortium composed of institutes (University of Zurich, Flemish Institute for Technological Research) and industries (RUAG, OIP, Netcetera) within the European Space Agency's (ESA) PRODEX programme. The imaging spectrometer (see Fig. 1) measures the solar reflected radiance in the wavelength range from 380 nm to 2500 nm, using two spectrometer channels that share a common ground imaging optics. Depending on the flight altitude, the achieved resolution of 1000 spatial across track pixels covering a Field of View (FOV) of 28°, is approximately 1.75 m at 3500 m above ground level, with more than 330 reconfigurable spectral bands [1].

The instrument has been designed to provide high quality spectroscopic data for scientific applications, with special emphasis on topics related to the Earth System's spheres [2], and to simulate and support the development of future spaceborne remote sensing instruments.

Table 1 gives an overview of the APEX performance. Besides a special focus on the calibration and validation concept (described in section II), a current status update and first results from this years flight campaign are also presented.

TABLE I. APEX SELECTED PERFORMANCES

APEX Performance		
Spectral Performance	***VNIR***	***SWIR***
Spectral Range	380.5 - 971.7 nm	941.2 - 2501.5 nm
Spectral Bands	up to 334, def.114	198
Spectral Sampling Interval	0.55-8 nm	5-10 nm
Spectral Resolution (FWHM)	0.6-6.3 nm	6.2-11 nm
Spatial Performance		
Spatial Pixels (across track)	1000	
FOV	28°	
IFOV	0.028° (~0.5 mrad)	
Spatial Sampling Interval (across track)	1.75 m @ 3500 m AGL	
Sensor Characteristics	***VNIR***	***SWIR***
Type	CCD	CMOS
Dynamic Range	14 bit	13 bit
Pixel Size	22.5 µm * 22.5 µm	30 µm * 30 µm
Smile	average < 0.35 pixel	
Keystone (Frown)	average < 0.35 pixel	
Co-Registration	average < 0.55 pixel	
Other Information		
Data Capacity	500 GB on SSD	
Data Transfer	Spectral frames: 30 MB/s, HK Data: 20 kB/s	
Data rate for default config.	0.4 GB/km (1250 km max.)	

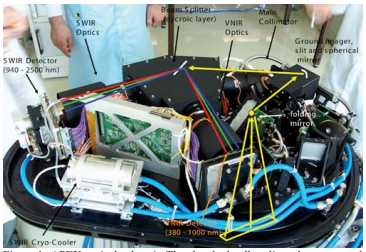

Figure 1. APEX optical sub-unit. The sketched yellow lines demonstrate the path of light from the observed area (rect.) to the prism.

II. Current Status: APEX Acceptance Flights and Verification Concept

As a result of the 2009 flight campaign the environmental controlling and regulation system was upgraded [3]. A new pressure regulation unit and an additional heating controller and elements were added. Recent measurements in the climate chamber facility hosted by RUAG in Emmen (CH) showed improved spectral performance and environmental stability [4].

A complete sensor characterization and calibration under laboratory conditions at the Calibration Home Base (CHB) in Oberpfaffenhofen (D) was performed. After system installation in the DLR Dornier Do-228 aircraft and on-ground system operation tests, the flight readiness was achieved.

Data acquisition took place in June / July 2010 over selected and well characterized vicarious calibration sites in Belgium and Switzerland [3]. In a total of nine flights (including one test flight) over more than 42 flight hours, all planned data acquisitions were performed under generally optimal conditions (stable, clear-sky measurements). This data set is proving to be valuable for the currently ongoing validation and acceptance process.

Verification of the acceptance requirements was planned using a broad variety of state-of-the-art measurements for airborne imaging sensors. Such a broad variety of performance monitoring approaches allows an independent validation of the instrument. The most relevant factors for the APEX validation are:

- In-flight characterization
- Vicarious validation
- Calibrated data assessment
- Cross validation using reflectance estimates

A detailed description of each validation approach applied for the APEX acceptance activities is presented in the following sections.

A. *In-Flight Characterization and Calibration*

Sensors operated in-flight are usually affected by movements and vibrations of the carrying platform or variations of environmental parameters, e.g. temperature and pressure. These factors affect the stability of the instrument and, therefore, the performance in-flight often differs from the one characterized in the laboratory.

APEX is the first airborne instrument carrying an onboard characterization facility able to monitor the instrument's spectral, radiometric *and* geometric performance for the entire instrument FOV. This In-flight Characterization (IFC) facility includes a quartz–tungsten–halogen 75W lamp, monitored and stabilized by means of a feedback loop sensor, and a filter wheel intercepting the optical path during calibration mode. One standard rare earth material NIST-certified filter, three bandpass filters, and one attenuation filter occupy five out of six positions on the wheel, with the last being empty.

Spectral monitoring is performed by tracking instrument-induced shifts of filter spectral features in-flight. Geometric monitoring relies on the position of geometric features present in the slit profile (i.e. slit irregularities) and resulting from the projection of two wires glued perpendicularly to the slit. Radiometric stability is investigated by comparing the onboard lamp signal measured in-flight with the one measured at the CHB.

Housekeeping information, co-registered with each imaging and calibration acquisition, is acquired thanks to a series of temperature and pressure sensors distributed within the optical compartment as well as the baffle.

The objective of this unit is to support the instrument performance analysis during standard in-flight operations and compare them with measurements achieved during calibration activities. The IFC provides a stable radiometric, geometric and spectral input to the system. Methods to investigate the instrument performance are currently under development [5].

The in-flight monitoring also allows identifying when instrument performances have fallen out of specifications and the instrument needs to return to the laboratory for a re-characterization. In specific cases, the monitoring can provide necessary correction coefficients for a data recalibration.

During the 2010 flight campaign over 90 GB of IFC and dark current data (DC) were collected which are currently being analysed. First results showed how environmental conditions on the airborne platform are controlled and stabilized.

B. *Vicarious Validation*

In addition to the in-flight characterization, vicarious validation provides an alternative, independent way to evaluate the performance of sensors in flight, whereby radiometrically and spectrally sufficiently characterized reference targets and corresponding sensor signals are compared. The correlation of both signals allows evaluation of the sensor performance in-flight. According to [6] and [7], several vicarious validation strategies are typically used,

namely *reflectance*, *radiance* and *irradiance (or improved reflectance) based methods*.

The APEX Processing and Archiving Facility (PAF) follows a *multi-target reflectance based vicarious validation* methodology. A multi-target approach based on reference targets spanning a wide dynamic range of radiometric signals enables evaluation of possible non-linear behavior in the sensor.

To provide a representative dynamic range of bright to dark reference signatures, only targets were selected, that were i) homogeneous and flat within a spatial area of at least 10 x 10m and ii) provided a high dynamic range of radiance values (Fig. 2). In total, 25 targets were measured in three different test sites under a variety of atmospheric conditions (urban, rural and high Alpine environments). Two test sites were covered repeatedly.

Ground reference data were acquired using a handheld ASD field spectrometer. The instrument registers reflected radiation within the spectral range of 350-2500 nm with a nominal full width half maximum (FWHM) of 3.0 nm (350-1050 nm) and 10.0 nm (1050-2500 nm), respectively. Data were acquired in radiance mode by observing the target, bracketed by radiance measurements of a Spectralon™ reference panel. Hemispherical-conical reflectance factor (HCRF) values were calculated in post-processing [8]. This strategy allows an evaluation of the measurement quality and target homogeneity. Data were acquired within +/- 1 hour of solar noon to avoid significant changes to the illumination geometry.

The measured reflectance factors were forward modeled to provide at-sensor radiances, comparable to the acquired sensor data. Atmospheric scattering and absorption effects were simulated using the radiative transfer model MODTRAN5. The model was parameterized using in-situ measurements of atmospheric and meteorological parameters (e.g. sun-photometer data to derive aerosol optical thickness and water vapor column, measurements of ozone concentrations, air pressure, humidity, temperature).

The agreement between modeled and measured radiance signals can be statistically described, and allows evaluation of the radiometric and spectral performance of the sensor. However, reflectance based vicarious validation approaches include an uncertainty that must be considered in the evaluation process. In optimal cases, the uncertainty sums to a total error ranging from 3.4% [9] to 4.9% [6]. Typical sources of uncertainty are i) the representativeness and homogeneity of the reference target, ii) the characterization of atmospheric properties at the time of overflight and iii) the spectral characteristics of the ground based spectrometers used [10].

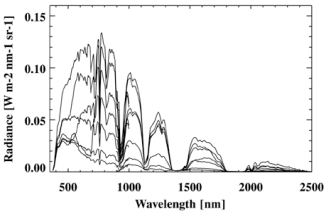

Figure 2. Dynamic range of simulated at-sensor radiance signals.

C. *CHB Data Calibration and Calibrated Data Assessment*

The generation of higher level products requires an accurate characterization and calibration of the sensor, done with the help of constantly repeated CHB [11] measurements. Results from these measurements are used in the PAF. The APEX processor is a software component developed at the University of Zurich and hosted operationally at VITO in Belgium [1]. The main functionality of the APEX processor is to transform raw instrument data into uniform radiometrically, spectrally and geometrically calibrated at-sensor radiances (Fig. 3) [12]. Data are transferred from the APEX CSU (Computer and Storage Unit) to the PAF using a tape device. Raw data are transformed into Level 0, i.e. digital numbers, by data segregation and basic bit operations. Level 0 comprises IFC, DC and image data, all accompanied by corresponding housekeeping data, the latter containing data about instrument settings per acquired data frame.

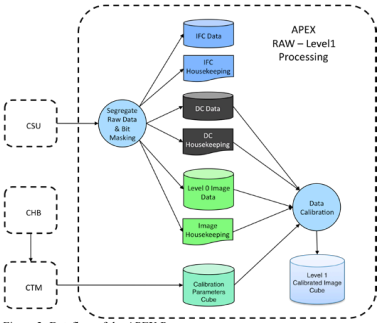

Figure 3. Dataflow of the APEX Processor.

Level 0-1 processing entails radiometric, spectral and geometric data calibration. It is based on calibration data acquired during CHB campaigns which has turned into so-called calibration cubes, comprising layers corresponding to specific instrument parameters, characterizing the system response at the detector pixel level (Fig. 4). This detailed information allows radiometric calibration of each detector pixel as well as correction for smile (spectral misregistration) and frown (keystone) effects, generating uniform data products. In a first step, validation of the products can be done visually. Fig. 5 shows a first result from the 2010 acceptance flights, a section of a flight-line over the Swiss National Parc located in southern Switzerland acquired on June 24, 2010. The two black lines in the image are hair-wires glued on the instrument slit and are used for geometric performance monitoring. First results from higher level products such as estimates of leaf area index, dry matter content, water content, and chlorophyll content were reported in [3].

D. Cross Validation Using Atmospheric Data Processing

An inverse approach to validating the image data is to convert the calibrated at-sensor radiance values to reflectance factors at the surface. This conversion is done by atmospheric data processing. During this step, the wavelength-dependent and view-angle specific scattering and extinction of energy through the atmosphere is modeled. Atmospheric correction accounts for adjacency effects as well as the spatial water vapor distribution, aerosol content variation and variation of diffuse illumination. Optionally, effects of haze, cloud shadow and directional as well topographic effects can be reduced. After atmospheric correction, APEX HCRF data can be compared to field-measured reflectance factors.

The ATCOR-4 software [13] is used for atmospheric correction. ATCOR implements a physical approach, based on inversion of the MODTRAN-4 radiative transfer code. ATCOR runs are parameterized by using in-situ measurements and (if available) external information on meteorological conditions. More details can be found in [14].

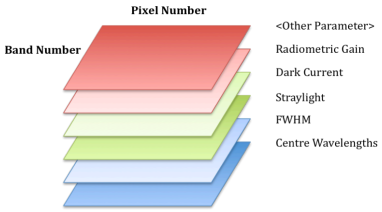

Figure 4. Structure of a calibration cube.

III. Conclusions

Performance assessment of APEX showed overall functionality of the system during the 2010 campaign. During this campaign in June / July 2010 a total of over 400 GB of imaging spectrometer data were collected over selected test sites in Belgium and Switzerland. Acquisitions include imaging data over forests, crops, glaciers, snow, inland water, urban, mountainous, and coastal areas. As the APEX calibration and validation concept foresees a broad variety of independent performance monitoring measurements, an expanded vicarious calibration campaign consisting of numerous ground truth measurements was organized simultaneously. In-flight calibration data were also continuously monitored during APEX flights, allowing one to track changes of the sensor calibration enabling derivation of absolute physical quantities from measured sensor data. Additionally, atmospherically corrected data were compared to field-measured reference spectra. First results show agreement between in-field measurements and the processed data. Sufficient adequate data were acquired during the 2010 flight campaign to support the current extensive evaluation of the instrument.

Acknowledgment

The authors acknowledge the scientific contribution of Edoardo Alberti. The authors acknowledge funding support of their respective employers and projects (SUK (Hyper-I-Net) and ESA (APEX Phase C/D)). All supporting personnel is thanked for their valuable support during field work.

Figure 5. Quicklook of a section of the Swiss National Parc flown with APEX on June 24th 2010. The two black lines in the image are wires mounted on the instrument slit, necessary for calibration and geometric performance tests.

REFERENCES

[1] K. I. Itten, F. Dell'Endice, A. Hueni, M. Kneubühler, D. Schläpfer, D. Odermatt, F. Seidel, S. Huber, J. Schopfer, T. Kellenberger, Y. Bühler, P. D'Odorico, J. Nieke, E. Alberti, and K. Meuleman, "APEX - the hyperspectral ESA Airborne Prism Experiment," Sensors, vol. 8, nr. 10, p. 6235-6259, 2008.

[2] M. E. Schaepman, S. L. Ustin, A. J. Plaza, T. H. Painter, J. Verrelst, and S. Liang, "Earth system science related imaging spectroscopy--An assessment," Remote Sensing of Environment, vol. 113, pp. 123-137, 2009.

[3] E. Alberti, F. Dell'Endice, P. D'odorico, A. Hueni, M. E. Schaepman, K. Meuleman, J. Biesemans, R. Dryemaeker, S. Sterckx, S. Adriaensen, S. Kempenaers, B. Bomans, D. Schläpfer, and Y. Rezaei, "APEX status PT.1: Instrument development and performance," ESA Hyperspectral Workshop, 17.-19.03., Frascati, Italy, 2010.

[4] P. D'Odorico, "Influence of system temperatures on instrument spectral performances," Technical Note, APX-RSL-IFC-0013-1, RUAG Climate Chamber Experiment, May 2010.

[5] P. D'Odorico, E. Alberti, and M. E. Schaepman, "In-flight spectral performance monitoring of the Airborne Prism Experiment," Appl. Opt., vol. 49, pp. 3082-3091, 2010.

[6] M. Dinguirard and P. N. Slater, "Calibration of space-multispectral imaging sensors: A review," Remote Sensing of Environment, vol. 68, pp. 194-205, 1999.

[7] P. N. Slater, S. F. Biggar, K. J. Thome, D. I. Gellman, and P. R. Spyak, "Vicarious radiometric calibrations of EOS sensors," Journal of Atmospheric and Oceanic Technology, vol. 13, pp. 349-359, 1996.

[8] G. Schaepman-Strub, M. E. Schaepman, T. H. Painter, S. Dangel, and J. V. Martonchik, "Reflectance quantities in optical remote sensing – definitions and case studies," Remote Sensing of Environment, vol. 103, pp. 27-42, 2006.

[9] M. Kneubühler, M. E. Schaepman, and K. Thome, "MERIS/ENVISAT Vicarious calibration over land," Proc. SPIE 5234, 10th Int. Symposium, Barcelona, pp. 614-623, 2003.

[10] J. Secker, K. Staenz, R. P. Gauthier, and P. Budkewitsch, "Vicarious calibration of airborne hyperspectral sensors in operational environments," Remote Sensing of Environment, vol. 76, pp. 81-92, 2001.

[11] P. Gege, J. Fries, P. Haschberger, P. Schötz, H. Schwarzer, P. Strobl, B. Suhr, G. Ulbrich, and W. J. Vreeling, "Calibration facility for airborne imaging spectrometers," ISPRS Journal of Photogrammetry & Remote Sensing, vol. 64, pp. 387–397, 2009.

[12] A. Hueni, J. Biesemans, K. Meuleman, F. Dell'Endice, D. Schläpfer, S. Adriaensen, S. Kempenaers, D. Odermatt, M. Kneubuehler, J. Nieke, and K. Itten, "Structure, components and interfaces of the Airborne Prism Experiment (APEX) processing and archiving facility," IEEE Transactions on Geoscience and Remote Sensing, pp. 68–73, 2009.

[13] R. Richter and D. Schlaepfer, "Geo-atmospheric processing of airborne imaging spectrometry data. Part 2: Atmospheric/Topographic correction," International Journal of Remote Sensing, vol. 23(13), pp. 2631-2649, 2002.

[14] A. Berk, G. P. Anderson, L.S. Bernstein, P. K. Acharya, H. Dothe, M. W. Matthew, S. M. Adler-Golden, J. H. Chetwynd, S. C. Richtsmeier, B. Pukall, C. L. Allred, L. S. Jeong, M. L. Hoke, and R. Green, "MODTRAN4 Radiative Transfer Modeling for Atmospheric Correction," 8th Ann. JPL Airb. Earth Science Workshop, pp. 55-61, 1999.

3 IN-FLIGHT SPECTRAL PERFORMANCE MONITORING OF APEX

This chapter has been published as: D'Odorico, P., Alberti, E. and Schaepman, M.E., 2010. In-flight spectral performance monitoring of the Airborne Prism Experiment. Applied Optics 49(16): 3082-3091.

In-flight spectral performance monitoring of the Airborne Prism Experiment

Petra D'Odorico,* Edoardo Alberti, and Michael E. Schaepman

Remote Sensing Laboratories, University of Zurich. Winterthurerstrasse 190, CH-8057 Zurich, Switzerland

*Corresponding author: petra.dodorico@geo.uzh.ch

Received 22 February 2010; revised 23 April 2010; accepted 23 April 2010;
posted 26 April 2010 (Doc. ID 124554); published 26 May 2010

Spectral performance of an airborne dispersive pushbroom imaging spectrometer cannot be assumed to be stable over a whole flight season given the environmental stresses present during flight. Spectral performance monitoring during flight is commonly accomplished by looking at selected absorption features present in the Sun, atmosphere, or ground, and their stability. The assessment of instrument performance in two different environments, e.g., laboratory and airborne, using precisely the same calibration reference, has not been possible so far. The Airborne Prism Experiment (APEX), an airborne dispersive pushbroom imaging spectrometer, uses an onboard in-flight characterization (IFC) facility, which makes it possible to monitor the sensor's performance in terms of spectral, radiometric, and geometric stability in flight and in the laboratory. We discuss in detail a new method for the monitoring of spectral instrument performance. The method relies on the monitoring of spectral shifts by comparing instrument-induced movements of absorption features on ground and in flight. Absorption lines originate from spectral filters, which intercept the full field of view (FOV) illuminated using an internal light source. A feature-fitting algorithm is used for the shift estimation based on Pearson's correlation coefficient. Environmental parameter monitoring, coregistered on board with the image and calibration data, revealed that differential pressure and temperature in the baffle compartment are the main driving parameters explaining the trend in spectral performance deviations in the time and the space (across-track) domains, respectively. The results presented in this paper show that the system in its current setup needs further improvements to reach a stable performance. Findings provided useful guidelines for the instrument revision currently under way. The main aim of the revision is the stabilization of the instrument for a range of temperature and pressure conditions to be encountered during operation.

OCIS codes: 280.0280, 110.0110, 300.0300, 120.4640.

1. Introduction

Imaging spectroscopy [1] data are being increasingly distributed to the user community at different quality levels. Uncertainties originating from acquisition, calibration, and processing reduce their usability at different levels of the data product chain. Nieke *et al.* [2] estimate the level of uncertainty to as high as 10% of the total radiance due to imperfections in the data resulting from punctual effects [3] (e.g., bad pixels), spectral and spatial misregistration [4], and sensor stability and degradation related effects, among other things. Since the advent of the first imaging spectrometers at the beginning of the 1980s [5], increasing attention has been devoted to the monitoring of these uncertainties and to improving the quality of the spectral data. Thanks to improved calibration concepts [6], new approaches [7,8], and advanced technology [9], it was possible to generate more accurate, i.e., uniform, imaging spectroscopy data and products. The same study [2] estimated how uncertainties of nonimaging and imaging instruments used in Earth observation could be reduced to values of $<5\%$.

Focusing on the spectral domain, we refer to spectral calibration as the process in which spectral response functions (SRF), associated with individual

0003-6935/10/163082-10$15.00/0

pixel elements across both dimension of the focal plane, are being defined. The latter usually foresees making an assumption on the shape of SRFs (e.g., Gaussian) and determining the center wavelengths (CW) as well as the full width at half-maximum (FWHM) describing each SRF. Spectral calibration is usually performed prior to a flight season in a standardization laboratory by means of a monochromator device [9]. A study by Green [10] estimated that a spectral calibration accuracy approaching 1% of the SRF's FWHM is required to obtain radiances without significant spectrally distinct errors. Spectral nonuniformities are usually present in the data in the form of band shifts or broadening [11], causing modification of the SRF with respect to the position and shape determined during the initial laboratory characterization. These effects are expected to vary with time and operation conditions. Pushbroom instruments present additional problems related to the spatial direction. In these systems, area arrays are used as focal planes generating three-dimensional imaging spectroscopy cubes corresponding to the parameters time, center wavelength position, and across-track view angle. For a uniform data set, the response curve in one dimension should be constant in the other two dimensions, e.g., the spectral response shall be constant with time and across-track view angle [12]. The effect for which spectral response is not constant with across-track pixel position is known as spectral misregistration or smile and is to a high extent intrinsic to the instrument design [10].

By not correcting systematically for these errors, and by relying on the initial nominal spectral laboratory calibration, artifacts will arise when converting the signal into physical meaningful units [13]. Guanter *et al.* [14] estimated that, for a synthetic data set, a shift of 1 nm for channels with a FWHM of 10 nm results in an error in the measured radiance of up to $\pm 25\%$ in the proximity of strong water vapor absorption bands [14].

Different strategies are chosen to monitor instrument stability and uniformity in the resulting spectral data. For spaceborne systems, these usually are based on an onboard calibration mechanism. The moderate-resolution imaging spectroradiometer (MODIS) system employs a light source in combination with a monochromator to monitor the spectral performance in orbit [15]. In a similar fashion, the medium resolution imaging spectrometer (MERIS) instruments make use of an erbium-doped Spectralon diffuser plate, which offers a number of spectral absorption features in the visible range. For characterization in the violet and near infrared, selected Fraunhofer lines and atmospheric features are covered by MERIS channels thanks to the instrument's spectral programmability [16]. The Hyperion system looks at the Sun rising through the limb of the Earth. In this way, light passes through the atmosphere before reflecting off the solar calibration panel into the instrument aperture, providing a spectrum rich in solar lines, atmospheric lines, and absorption lines from the paint that coats the panel [17].

Airborne imaging spectrometers face a different operational scenario than their spaceborne counterparts. Two major differences influence the calibration strategy to be adopted: the first is that airborne instruments can return on ground to undergo a recharacterization in the laboratory; the second is that being airborne implies a higher exposure to stresses caused by variation of environmental factors (e.g., pressure/temperature). This eventually meant that differences between the laboratory setting and the airborne platform, in terms of environmental conditions, observational geometry, mechanical, electrical, and operational interfaces [18], could no longer be neglected in the data calibration process. The need for an in-flight monitoring approach was thus addressed by so-called scene-based methods, as presented extensively for airborne sensors, such as the compact airborne spectrographic imager (CASI) [14] and the airborne visible/infrared imaging spectrometer (AVIRIS) [18]. These methods rely on features present in the imagined spectra, which by nature always occur at the same wavelength; these are atmospheric absorption features and solar Fraunhofer lines [14,19]. In short, a scene-based approach works by comparing a spectrum acquired by the sensor in flight with a simulated reference spectrum (S). The simulated references result from the convolution of the highly resolved incoming signal with instrument SRF, which are shifted by iterating on $\Delta\lambda$:

$$S = \int \mathrm{SRF}(\lambda + \Delta\lambda) \times L(\lambda) \times T(\lambda) \mathrm{d}\lambda, \qquad (1)$$

where $\mathrm{SRF}(\lambda + \Delta\lambda)$ are the "new" SRF of the instrument, $L(\lambda)$ is the incoming signal, and $T(\lambda)$ is the atmospheric transmission function. The process reaches a halt when the best match between the acquired and a simulated spectrum is found, whereby the corresponding $\Delta\lambda$ represents the shift.

Three fundamental limitations are associated with scene-based methods. The first is the disputable assumption for which the variability in time and heterogeneity in space of the atmospheric layer [14], as well as the directional effects in the scene, are negligible compared to spectral nonuniformities introduced by the instrument instability. The second constraint is seen in the inability to establish traceability between characterization measurements performed in flight and characterization measurement acquired on ground by using the same measurement techniques and references. Last but not least, the generation of simulated reference spectra obtained by iterating on SRF position and/or width, requires the nominal SRFs from laboratory characterization. Thus, the uncertainties linked with the determination of the latter are propagated throughout the estimation of the new spectral parameters.

An alternative approach able to overcome these limitations is technically feasible by including

characterization equipment in the instrument design concept, as previously presented for spaceborne systems. In the early 1990s, the use of onboard characterization equipment was first attempted with AVIRIS. In this instrument, the onboard signal source is given by a 10 W quartz halogen lamp stabilized by a silicon detector feedback circuit. The light is transmitted through optical fibers to the back of the foreoptics shutter and reflected from there to the AVIRIS spectrometer [20,21]. Similarly, in 1997 a revision of the reflective optics system imaging spectrometer (ROSIS) airborne instrument brought the inclusion of a mercury lamp for onboard spectral calibration before and after each flight line [22]. Since then—to the best of our knowledge—no further development has taken place in this direction.

The Airborne Prism Experiment (APEX) imaging spectrometer [23] is, to the best of our knowledge, the first pushbroom instrument including an in-flight characterization (IFC) facility that allows a full characterization of system properties, i.e., radiometric, spectral, and geometric, during flight as well as on ground for the full instrument field of view (FOV). In this paper, we present the findings of a series of ground and flight experiments in which data acquired with the IFC are used to understand the system behavior in different operational conditions. A spectral performance monitoring methodology, using IFC filter features to monitor spectral data uniformity, has been developed in this context.

2. APEX and Its In-Flight Characterization Facility

The APEX project started in 1997 [24] by performing a feasibility study on the design of an imaging spectrometer. System specifications were defined based on user requirements and on a subsequently derived forward-performance model built on these requirements [25]. Key instrument requirements are reported in Table 1. APEX serves a multitude of purposes, including future sensor simulation, regional-scale biogeochemical cycle assessment, and technology studies. In the summer of 2009, the first extensive flight and field campaigns were carried out in Europe as part of the instrument acceptance process.

APEX mechanical and thermal design is conceived to minimize the impact of environmental parameters, such as pressure, temperature, and vibrations. During exploitation, airborne instruments experience a standard atmosphere at 5.5 km a.s.l., an external temperature of about −21 °C, and an absolute pressure of 50 kPa. The APEX mechanical interface plate (MIP) allows the installation and interface of the instrument, for example, with the aircraft or the calibration bench. The APEX optical base plate (OBP), the supporting core of the instrument, is linked to the MIP by a system of six studs with spherical head joints, aiming at minimizing the distortions on the OBP itself induced by external thermo-mechanical effects. A carbon fiber cover, which is gas tight by means of an O-ring, is mounted on the MIP. The aim is to seal the optical subunit in a nitrogen atmosphere, protecting the optical instrument from contamination and degradation (e.g., chemicals, condensation) during flight operations. The internal pressure at takeoff ranges between 110 and 130 kPa. An optical window mounted on the MIP allows the radiance input inside the optical system. To support instrument thermal conditioning within the operating temperature range, the aircraft installation includes an environmental control box (ETC) to generate a stabilized temperature environment surrounding the page. The instrument baffle is connected to the MIP with a system designed to minimize thermal conduction through the mechanical structure. Nevertheless, convective heat exchange happens by means of airflow streaming through the optical baffle aperture, reaching the bottom of the MIP plate and streaming inside the ETC box. The instrument is installed on a Leica PAV30 stabilizing platform, allowing it to be a nadir-looking system within ±5° of roll and pitch angles.

The instrument design is a dispersive pushbroom spectrometer, acquiring the spectral and across-track domain on area detectors. Imaging is performed through the forward motion of the aircraft. The FOV is projected by the ground imager onto the spectrometer slit using a path folding mirror. To minimize the polarization sensitivity, a scrambler can be inserted to randomize the polarization of the incoming light at the expense of spatial resolution. A collimator lens group directs the light on the first prism. A dichroic coating separates the short-wave infrared (SWIR) and visible near infrared (VNIR) channels. The VNIR channel is then dispersed further using a second prism. The VNIR detector is a commercial charged coupled device (CCD) ranging from 380–1000 nm. For the SWIR channel, a specific comple-

Table 1. APEX Instrument—Key Requirements

Parameter	Requirement
Field of view (FOV)—pushbroom techniques	Swath: ±14 deg with 1000 across-track pixels
Instantaneous field of view (IFOV)	0.028 deg.
Flight altitude range	3.5–10 km a.s.l.
Standard aircraft interface	For Dornier Do-228 on stabilizing platform PAV-30
Spectral coverage	VNIR: 380–970, SWIR: 940–2500
Spectral channels	VNIR: 334 (prior binning) or 114 (default binning). SWIR: 198
Spectral sampling interval (SSI)	VNIR: 0.5–8 nm. SWIR: 5–10 nm
FWHM	~1.5 SSI
Center wavelength accuracy	<0.2 nm
Smile/Keystone	<0.35 pixel
Coregistration	<0.9 pixel
Instrument temporal radiometric uncertainty within a flight section	<2%
Interval for instrument recalibration	Before and after a complete flight season.

mentary metal oxide semiconductor (CMOS) mercury cadmium telluride (MCT) detector array was developed [26] ranging from 940–2500 nm. The two spectrometer channels are aligned to minimize the geometric coregistration error.

An integral part of the APEX spectrometer is a built-in IFC facility (Fig. 1). During the in-flight characterization operation, the main instrument shutter is closed to avoid any light penetrating from the outside. A stabilized quartz–tungsten–halogen (QTH) 75 W lamp in a dedicated housing is attached to an optical fiber. The optical fiber guides the light from the lamp through the calibration shutter, which is usually closed to prevent the IFC light from entering the spectrometer during image acquisition. Diffusers are placed before and after a fixed folding mirror to improve the uniformity of the illumination. A sensor is used to monitor the light level and to control the lamp power accordingly in a closed control loop. A sliding folding mirror is moved into the optical path to reflect the light generated by the IFC toward a filter wheel mounted in front of the ground imager. The wheel holds four spectral filters to be used for instrument spectral stability monitoring; these are three bandpass filters (Spectrogon) with absorption features at 700, 1000, and 2218 nm and a standard reference material (SRM) filter from the National Institute for Standards and Technology (NIST) (Fig. 2). The NIST certified SRM filter holds many distinct absorption features and can be used as a secondary spectral calibration standard. A fifth filter, an NG4 attenuation filter, is used to avoid saturation in the VNIR channel at maximum radiance levels (image acquisition over snow). The sixth filter wheel position is left empty for standard data acquisition. Deterioration of the spectral filters is not expected as they are located inside the enclosed and temperature-stabilized optical subunit.

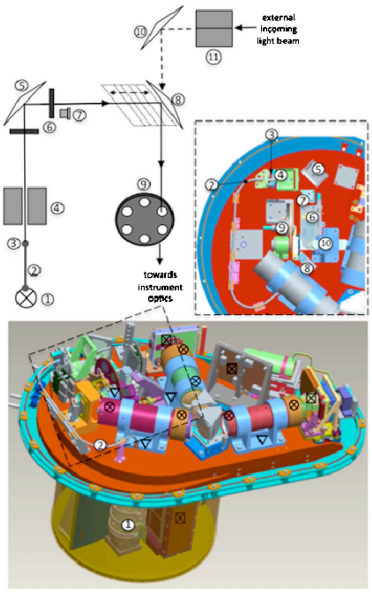

Fig. 1. (Color online) IFC facility onboard APEX: (1) QTH lamp; (2) optical fiber; (3) fiber output; (4) calibration shutter; (5) fixed folding mirror; (6) diffusers; (7) feedback loop sensor; (8) sliding folding mirror; (9) filter wheel; (10) fixed folding mirror; (11) global shutter; □ temperature sensor; ∇ temperature sensor on optical base plate (averaged); ⊗ differential temperature sensors.

For each filter used, the IFC light is dispersed onto the detectors in exactly the same fashion as ground observations. With this design, all relevant optical elements of APEX can be calibrated in flight. A default IFC spectral calibration measurement consists of 316 × 1000 × 20 pixels, where 316 is the combination of VNIR (117) and SWIR (199) spectral pixels, 1000 is the number of across-track detector pixels, and 20 is the average number of frames per default measurement. IFC measurements can be acquired at different integration times (ITs), with a default of 29 ms. Once the instrument becomes operational, it is planned to perform IFC measurements regularly during each laboratory and flight campaign.

3. Materials and Methods

A. Methods

Spectral monitoring techniques that rely on the position of stable and known spectral features, are all based on a common assumption. The latter states that a shift in SRFs (i.e., center wavelength) causes spectral features to be sampled differently, namely, higher or lower in the absorption slopes. As a result, features which, "by nature," are always found at the same wavelengths, happen to be "apparently" shifted toward lower or higher wavelengths. As an example, SRFs shifted toward the lower wavelength slope of

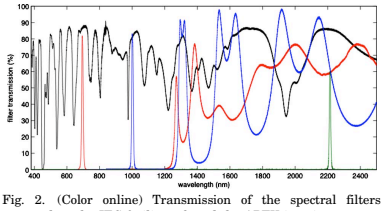

Fig. 2. (Color online) Transmission of the spectral filters mounted on the IFC facility onboard the APEX imaging spectrometer (SRM NIST, black; BP700, red; BP1000, blue; BP2218, green).

the absorption feature, i.e., wavelengths are decreased, result in an apparent feature shift toward higher wavelengths as seen in Fig. 3. This is explained by the fact that SRFs shifted toward lower wavelengths cause a higher signal to be sampled for the lower wavelength slope and a lower signal to be sampled for the higher wavelength slope (i.e., just imagine sampling the same feature slightly to the left of the original points). It is thus possible to estimate the shift in the instrument SRFs by retrieving the observed shift in the imagined features.

The approach proposed for the APEX instrument foresees looking at the same IFC feature-rich spectrum on ground and at different moments during flight and searching for the spectral shift of the nominal channel positions by finding the best fit. To achieve the best sensitivity, the fitting is evaluated only around predefined spectral regions where the filter's features occur. Features located in a region of the spectrum characterized by too low a signal were excluded from the analysis.

The fundamental difference between the methodology proposed here and the scene-based approach described earlier is that in the former, spectra directly measured by the instrument are used for the estimation, while in the latter, modeled quantities obtained by moderate resolution atmospheric transmission (MODTRAN) simulations and convolution operations are taken as a reference. To better understand this difference, a more detailed algorithm description is provided in the following.

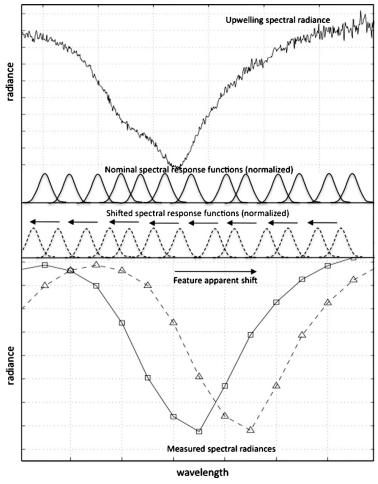

Fig. 3. Example of an absorption feature seen by a sensor with nominal (continuous) and with shifted (discontinuous) SRF: where □ points sampled with nominal SRF and △ point sampled with shifted SRF.

It is assumed that for an operational instrument spectral shifts occur mostly at the subpixel level. Estimation at this resolution requires the measured IFC spectra to be resampled to a finer sampling interval. This was achieved by linear interpolation of spectra. A brief assessment of other interpolation techniques (e.g., spline) showed negligible differences between techniques. In a first step, spectral features in the reference IFC onground spectrum are identified. Features usually extend over 5–10 spectral bands. Individual features are indexed by defining a lower (x_L) and an upper (x_U) spectral pixel number. While x_L and x_U remain fixed for the ground spectrum, they are iteratively changed for the flight spectrum for which the feature position shall be determined. In practice, this step is carried out by employing a sliding window, which scans across the flight spectrum as shown in Fig. 4. The step $\mathbf{\Delta x}$ size by which the window moves corresponds to the step defined earlier for the interpolation of the spectrum and represents the resolution of the algorithm (i.e., the minimum shift that can be retrieved). The step size $\mathbf{\Delta x}$ was set to a value of 0.01 pixels. This threshold was determined using a sensitivity analysis accounting for system intrinsic fluctuations (e.g., random noise) during spectra acquisition and method uncertainty [27,28]. Each spectral interval identified by the sliding window is iteratively compared with the reference feature using feature matching. The best feature match is identified by means of an optimization procedure that minimizes the deviation between the ground reference feature and the feature in the flight spectrum. Different merit functions can be used to assess the goodness of each iterative match, such as position of the feature's peak, position of the feature's center of gravity (COG), standard deviation, or Pearson's correlation coefficient. Pearson's correlation coefficient has been chosen for this study as the merit function to be maximized; reasons for this choice lie in the results obtained by means of a sensitivity study [27] and on a review of literature [16,17,29–32]. In the sensitivity analysis,

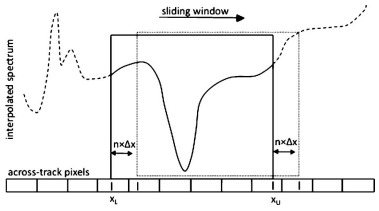

Fig. 4. Sliding window progressively shifting of Δx and defining a lower ($x_L + \Delta x$) and an upper ($x_U + \Delta x$) spectral pixel position by which a portion of the flight spectrum is indexed. The sliding window is shown for two iteration steps.

simulated datasets were used to compare different merit functions, whereby the correlation analysis gave the best results with uncertainties in the order of 1%–3% of a pixel. Furthermore, in a comparison study, Neville *et al.* [33] identified the correlation function as very suitable when working with uncalibrated data due to its insensitivity toward calibration gain/offset uncertainties [32]. An additional advantage is found in the fact that the correlation coefficient is the result of directly comparing the feature's shapes; thus, all sampling points are weighted in the comparison. On the other hand, metrics, such as the peak or the COG, first compute the value representative of each feature and then compare the two features based on this one value, which can be the peak or the COG position.

The described feature matching process is repeated for all detector pixels in the across-track direction so as to obtain an across-track shift profile (or differential smile profile), as shown in Fig. 5. By means of simple linear least-squares regression analysis, a function is fitted to the across-track spectral shifts as follows:

$$f(x) = \beta_0 + \beta_1 x, \tag{2}$$

where x is the across-track pixel position. Because the number of data points is large compared to the number of fit parameters, the noise introduced in the estimation of individual shifts is believed to cancel out when using the fit. Two indices derived by the fit are used to synthesize the system's spectral performance as compared to the reference's performance. These indices are the mean spectral shift (mss), obtained by Eq. (2) when calculating the fit value for the central across-track detector pixel ($x = 500$), and the rotation given by the angular coefficient (ac) of the fit function (ac $= \beta_1$). The former index will be used to compare spectral performance uniformity in the time domain, i.e., between IFC recordings performed at different moments during a flight season. The latter index will be used to describe the uniformity of the spectral performance in the spatial dimension, i.e., the across-track direction.

The proposed methodology can be considered independent from the laboratory characterization process and the associated uncertainties. This, however, is true as long as we are only interested in the estimation of spectral shifts expressed in units of pixel, as was the case for this study. The independence is granted by the fact that no *a priori* calibration information (e.g., nominal center wavelength positions) is needed to produce shift estimates.

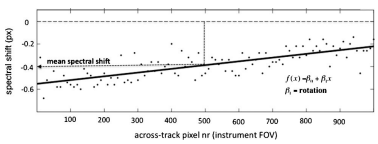

Fig. 5. Spectral shift estimated for each across-track pixel using one filter absorption feature. The indices adopted to synthesize the instrument spectral performance at a specific time instance are (1) the mss, given by the value of the fit for the central detector pixel and (2) the rotation, given by the angular coefficient of the fit function.

B. Data

In the frame of the APEX instrument acceptance phase, a series of IFC acquisition experiments were carried out to test the system.

It is known that different flight levels and the derived pressure/temperature stresses can cause changes in the dispersion element (prism or grating), aberrations in the collimator and imaging optics, or misalignment of the detector array in the instrument's focal plane [32,33]. Two ground experiments were carried out to test the independent influence of individual environmental parameters on the instrument behavior. In the first experiment, a pressure profile resembling that encountered in flight is simulated by means of nitrogen overpressure. In a second experiment, the influence of system temperatures is investigated by exposing the system to controlled heating/cooling within a climate chamber. Furthermore, data were acquired during a flight campaign in June 2009 to study the instrument's spectral behavior in a complex operational setting. IFC measurements were taken over three flight days, whereby in the second and third day measurements were subdivided into morning and afternoon acquisitions for a total of five separate data sets.

For all IFC acquisitions, the same reference data set was used for the spectral shift analysis. The reference IFC frame was obtained by averaging an IFC cube acquired on ground at the calibration home base (CHB), located at DLR in Oberpfaffenhofen, Germany [9]. The time of the IFC reference cube acquisition preceded all other acquisitions and coincided with the most recent APEX laboratory characterization campaign.

Coregistered onboard with the image and calibration data were environmental parameters, reflecting the state of the system during a particular acquisition. For this purpose, a number of temperature sensors were positioned within the optical subunit (e.g., on both detectors, on the optical base plate) and the baffle compartment [on the power supply unit (PSU)] (see Fig. 1), while pressure sensors were located inside as well as outside the optical subunit compartment.

Last but not least, dark current (DC) cubes were always acquired before and after each IFC cube and used in the preprocessing for DC correction.

4. Results

Least-square regression analysis was used to identify the environmental parameters most significant in explaining the trend in spectral performance deviations. The deviation from a reference performance was synthesized by using the mss and the rotation

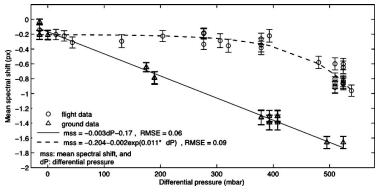

Fig. 6. Spectral mean shifts estimated for flight data (∘) and for on-ground data (△) acquired at different pressure regimes. The size of the vertical bar (|) represents the standard deviation of the estimates. Linear (continuous line) and exponential (discontinuous line) regression models have been fitted to the data. Results are for the feature at 784–815 nm.

(ac) indices. In the controlled ground experiment, the variation of differential pressure (dP), calculated as the difference between pressures registered internally and externally the optical subunit, was found to explain the spectral performance nonuniformities in time (mean $r^2 = 0.98$). For dP ranging from −100 to 550 mbar, a linear absolute increase of mss was estimated, where the highest absolute shifts of about 1.6 pixels occurred in concomitance with maximal dP conditions. Results are depicted in Fig. 6, where triangles represent the mss associated with an IFC measurement performed at a specific time and dP condition. Standard deviations (size of the vertical bars) provide an indication of the dispersion of across-track shifts around the mean shift, i.e., the shift associated with the central detector pixel.

The correlation analysis carried out between each housekeeping parameter and the mss for the flight data confirmed dP as being the most influential parameter. The comparison with the relation found for the ground experiment revealed, however, a less steep drop in spectral performance with rising dP. The latter can be ascribed to the fact that on ground the influence of dP was assessed in an independent manner, i.e., all other environmental parameters were kept stable, while in-flight joint dynamics influence system behavior. Residual analysis showed how this relationship, when modeled for a complex operational setting, is best described by an exponential regression model (Fig. 6).

The analysis was repeated for four spectral regions in the VNIR and four in the SWIR, based on the data acquired over the three flight days. The day-to-day differences in dP values can be ascribed to the different IFC measuring scenarios, in terms of flight altitude and time elapsed since takeoff.

The results of the trend analysis presented in Fig. 7 evidenced good agreement for all investigated spectral regions, with mss increasing exponentially as a function of the rising dP. Small shift differences along the spectral domain were expected because, for each spectral region, a different filter feature was used in the estimation. The difference in feature shape, as well as in number of points encompassed by each feature, is responsible for the small variations.

A constant absolute shift in the range of 0.2–0.4 pixels in the VNIR and 0.4–0.6 pixels in the SWIR was estimated for dP below 400 mbar. It is assumed that the climbing of the dP beyond this value released the system from what was a state of static equilibrium and provoked an exponential increase of the shift, reaching 1 pixel in the VNIR and 1.3 pixel in the SWIR for dP of 550 mbar.

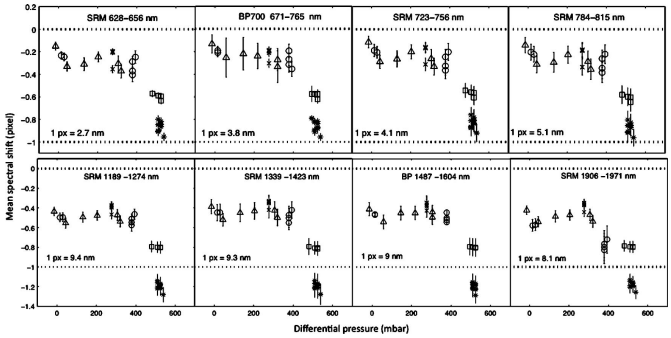

Fig. 7. Mean spectral shift estimates for four spectral regions of the VNIR (top) and SWIR (bottom) detector, plotted against the differential pressure trend. Data were acquired over three flight days: ∘17/06, □18/06 AM, △18/06 PM, *23/06 AM, ×23/06 PM. Data were acquired with the NIST SRM and with the bandpass filters. The size of the vertical bar (|) represents the standard deviation of the estimates. The dotted horizontal lines enclose the interval corresponding to one unbinned detector pixel and report the nanometers for the specific wavelength region.

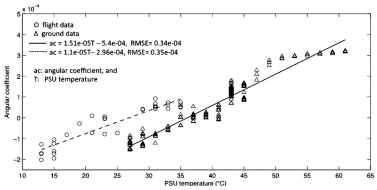

Fig. 8. Rotation estimated for flight data (∘) and for onground data (△) acquired at different PSU temperatures. Linear regression models have been fitted to the data (continuous line, ground data; discontinuous line, flight data). Results are for the feature at 784–815 nm.

Making the needed assumptions, the shift can be converted to nanometers by multiplying its value, expressed in units of pixels, by the average spectral sampling interval (SSI), derived from the most recent laboratory characterization and corresponding to the spectral region covered by the feature. This implies two conditions. These are that the interval covered by a feature should be small enough for (1) an average SSI to be a plausible approximation and (2) the estimated shift to be assumed constant for all bands covered by the feature. Overall, APEX bands were estimated to shift toward shorter wavelengths, meaning that spectral absorption features were found apparently shifting toward longer wavelengths.

Spectral performance nonuniformities in the space domain, i.e., across track, were synthesized by the second indicator, termed rotation and expressed as the angular coefficient of the regression fit function. Further, as was already done for the first indicator, least-square regression analysis was used to correlate rotations with the environmental parameters trends.

The second controlled ground experiment, which took place in a climate chamber at stable pressure conditions, revealed a temperature dependency of the across-track spectral nonuniformities (i.e., rotations). The temperature correlating best with the spectral performance trend was the one recorded in the baffle compartment at the level of the PSU. As depicted in Fig. 8, a linear regression model was found to best describe the trend in rotation as a function of varying PSU temperature. For a right-handed coordinate system placed at the central detector pixel position, the rotation was estimated to occur clockwise for PSU temperatures below 35 °C and counterclockwise for temperatures exceeding this value. A PSU temperature of 50 °C marked a leveling off of the rotation to constant values.

The temperature dependency was confirmed by the flight data (Fig. 8), although temperature ranges simulated on ground and registered in flight did not fully overlap. In the overlapping temperature range, the observed offset between ground and flight estimates is believed to be due to the combined influence of environmental parameters during flight.

In Fig. 9, angular coefficient estimates are reported for four spectral regions in the VNIR and four in the SWIR, considering the data acquired during the three flight days. The trend analysis revealed overall consistency for all investigated spectral regions in the VNIR as well as good correlation (mean $r^2 = 0.82$), which was only partially present for the SWIR (mean $r^2 = 0.53$). The highest estimated rotations are given by angular coefficients in the order of $3e^{-04}$ occurring in concomitance with lower PSU temperatures (about 10 °C–15 °C). The mentioned

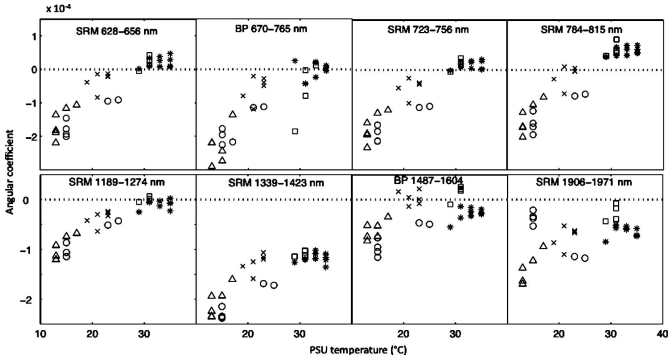

Fig. 9. Rotation for four spectral regions of the VNIR (top) and SWIR (bottom) detector plotted against the PSU temperature trend. Data were acquired over three flight days: ∘17/06, □ 18/06 AM, △18/06 PM, *23/06 AM, ×23/06 PM. Data were acquired with the NIST SRM and with the bandpass filters.

angular coefficient value corresponds to angles of about 0.017 deg (angle = arctan(ac) * 180/π) or to maximal rotations of 0.3 pixels.

It should be noted at this point that what was here termed rotation is in reality a change in the intrinsic smile profile. The latter can have two main origins. The first, most likely source, is a mechanical misalignment causing the image of the slit to be projected differently on the detector array (i.e., the whole detector is rotating). The second source is linked to aberrations in the instrument optics and usually causes spectrally dependent nonuniformities. The contributions of these two sources to the overall change in smile profile are difficult to separate based exclusively on the current analysis. The fact that mechanical misalignments are more likely to occur than optical aberrations, coupled with a relatively good spectral independence of the results, made us prefer the term rotation.

Further work is needed to confirm these hypotheses, such as the integration with results coming from the geometric analysis, in which the position of the features intrinsic to the slit across-track profile are monitored in the same fashion as spectral features.

5. Conclusion

In this paper, the potential of built-in characterization equipment for monitoring system spectral performances over a wide range of operational conditions is shown for the first time, to the best of our knowledge, for an airborne dispersive pushbroom imaging spectrometer. The presented methodology was found suitable for the monitoring and quantification of spectral nonuniformities in the time and space (across-track) domains. Two indices, synthesizing the instrument spectral performance compared to a reference (on ground) performance, were used; these are the mean shift and the rotation.

The system spectral performance during flight was found to deviate from the reference performance characterized on ground prior to flight. Maximal mean shift of about 1 pixel and maximal rotation of about 0.017 deg were estimated on average for both detectors. The availability of housekeeping information (e.g., temperatures and pressure), associated with the system at each acquisition, was fundamentally important for the study. As a result, environmental performance dependencies advanced the understanding of the system behavior during operation. This study showed the importance of having well-distributed thermal sensors within the instrument. The relevance of monitoring the internal and external pressure as a possible instrument performance driver was further evidenced.

A trend analysis of data acquired in a controlled environment in the frame of two ground experiments revealed that differential pressure and temperature in the baffle compartment were the driving factors for spectral performance deviations in the time and the spatial domains, respectively. These findings provide valuable information for the realization of instrument design changes aimed at minimizing the effects investigated in this study.

Future work foresees the integration of results obtained from scene-based approaches, using spectral features present in the image scene itself (e.g., atmospheric features and solar Fraunhofer lines), as well as geometric stability monitoring, based on features present in the across-track slit profile (slit irregularities). These may further improve the interpretation of the system behavior in regard to external factors as treated within this study.

This work has been done in the frame of the APEX project funded by an ESA/PRODEX contract. P. D'Odorico acknowledges the support of a Marie Curie Fellowship awarded in the frame of the Sixth Framework Program through the Hyper-I-Net network. The authors thank A. Hüni and F. Dell'Endice from University of Zurich for data collection and V. Mogulsky from Kayser Threde and D. Schläpfer from ReSe for beneficial discussions. A special thanks goes to A. Gonsamo for valuable comments on an earlier version of this paper. Last but not least, we acknowledge the thoughtful comments of three anonymous reviewers.

References

1. M. E. Schaepman, S. L. Ustin, A. J. Plaza, T. H. Painter, J. Verrelst, and S. Liang, "Earth system science related imaging spectroscopy-an assessment," Remote Sens. Environ. **113**, S123–S137 (2009).
2. J. Nieke, D. Schlaepfer, F. Dell'Endice, J. Brazile, and K. I. Itten, "Uniformity of imaging spectrometry data products," IEEE Trans. Geosci. Remote Sens. **46**, 3326–3336 (2008).
3. D. Schlaepfer, J. Nieke, and K. I. Itten, "Spatial PSF nonuniformity effects in airborne pushbroom imaging spectrometry data," IEEE Trans. Geosci. Remote Sens. **45**, 458–468 (2007).
4. F. Dell'Endice, J. Nieke, D. Schlaepfer, and K. I. Itten, "Scene-based method for spatial misregistration detection in hyperspectral imagery," Appl. Opt. **46**, 2803–2816 (2007).
5. G. Vane, A. F. H. Goetz, and J. B. Wellman, "Airborne imaging spectrometer: a new tool for remote sensing," IEEE Trans. Geosci. Remote Sens. **GE-22**, 546–549 (1983).
6. M. E. Schaepman and S. Dangel, "Solid laboratory calibration of a nonimaging spectroradiometer," Appl. Opt. **39**, 3754–3764 (2000).
7. N. Fox, J. Aiken, J. J. Barnett, X. Briottet, R. Carvell, C. Frohlich, S. B. Groom, O. Hagolle, J. D. Haigh, H. H. Kieffer, J. Lean, D. B. Pollock, T. Quinn, M. C. W. Sandford, M. Schaepman, K. P. Shine, W. K. Schmutz, P. M. Teillet, K. J. Thome, M. M. Verstraete, and E. Zalewski, "Traceable radiometry underpinning terrestrial- and helio-studies (TRUTHS)," Adv. Space Res. **32**, 2253–2261 (2003).
8. P. N. Slater, S. F. Biggar, J. M. Palmer, and K. J. Thome, "Unified approach to absolute radiometric calibration in the solar-reflective range," Remote Sens. Environ. **77**, 293–303 (2001).
9. P. Gege, J. Fries, P. Haschberger, P. Schötz, H. Schwarzer, P. Strobl, B. Suhr, G. Ulbrich, and W. J. Vreeling, "Calibration facility for airborne imaging spectrometers," ISPRS J. Photogramm. Remote Sens. **64**, 387–397 (2009).
10. R. Green, "Spectral calibration requirements for Earth-looking imaging spectrometers in the solar-reflected spectrum," Appl. Opt. **37**, 683–690 (1998).

11. P. Mouroulis, R. Green, and T. Chrien, "Design of pushbroom imaging spectrometer for optimum recovery of spectroscopic and spatial information," Appl. Opt. **39**, 2210–2220 (2000).
12. D. Schläpfer, J. Nieke, and K. I. Itten, "Spatial PSF nonuniformity effects in airborne pushbroom imaging spectrometry data," IEEE Trans. Geosci. Remote Sens. **45**, 458–468 (2007).
13. L. Guanter, K. Segl, B. Sang, L. Alonso, H. Kaufmann, and J. Moreno, "Scene-based spectral calibration assessment of high spectral resolution imaging spectrometers," Opt. Express **17**, 11594–11606 (2009).
14. L. Guanter, V. Estellès, and J. Moreno, "Spectral calibration and atmospheric correction of ultra-fine spectral and spatial resolution remote sensing data. Application to CASI-1500 data," Remote Sens. Environ. **109**, 54–65 (2007).
15. H. Montgomery, N. Che, K. Parker, and J. Bowser, "The algorithm for MODIS wavelength on-orbit calibration using the SRCA," IEEE Trans. Geosci. Remote Sens. **38**, 877–884 (2000).
16. S. Delwart, R. Preusker, L. Bourg, R. Santer, D. Ramon, and J. Fischer, "MERIS in-flight spectral calibration," Int. J. Remote Sens. **28**, 479–496 (2007).
17. P. S. Barry, J. Shepanski, and C. Segal, "Hyperion on-orbit validation of spectral calibration using atmospheric lines and an on-board system," Proc. SPIE **4480**, 231–235 (2002).
18. R. Green and B. Pavri, "AVIRIS inflight calibration experiment measurements, analysis and results in 2000," in *Proceedings of the Tenth JPL Airborne Earth Science Workshop* (Jet Propulsion Laboratory, 2001), pp. 205–219.
19. L. Guanter, R. Richter, and J. Moreno, "Spectral calibration of hyperspectral imagery using atmospheric absorption features," Appl. Opt. **45**, 2360–2370 (2006).
20. R. Green, M. Eastwood, C. Sarture, T. Chrien, M. Aronsson, B. Chippendale, J. Faust, B. Pavri, C. Chovit, M. Solis, M. Olah, and O. Williams, "Imaging spectroscopy and the airborne visible/infrared imaging spectrometer (AVIRIS)," Remote Sens. Environ. **65**, 227–248 (1998).
21. T. Chrien, M. Eastwood, R. Green, C. Sarture, H. Johnson, C. Chovit, and P. Hajek, "airborne visible/infrared imaging spectrometer (AVIRIS) onboard calibration system," in *Summaries of the Fifth Annual JPL Airborne Earth Science Workshop* (Jet Propulsion Laboratory, 1995), pp. 31–32.
22. P. S. S. Thiemann, P. Gege, N. Stahl, W. Mooshuber, and H. van der Piepen, "Das abbildende spektrometer ROSIS," in *Publikationen der Deutschen Gesellschaft für Photogrammetrie und Fernerkundung*, E. Seyfert, ed. (DLR, 2001), pp. 147–153.
23. K. Itten, F. Dell Endice, A. Hueni, M. Kneubuehler, D. Schlaepfer, D. Odermatt, F. Seidel, S. Huber, J. Schopfer, T. Kellenberger, Y. Buehler, P. D'Odorico, J. Nieke, E. Alberti, and K. Meuleman, "APEX—the hyperspectral ESA airborne prism experiment," Sensors **8**, 6235–6259 (2008).
24. K. I. Itten, M. Schaepman, L. De Vos, L. Hermans, H. Schlaepfer, and F. Droz, "APEX—airborne PRISM experiment: a new concept for an airborne imaging spectrometer," in *Proceedings of the Third International Airborne Remote Sensing Conference and Exhibition* (Environmental Research Institute of Michigan, 1997), pp. 181–188.
25. D. Schläpfer and M. Schaepman, "Modelling the noise equivalent radiance requirements of imaging spectrometers based on scientific applications," Appl. Opt. **41**, 5691–5701 (2002).
26. P. Chorier and P. Tribolet, "High performance HgCdTe SWIR detectors for hyperspectral instruments," Proc. SPIE **4540**, 328–341 (2001).
27. P. D'Odorico, E. Alberti, F. Dell'Endice, A. Hüni, and K. Itten, "An algorithm for tracking APEX spectral stability by means of the in-flight characterizarion facility (IFC)," in *Proceedings of the 6th EARSeL Workshop on Imaging Spectroscopy* (EARSeL, 2009), p. 5.
28. P. D'Odorico, E. Alberti, F. Dell'Endice, A. Hüni, and M. Schaepman, "Spectral stability monitoring of an imaging spectrometer by means of onboard sources.," in *Proceedings of IEEE International Geoscience and Remote Sensing Symposium* (IEEE, 2009), I-72–I-75.
29. C. Zhu and L. M. Hanssen, "Comparison and development of absorption peak determination algorithms for wavelength standards," Proc. SPIE **4103**, 62–68 (2000).
30. C. Zhu and L. M. Hanssen, "Absorption-line evaluation methods for wavelength standards," Proc. SPIE **3425**, 111–118 (1998).
31. B. C. Gao, M. Montes, and C. Davis, "Refinement of wavelength calibrations of hyperspectral imaging data using a spectrum-matching technique," Remote Sens. Environ. **90**, 424–433 (2004).
32. R. A. Neville, L. Sun, and K. Staenz, "Spectral calibration of imaging spectrometers by atmospheric absorption feature matching," Can. J. Remote Sens. Suppl. 1 **34**, S29–S42 (2008).
33. R. A. Neville, L. Sun, and K. Staenz, "Detection of spectral line curvature in imaging spectrometer data," Proc. SPIE **5093**, 144–154.

4 PERFORMANCE ASSESSMENT OF ONBOARD AND SCENE-BASED METHODS FOR APEX SPECTRAL CHARACTERIZATION

This chapter has been published as: D'Odorico, P., Guanter, L., Schaepman, M.E. and Schläpfer, D., 2011. Performance assessment of onboard and scene-based methods for Airborne Prism Experiment spectral characterization. Applied Optics, 50(23): 4755-4764.

Performance assessment of onboard and scene-based methods for Airborne Prism Experiment spectral characterization

Petra D'Odorico,[1,*] Luis Guanter,[2] Michael E. Schaepman,[1] and Daniel Schläpfer[3]

[1]Remote Sensing Laboratories, University of Zurich, Winterthurerstrasse 190, CH-8057 Zurich, Switzerland

[2]Atmospheric, Oceanic and Planetary Physics, University of Oxford, Parks Road, OX1 3PU Oxford, UK

[3]ReSe Applications, Langeggweg3, CH-9500 Wil SG, Switzerland

*Corresponding author: petra.dodorico@geo.uzh.ch

Received 4 February 2011; revised 23 May 2011; accepted 17 July 2011;
posted 18 July 2011 (Doc. ID 142221); published 12 August 2011

Accurate spectral calibration of airborne and spaceborne imaging spectrometers is essential for proper preprocessing and scientific exploitation of high spectral resolution measurements of the land and atmosphere. A systematic performance assessment of onboard and scene-based methods for in-flight monitoring of instrument spectral calibration is presented for the first time in this paper. Onboard and ground imaging data were collected at several flight altitudes using the Airborne Prism Experiment (APEX) imaging spectrometer. APEX is equipped with an in-flight characterization (IFC) facility allowing the evaluation of radiometric, spectral, and geometric system properties, both in-flight and on-ground for the full field of view. Atmospheric and onboard filter spectral features present in at-sensor radiances are compared with the same features in reference transmittances convolved to varying instrument spectral configurations. A spectrum-matching algorithm, taking advantage of the high sensitivity of measurements around sharp spectral features toward spectrometer spectral performance, is used to retrieve channel center wavelength and bandwidth parameters. Results showed good agreement between spectral parameters estimated using onboard IFC and ground imaging data. The average difference between estimates obtained using the O_2 and H_2O features and those obtained using the corresponding filter features amounted to about 0.3 nm (0.05 of a spectral pixel). A deviation from the nominal laboratory instrument spectral calibration and an altitude-dependent performance was additionally identified. The relatively good agreement between estimates obtained by the two approaches in similar spectral windows suggests they can be used in a complementary fashion: while the method relying on atmospheric features can be applied without the need for dedicated calibration acquisitions, the IFC allows assessment at user-selectable wavelength positions by custom filters as well as for the system on-ground.

OCIS codes: 280.0280, 110.0110, 300.0300, 120.4640.

1. Introduction

A large variety of imaging spectrometers exists [1], and they are successfully being used to simultaneously retrieve variables from different spheres of the Earth [2]. However, numerous studies evidenced severe inaccuracies in retrieved reflectance and higher level products due to errors in instrument spectral calibration [3–5]. The conversion of at-sensor radiance to physical surface reflectance quantity requires compensating for the presence of the atmosphere and its effects, such as absorption and scattering [6,7]. An erroneous instrument spectral calibration would induce compensation at the wrong wavelengths, causing the appearance of atmospheric residual features in the reflectance spectrum. The subsequent exploitation of the spectral features

0003-6935/11/244755-10$15.00/0

present in the retrieved surface reflectance spectra would also introduce a bias in the further analysis and propagate uncertainties into final products.

Errors in spectral calibration parameters are defined as deviations from the nominal parameter values assigned during previous instrument characterization. Errors may occur as shifts in center wavelengths and/or changes in bandwidth i.e., full width at half-maximum (FWHM) of spectral response functions (SRF) associated with individual detector pixels. For area detectors, a further artifact is caused by a variation in dispersion along the dimension of the entrance slit. This leads to a spectral shift that depends on the pixel location along the cross-dispersion direction of the detector, causing a change in detector smile [8]. Technical limitations of instrument design, mechanical tolerances, vibrations, and changes in instrument temperature and pressure are among the most common causes generating deviations in spectral calibration of pushbroom dispersive airborne and spaceborne systems [4].

Due to the high sensitivity of the measured spectrum to the instrument spectral performance in spectral windows where abrupt radiance changes occur, most of the methods for in-flight spectral characterization of imaging spectrometers are based on the evaluation of sharp absorption features present in given radiance spectra used as a reference [9,10]. Typical strategies for in-flight spectral characterization are broadly divided into two groups. The first compares the position of a spectral feature in the observed spectrum to the position of the same feature in a modeled reference spectrum and calculates model parameters producing the best match [4,10]. The second group builds on the notion that links a smooth reflectance-spectrum appearance with an accurate atmospheric compensation model, which in turn is associated with a valid wavelength calibration [5,9,11]. Hence, it looks for the set of spectral parameters, which, when used as an input in the atmospheric correction, results in the smoothest surface reflectance spectrum. Smoothing techniques work well if instrument spectral deviations are small. For larger band shifts, the operation of smoothing, usually performed by moving average, might fail to remove residual features in the smoothed reference spectrum used as surrogate for the true surface [9,12].

To be able to use feature-matching approaches in the spectral domain, the measured spectrum must have distinguishable features occurring at the spectral resolution limit of the instrument at hand and transferable to a known reference spectrum. When relying solely on image data, the reference spectrum is usually given by the modeled at-sensor radiance [5], transmittance, or irradiance [4] signals containing atmospheric absorption features. When available, onboard spectral calibration sources may provide a valid alternative to image data as well as a useful complement covering spectral regions devoid of atmospheric features; reference signals are then usually diffuser plates' absorption lines or dedicated filter transmittances [13–16].

In this paper, a systematic evaluation and comparison of two independent approaches aimed at instrument in-flight spectral characterization is presented for the first time. The first approach relies on dedicated calibration acquisitions performed with characterization equipment onboard the APEX imaging spectrometer. The second approach uses atmospheric features present in standard ground imaging. The investigation focused on the APEX instrument [17], yet outcomes are considered relevant for other operational and upcoming sensor systems holding onboard characterization equipment, such as the Environmental Mapping and Analysis Program (EnMAP) [18]. Among other existing airborne systems, AVIRIS [16,19] and ROSIS [20] also hold internal characterization sources, both used before and after acquisition of a flight line.

2. Materials and Methods

A. APEX Imaging Spectrometer

APEX is an airborne dispersive pushbroom imaging spectrometer developed by a joint Swiss–Belgian consortium in the frame of the European Space Agency's (ESA) PRODEX (PROgramme de Développement d'EXpériences scientifiques) programme. It is designed to validate and calibrate spaceborne missions and contribute to advanced product development. Table 1 presents an overview of APEX performances.

Table 1. APEX Instrument Performance

Spectral Performance		
	VNIR	**SWIR**
Spectral range	375–983 nm	991–2500 nm
Spectral bands	334 (unbinned), 114 (def. binned)	198
Spectral sampling interval	0.45–7.5 nm	5–10 nm
Spectral resolution (FWHM)	0.7–9.7 nm	6.2–12 nm
Spatial Performance		
Spatial pixels (across track)	1000	
FOV	28°	
IFOV	0.028° (~0.5 mrad)	
Spatial sampling interval (across track)	1.75 m at 3500 m above ground level	
Detector Characteristics		
	VNIR	**SWIR**
Type	CCD	CMOS
Dynamic range	14 bit	13 bit
Pixel size	22.5 μm by 22.5 μm	30 μm by 30 μm
Smile	average $<$ 0.35 pixel	
Keystone (frown)	average $<$ 0.35 pixel	
Coregistration	average $<$ 0.55 pixel	
Other Information		
Data capacity	500 GB on solid state disks	
Data transfer	Spectral frames: 30 MB/s	
Data rate for default configuration	0.4 GB/km (1250 km max.)	

The instrument design (Fig. 1) is a dispersive pushbroom spectrometer acquiring the spectral and across-track domain on area detectors. Imaging is performed through forward motion of the aircraft. The field of view (FOV) is projected by the ground imager onto the spectrometer slit using a path folding mirror. To minimize the polarization sensitivity, a scrambler can be inserted to randomize the polarization of the incoming light at the expense of spatial resolution. A collimator lens group directs the light on the first prism. A dichroic coating separates the short-wave infrared (SWIR) and visible and near-infrared (VNIR) channels. The VNIR channel is then dispersed further using a second prism. The VNIR detector is a commercial charged coupled device (CCD) ranging from 380–1000 nm, as of instrument design. For the SWIR channel, a specific complementary metal oxide semiconductor (CMOS) mercury cadmium telluride detector array was developed ranging from 940–2500 nm. The two spectrometer channels are aligned to minimize the geometric coregistration error.

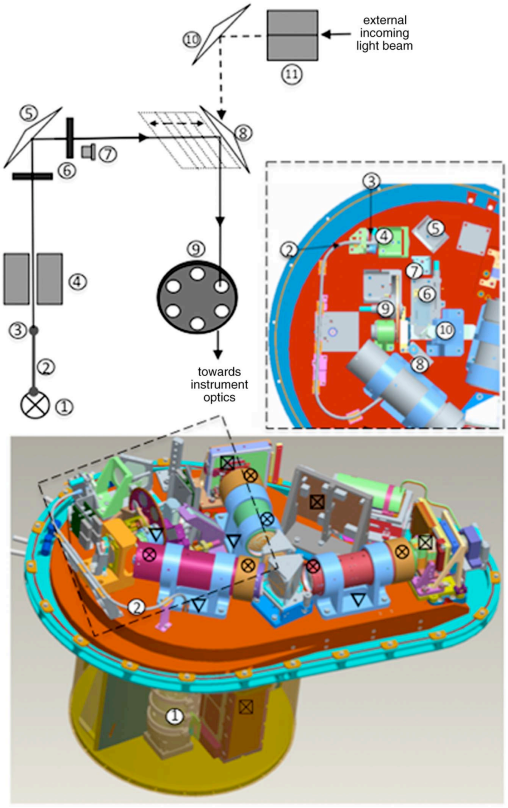

Fig. 1. (Color online) IFC facility onboard APEX: (1) QTH lamp, (2) optical fiber, (3) fiber output (4) calibration shutter, (5) fixed folding mirror, (6) diffusers, (7) feedback loop sensor, (8) sliding folding mirror, (9) filter wheel, (10) fixed folding mirror, (11) global shutter, □ temperature sensor, ∇ temperature sensor on optical base plate (averaged),⊗ differential temperature sensors.

APEX holds an IFC facility (Fig. 1) allowing the characterization of radiometric, spectral, and geometric system properties, both in-flight and on ground covering the full FOV. During in-flight characterization operation, the main instrument shutter is closed to avoid any light penetrating from the outside. A stabilized quartz tungsten halogen (QTH) 75 W lamp in a dedicated housing is attached to an optical fiber. The optical fiber guides the light from the lamp through the calibration shutter, which is usually closed to prevent the IFC light from entering the spectrometer during image acquisition. Diffusers are placed before and after a fixed folding mirror to improve the uniformity of the illumination. A sensor is used to monitor the light level and to control the lamp power accordingly in a closed control loop. A sliding folding mirror is moved into the optical path to reflect the light generated by the IFC toward a filter wheel mounted in front of the ground imager. The wheel holds four spectral filters to be used for instrument spectral stability monitoring, these are three bandpass filters (Spectrogon) with transmission features at 700, 1000, and 2218 nm; and a standard reference material (SRM) filter from the National Institute for Standards and Technology (NIST) holding many distinct absorption features throughout the VNIR and SWIR spectral range. A fifth filter, an NG4 attenuation filter, is used to avoid saturation in the VNIR channel at maximum radiance levels (image acquisition over snow). The sixth filter wheel position is left empty for standard data acquisition. Deterioration of the spectral filters is not expected as they are located inside the enclosed and temperature stabilized optical subunit.

For each filter position, the IFC light is dispersed onto the detectors in exactly the same fashion as ground observations. With this design, the most relevant parameters of APEX's optical performance can be characterized in-flight. IFC measurements will be carried out during each laboratory and flight campaign.

Coregistered onboard with the image and IFC data the system measures environmental parameters, reflecting the state of the instrument during a particular acquisition. For the collection of these housekeeping (HK) data, a number of temperature sensors are placed within the optical subunit (e.g., on both detectors, on the optical base plate) and the baffle compartment (on the power supply unit), while pressure sensors are located inside as well as outside the optical subunit compartment (Fig. 1). In 2009, the recording of HK data coregistered with IFC measurements during targeted on-ground and in-flight experiments allowed identification of a temperature and pressure driven trend on instrument spectral performance. The highest correlation was found with the temperature in the baffle and with the differential pressure [17]. Following these findings an instrument revision took place, aimed at the stabilization of the system for a range of temperature and pressure conditions to be encountered during operation. The revision included the manufacturing of a pressure regulation mechanism for the automatic release or fill-in of nitrogen according to the change in-flight altitude and an optimization of the system heating/cooling regulation.

B. APEX Data

APEX data acquired during a flight campaign in June 2010 were used in this study. APEX has an electronic binning pattern implemented, allowing variable spectral sampling intervals in the 375–616 nm VNIR spectral region for which lower signal-to-noise ratios (SNRs) are expected. In this study, data acquired using the default VNIR binning pattern were used; however, the data analysis focused on spectral regions falling outside of the binned region. A total of 114 and of 198 spectral bands were acquired in this configuration for the VNIR and SWIR, respectively.

Four different flight heights, corresponding to 2500, 3500, 4100, and 6500 m above sea level, were selected based on previous experience suggesting differential pressure and system temperatures having an impact on instrument performance [17]. IFC data were acquired before and after each flight line. The timely proximity of ground imaging and IFC data-takes secured acquisition under comparable environmental conditions verified by means of the coregistered HK data.

Flight lines were flown on consecutive days and slightly differing acquisition times and locations within Switzerland. Simultaneously, vicarious measurements were performed on ground. Before data acquisition, a full laboratory characterization was performed at the Calibration Home Base located at DLR Oberpfaffenhofen in Germany. Laboratory calibration resulted in nominal sensor spectral parameters, i.e., center wavelength and FWHM, measured under controlled conditions. These provided the initial calibration parameters toward which estimates by both in-flight approaches were compared. Data preprocessing included radiometric calibration, spatial resampling, detector coregistration, bad pixel replacement, and a smear correction. For the spectral calibration task, along-track averaging of image data is performed to reduce spatial heterogeneity effects.

C. Estimation of Spectral Parameters

In this study, a methodology was devised aimed at the estimation of instrument spectral parameters (center wavelength and FWHM) by monitoring the position and shape of spectral features, which by nature occur always at the same wavelengths in an APEX spectrum. Three atmospheric absorption features were chosen for the approach relying on ground imaging, these are the O_2-A feature at 760 nm, the H_2O feature at 1135 nm, and the CO_2 feature at 2010 nm. For the IFC-based approach, absorption features were chosen overlapping with atmospheric features as well as in spectral regions devoid of atmospheric features. Figure 2 shows the distribution of spectral features available from the atmosphere and from IFC filters

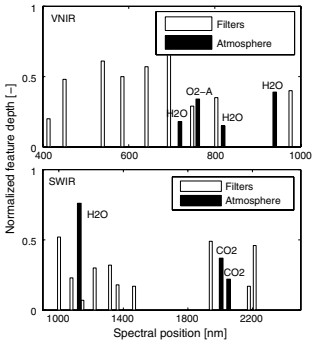

Fig. 2. Position of spectral features of the IFC filters (white) and the atmosphere (black), detectable with APEX spectral resolution. Insufficient signal-to-noise ratio might limit the detectability of some of these features.

mounted on APEX, whose detectability is feasible at APEX's spectral resolution but might still be limited by insufficient SNR (compare [8] for a list of available natural features). The suitability of a feature for the purpose of spectral parameter estimation cannot be determined *a priori*; in this study, features with greater depth were generally preferred. The O_2-A feature is known to hold the greatest potential for spectral characterization because O_2 is very well mixed in the atmosphere and the O_2-A feature is narrow and deep. Absorption features used for the methods' comparison are depicted in Fig. 3.

In the onboard approach, the reference spectrum is given by the transmittance of the SRM filter included in the IFC. The filter characterization is provided by

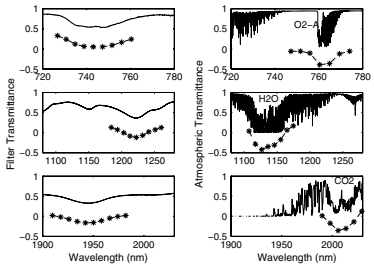

Fig. 3. Absorption features used for VNIR (top) and SWIR (middle, bottom) detectors for instrument spectral parameter estimation. Left: IFC NIST filter features, and right: atmospheric features. The continuous lines show the transmittance spectra while the discontinuous lines represent the same spectra convolved with APEX bands (offset for clarity).

NIST in measurement intervals of 0.1 nm from 350 to 850 nm and 0.25 nm from 850 to 2500 nm.

When using the scene-based approach, a transmittance spectrum is preferred over a radiance spectrum based on the assumption that the shape of atmospheric absorption features in radiance data remains essentially unvaried with respect to the corresponding transmittance spectra. Different studies have favored the former [5,21], others preferred the latter [4], although none of these sources provided clear evidence for the superiority of using one over the other reference. The choice between a generic reference transmittance spectrum and scene-specific ones was made based on a sensitivity analysis investigating the impact of changing atmospheric characteristics on instrument spectral parameters retrieval. Simulations were performed for a simplified scenario, e.g., no instrument noise was assumed and spectral parameters were varied one at a time. Results showed how the influence of varying atmospheric parameterization is merely confined to FWHM estimation and even there it exclusively affected results based on the H_2O and CO_2 features. Large deviations in assumed water vapor content and the derived nonlinearity of the transmittance as a function of it, made it particularly difficult to derive accurate FWHM change estimates using the water vapor feature. The FWHM retrieval based on the latter two features was excluded regardless of these findings due to the insufficient instrument spectral sampling (at 1135 nm: SSI = 9.6 nm; at 2004 nm: SSI = 7.8 nm). A generic transmittance spectrum was found to provide no significant errors for the further analysis and was, therefore, preferred in this study to reduce processing time and efforts associated with the spectral parameter estimation.

The calculation of atmospheric parameters is based on MODTRAN 5 [22], which uses the HITRAN2008 line database [23]. Total upward transmittance ($T^{\uparrow}$) was calculated as the sum of the spectral transmittances for diffuse ($t^{\uparrow}_{\mathrm{dif}}$) and direct ($t^{\uparrow}_{\mathrm{dir}}$) upwelling radiation from the surface to the sensor ($T^{\uparrow} = t^{\uparrow}_{\mathrm{dif}} + t^{\uparrow}_{\mathrm{dir}}$). The direct transmittance is given as a standard MODTRAN output, while the diffuse transmittance can be obtained by a 2-run MODTRAN process as described by Guanter *et al.* [24]. The spectral resolution of the MODTRAN output was set to 8.2 cm^{-1}.

Each reference transmittance spectrum point $T(\lambda_j)$ was convolved with the instrument's calibrated response for those spectral regions encompassing the predefined absorption features (see Fig. 3). Predefined absorption features fall outside the spectral region subject to APEX spectral binning; thus, no pixel binning function needs to be implemented in the convolution. The following equation was used:

$$S_i(\Delta\lambda, \Delta\mathrm{FWHM}) = \sum_{j=1}^{j=N} T(\lambda_j) * \mathrm{SRF}_i(\Delta\lambda, \Delta\mathrm{FWHM}), \quad (1)$$

where $SRF_i(\Delta\lambda, \Delta FWHM)$ stands for an SRF approximated by a Gaussian function to which a spectral shift ($\Delta\lambda$) and a bandwidth change ($\Delta FWHM$) have been applied and where N is the number of spectral points at which the input reference spectrum was originally sampled.

The convolved transmittances are iteratively fed into an optimization loop, which searches for the band shift and width change that results in the smallest difference between the references and the measured APEX spectra. The optimization is performed based on the Nelder–Mead simplex algorithm as described in Lagarias *et al.* [25]. In order to achieve the best sensitivity, the best match is evaluated using correlation analysis in the region of the absorption features. Features in both the reference and the measured spectrum are continuum normalized assuming a linear continuum. Changes to the spectral parameters fed into the convolution are defined with respect to the initial parameter grids coming from the laboratory characterization. The search uses zero as a starting deviation value for both parameters without upper constraining thresholds for the magnitude of deviations. In few cases, the process ended before the function converged into its optimal value and corresponding estimates were thus removed from the final output.

3. Results and Discussion

A. Spectral Parameters Estimation

Results of the APEX spectral parameter estimation for selected acquisitions are presented in this section. For each detector, we first cross-validated estimates obtained for the same wavelength region using IFC filter features and corresponding atmospheric features. Next, the linearity of retrieved shifts over the detector's spectral dimension was investigated using IFC filter features at different wavelength positions. This second set of results is meant to assess whether the spectral shift derived by one single wavelength position can be used to update the entire spectral range. Estimates obtained with the IFC for the instrument on-ground, before and after the flight, are also presented.

Figure 4 shows the nominal versus the updated smile profiles obtained over four flight altitudes for the VNIR band centered at 760 nm. Estimations based on the O_2-A and corresponding NIST filter feature yield comparable results, differing in average of 0.3 nm, corresponding to 0.05 of a spectral pixel in this particular wavelength region. A deviation from the nominal instrument spectral calibration and an altitude-dependent performance are evident, confirming the unsolved pressure/temperature dependency of the system. For prism-based instruments as APEX, performance changes with altitude are often connected to pressure-dependant dispersion changes of the prism. Results were remarkably reproducible when the instrument was flown at the same altitude on different dates and sites (figures

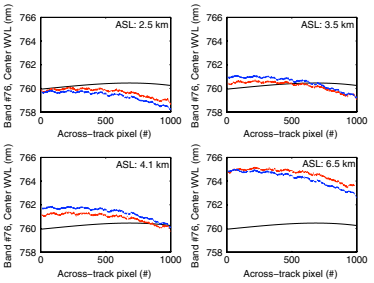

Fig. 4. (Color online) Smile characterization at 760 nm for four flight altitudes. The continuous black line represents the nominal smile as measured in the lab, while the dotted lines represent the estimates based on the O_2-A absorption feature (blue) and on the NIST filter absorption feature (red).

not included here). In the future, the development of a correction model in function of flight height is thus something worth investigating. System performance estimated at the highest flight altitude of 6.5 km shows the greatest deviation from nominal value. A shift of 4.1 nm (0.70 of a spectral pixel) and 4.4 nm (0.75 of a spectral pixel) for the central detector pixel position was estimated by the onboard-based and scene-based approaches, respectively. An increase in smile is further identified by both approaches. Smile, computed as the greatest difference found between the center wavelength values of two detector pixels, amounts to 1.5 nm (0.26 of a spectral pixel) and 2 nm (0.34 of a spectral pixel) for onboard-based and scene-based estimates, respectively, compared to the 0.6 nm (0.1 of a spectral pixel) nominal value.

Figure 5 shows a good overlap between estimates based on the three IFC filter features centered at 644 nm, 743 nm, and 803 nm, respectively. For the VNIR detector, the shift estimates in one wavelength region can thus be considered representative for the entire spectral range. Further, measurements taken with the IFC on-ground before and after the flights indicate a good correspondence with the instrument laboratory characterization with across-track spectral shifts close to zero.

For the SWIR detector, two wavelength regions were identified for which NIST-filter and atmospheric features are partly overlapping. Agreement between the estimates obtained with the two approaches is observable in the first of the two examined regions, encompassing the H_2O feature at 1130 nm (Fig. 6). Deviation from nominal performances is greater for the lower of the flown altitude, reaching values of −13 nm, being the equivalent of 1 spectral pixel in this particular wavelength region featuring FWHM of about 12 nm. Values refer to the position of the central detector pixel. A shift amounting to −2 nm (0.17 of a spectral pixel) is estimated

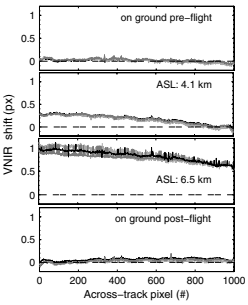

Fig. 5. Estimated spectral shift in the across-track direction expressed as fraction of spectral pixel. Retrieval based on IFC data acquired on ground before (top) and after (bottom) the flight, as well as for two different flight heights. Three VNIR wavelength regions are considered: 630–658 nm (black), 726–760 nm (light gray), 788–819 nm (dark gray).

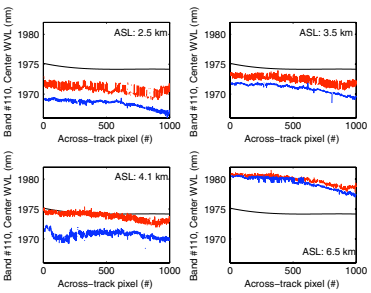

Fig. 7. (Color online) Smile characterization at 1974 nm for four flight altitudes. The continuous black line represents the nominal smile as measured in the lab, while the dotted lines represent the estimates based on the CO_2 absorption feature centered at 2004 nm (blue) and a NIST filter absorption feature centered at 1934 nm (red).

when the system is flown at 6.5 km. The smile for the investigated spectral region amounts to 2 nm (0.17 of a spectral pixel) and 3 nm (0.25 of a spectral pixel) for onboard-based and scene-based estimates, respectively, compared to the 1 nm (0.08 of a spectral pixel) nominal value found in laboratory conditions. In the second SWIR region, estimations based on the CO_2 feature at 2001 nm and analogous NIST-filter feature, confirmed the general direction of the shift evidenced in the former SWIR region, with shifts going from shorter to higher wavelengths with increasing flight altitude (Fig. 7), but significantly differed in magnitude. Smile profiles are characterized by a noisy appearance in the across-track direction particularly for the IFC-based estimates. The two approaches yield estimates diverging in average by 2 nm (0.2 of a spectral pixel), with the exception of the flight performed at the highest altitude for which a nearly perfect overlap of smile profiles is provided. The low at-sensor signal within this absorption feature and the overlap between water vapor and CO_2 absorption (double feature) may have led to the less stable parameter retrieval.

Estimates for three IFC SWIR features confirmed and added to these findings. Results in Fig. 8 show that the two IFC NIST features at 1381 nm and 1934 nm provide concurring shift estimates, while those based on the feature at 1222 nm systematically

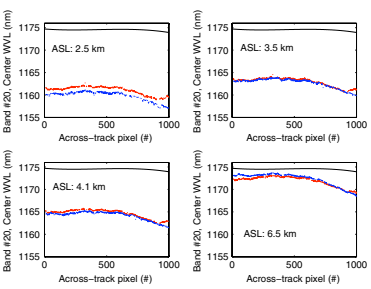

Fig. 6. (Color online) Smile characterization at 1175 nm for four flight altitudes. The continuous black line represents the nominal smile as measured in the lab, while the dotted lines represent the estimates based on the water vapor absorption feature centered at 1130 nm (blue) and a NIST filter absorption feature centered at 1222 nm (red).

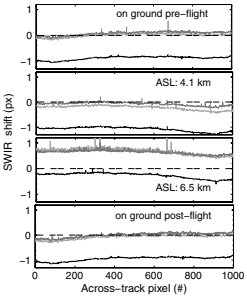

Fig. 8. Estimated spectral shift in the across-track direction expressed as fraction of spectral pixel. Retrieval based on IFC data acquired on ground before (top) and after (bottom) the flight, as well as for two different flight heights. Three SWIR wavelength regions are considered: 1193–1269 nm (black), 1339–1423 nm (light gray), and 1909–1974 nm (dark gray).

diverge by 1 spectral pixel. This holds true as well when on-ground IFC data are considered, thus ruling out the possibility of nonlinear spectral shifts affecting the SWIR detector during flight. Targeted measurements are planned for the next laboratory characterization to help identify the causes of these observations. A faulty instrument laboratory characterization or inaccuracies in the NIST SRM filter characterization in the 1193–1269 nm SWIR region are only two possible hypotheses.

The estimation of the FWHM change in addition to the center wavelength shift in a single inversion step is only recommended if an adequate number of spectral bands, sampling the absorption feature, was provided. A spectral sampling interval (SSI) of 5 nm has been identified as the threshold value above which the number of bands might result insufficient for the inversion of two parameters. For the same reason the impact of not updating the nominal FWHM would not be significant for this type of data [26]. These considerations automatically lead to the exclusion of the FWHM estimation for the SWIR region characterized by SSI ranging between 5–10 nm. For the investigated VNIR region around 760 nm the SSI varies between 3.8 and 4.6 nm and is thus bordering useful limit conditions. Figure 9 presents the nominal FWHM for the VNIR band centered at 760 nm compared to the updates provided by means of the onboard-based and scene-based approaches. It is readily observable that the estimates obtained by the two approaches disagree between each other as well as with the nominal reference. The O_2-A feature provides a less noisy estimate in the across-track direction, which, however, deviates immediately from the nominal FWHM. On the other hand, the IFC filter feature, despite the noise, follows the trend of the ground calibration measurements at low altitude and deviates only for higher altitude. Based on these estimates and those obtained by other IFC filter features (results not shown here) it is not possible to draw any definitive conclusion on changes affecting the FWHM parameter. The insufficient instrument spectral resolution was hypothesized to be among the reasons why an accurate FWHM change retrieval could not be devised.

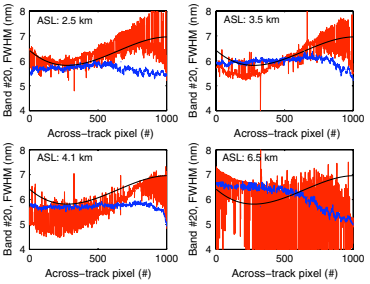

Fig. 9. (Color online) FWHM characterization at 760 nm for four flight altitudes. The continuous black line represents the nominal FWHM as measured in the lab, while the discontinuous lines represent the estimates based on the O_2-A absorption feature (blue) and on the corresponding NIST filter absorption feature (red).

B. APEX Spectral Calibration Updates Verification

The validity of APEX spectral calibration update was verified using a simple atmospheric correction equation. The MODTRAN 5 code was used to compute the different atmospheric parameters required to convert a radiance signal into a reflectance signal [22]. Scene-specific parameterization and a 2-MODTRAN run (see [24]) were needed for this purpose. Reflectances obtained assuming the nominal and the updated spectral calibration are compared. The IFC filter absorption feature around 743 nm was used for updating the VNIR spectral calibration, after previous analysis had shown that the spectral characterization derived from one single spectral position is representative of the entire spectral range covered by the detector. This could not be demonstrated for the SWIR detector, for which a disagreement between estimates was found when using features at different wavelength positions. As a consequence the update of spectral calibration parameters is performed separately for each SWIR spectral region corresponding to an IFC filter feature. Results for the scene acquired at a flight altitude of 6.5 km are shown in Fig. 10 for VNIR and SWIR regions, respectively. Different targets (vegetation, gravel) were selected from the scene, each corresponding to a different across-track position on the detector. The overall perception is that spectra obtained by assuming the updated instrument parameters during atmospheric correction are much smoother than those

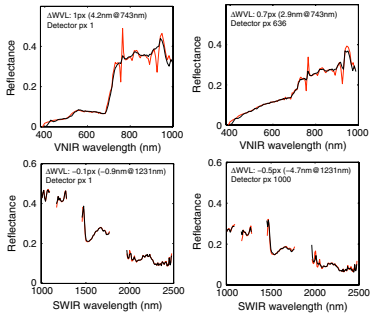

Fig. 10. (Color online) Surface reflectance spectra obtained based on nominal (red) and updated (black) spectral calibration parameters. For the VNIR the update is based on the IFC feature located around 743 nm. For the SWIR the update was performed for each spectral region separately based on the corresponding IFC feature.

derived based on the laboratory spectral calibration. For the VNIR region, the absence of spikes around the O_2-A band, when the updated instrument parameters are assumed, further validates the correctness of the new spectral calibration. Remaining spikes around 940 nm could be explained by water vapor residuals and uncertainties in the radiometric calibration. In the SWIR region, while major error spikes caused by the spectral miscalibration were eliminated, few residual spikes and dips are still present most likely due to an inaccurate water vapor column estimate. However, findings for the SWIR remain to be proven by further measurements and analysis as discussed in Section 3.A.

4. Conclusions and Outlook

In this paper, a systematic analysis of both atmospheric-based and onboard approaches to spectral characterization is presented for the first time. Both approaches rely on the same feature-matching technique and are aimed at improving APEX in-flight spectral calibration. Deviations of instrument spectral parameters are estimated in relation to an initial calibration state defined during laboratory characterization. The hypothesis is that spectral calibration during flight will deviate from the laboratory calibration and can be updated using the employed methods. The calibration process remains fully independent of an atmospheric correction, which in turn can be used as further validation.

Estimates based on onboard filter features showed good agreement with estimates based on O_2 and H_2O atmospheric absorption features, differing in average of about 0.3 nm (0.05 of a spectral pixel) at the central detector pixel position. Differences might be explained by suboptimal features' shape, method uncertainties, and different sampling frequencies of the reference spectra. Within the second investigated SWIR region, efforts resulted in poorer correspondence between the two methods. Estimates based on the CO_2 feature and its corresponding onboard feature showed disagreement of up to 2 nm (0.2 of a spectral pixel) in this region. Cross sensitivities between the solar function and the absorption of CO_2 and H_2O in the atmospheric model and the laboratory calibration uncertainties in this region can explain the observed disagreement. In addition, results showed an altitude-dependent performance deviation for both detectors. Pressure-dependent dispersion changes are known effects in prism-based instruments and future work will include improved pressure and temperature measurements with sensors placed on the dispersing elements.

Combining onboard and scene data for the in-flight monitoring of spectral calibration holds a number of advantages. Cross-validation of calibration efforts is possible, where sufficient features in the same spectral region exist. Further, spectral filters complementing the number and distribution of atmospheric features allow the monitoring of the full wavelength range. The relatively good agreement between estimates obtained by the two approaches in similar spectral windows suggests they can be used in a complementary fashion: while the method relying on atmospheric features can be applied without the need for dedicated calibration acquisitions, the IFC allows assessment at user-selectable wavelength positions by custom filters as well as for the system on-ground. The latter is also the reason why at comparable performances by the two methods, the IFC should be preferred over more conventional approaches relying on ground imaging and related atmospheric features. In the future, with the manufacturing of materials providing even sharper absorption features, onboard spectral characterization sources are expected to gain even more importance over atmospheric-based approaches, particularly in the SWIR region.

Because of the physical nature of the approach, findings of this study are transferable to other instruments as long as boundary conditions are met (e.g., instrument spectral resolution not exceeding atmospheric line database resolution and availability of onboard sources).

This work was carried out in the framework of the APEX project funded by a European Space Agency (ESA) PRODEX (PROgramme de Développement d'EXpériences scientifiques) contract [15449/01/NL/SFe(IC)]. P. D'Odorico acknowledges the support of a Marie Curie Fellowship awarded in the frame of the Sixth Framework Programme through the Hyper-I-Net network. A special thanks goes to A. Hüni for data collection and technical support and to A. Gonsamo for beneficial discussions. The authors also thank two anonymous reviewers for their valuable comments that contributed to the improvement of this work.

References

1. M. E. Schaepman, "Imaging spectrometers," in *The SAGE Handbook of Remote Sensing*, T. A. Warner, M. D. Nellis, and G. Foody (eds.) (SAGE, 2009), pp. 166–178.
2. M. E. Schaepman, S. L. Ustin, A. J. Plaza, T. H. Painter, J. Verrelst, and S. Liang, "Earth system science related imaging spectroscopy—An assessment," Remote Sens. Environ. **113**, S123–S137 (2009).
3. R. Green, "Spectral calibration requirements for Earth-looking imaging spectrometers in the solar-reflected spectrum," Appl. Opt. **37**, 683–690 (1998).
4. B. C. Gao, M. Montes, and C. Davis, "Refinement of wavelength calibrations of hyperspectral imaging data using a spectrum-matching technique," Remote Sens. Environ. **90**, 424–433 (2004).
5. R. A. Neville, L. Sun, and K. Staenz, "Spectral calibration of imaging spectrometers by atmospheric absorption feature matching," Can. J. Remote Sens. **34**, 29–42 (2008).
6. B.-C. Gao, M. J. Montes, C. O. Davis, and A. F. H. Goetz, "Atmospheric correction algorithms for hyperspectral remote sensing data of land and ocean," Remote Sens. Environ. **113**, S17–S24 (2009).
7. F. C. Seidel, A. A. Kokhanovsky, and M. E. Schaepman, "Fast and simple model for atmospheric radiative transfer," Atmos. Meas. Tech. **3**, 1129–1141 (2010).
8. R. Richter, D. Schläpfer, and A. Müller, "Operational atmospheric correction for imaging spectrometers accounting for

the smile effect," IEEE Trans. Geosci. Remote Sens. **49**, 1772–1780 (2011).
9. L. Guanter, R. Richter, and J. Moreno, "Spectral calibration of hyperspectral imagery using atmospheric absorption features," Appl. Opt. **45**, 2360–2370 (2006).
10. J. Brazile, R. A. Neville, K. Staenz, D. Schläpfer, L. Sun, and K. Itten, "Towards scene-based retrieval of spectral response functions for hyperspectral imagers using Frauenhofer features," Can. J. Remote Sens. **34**, S43–S58 (2008).
11. Z. Qu, B. C. Kindel, and A. F. H. Goetz, "The high accuracy atmospheric correction for hyperspectral data (HATCH) model," IEEE Trans. Geosci. Remote Sens. **41**, 1223–1231 (2003).
12. A. Rodger, "SODA: A new method of in-scene atmospheric water vapor estimation and post-flight spectral recalibration for hyperspectral sensors: Application to the HyMap sensor at two locations," Remote Sens. Environ. **115**, 536–547 (2011).
13. S. Delwart, R. Preusker, L. Bourg, R. Santer, D. Ramon, and J. Fischer, "MERIS in-flight spectral calibration," Int. J. Remote Sens. **28**, 479–496 (2007).
14. H. Montgomery, N. Che, K. Parker, and J. Bowser, "The algorithm for MODIS wavelength on-orbit calibration using the SRCA," IEEE Trans. Geosci. Remote Sens. **38**, 877–884 (2000).
15. P. S. Barry, J. Shepanski, and C. Segal, "Hyperion on-orbit validation of spectral calibration using atmospheric lines and an on-board system," Proc. SPIE **4480**, 231–235 (2002).
16. T. Chrien, M. Eastwood, R. Green, C. Sarture, H. Johnson, C. Chovit, and P. Hajek, "Airborne visible/infrared imaging spectrometer (AVIRIS) onboard calibration system," in *Proceeding of the Fifth Annual JPL Airborne Earth Science Workshop* (Jet Prop. Lab., 1995), pp. 31–32.
17. P. D'Odorico, E. Alberti, and M. Schaepman, "In-flight spectral performance monitoring of the Airborne Prism Experiment," Appl. Opt. **49**, 3082–3091 (2010).
18. B. Sang, J. Schubert, S. Kaiser, V. Mogulsky, C. Neumann, K. P. Forster, S. Hofer, T. Stuffler, H. Kaufmann, A. Muller, T. Eversberg, and C. Chlebek, "The EnMAP hyperspectral imaging spectrometer: instrument concept, calibration, and technologies," in *Imaging Spectrometry XIII* (SPIE, 2008), 708605–708615.
19. R. Green, M. Eastwood, C. Sarture, T. Chrien, M. Aronsson, B. Chippendale, J. Faust, B. Pavri, C. Chovit, M. Solis, M. Olah, and O. Williams, "Imaging Spectroscopy and the Airborne Visible/Infrared Imaging Spectrometer (AVIRIS)," Remote Sens. Environ. **65**, 227–248 (1998).
20. S. Thiemann, P. Strobl, P. Gege, N. Stahl, W. Mooshuber, and H. van der Piepen, "Das abbildende spektrometer ROSIS," in *Publikationen der Deutschen Gesellschaft für Photogrammetrie und Fernerkundung*, E. Seyfert (ed.) (DLR, 2001), pp. 147–153.
21. R. O. Green, "Determination of the in-flight spectral calibration of AVIRIS using atmospheric absorption features," in *Proceedings of the Fifth Annual JPL Airborne Earth Science Workshop*, Vol. 1, R. O. Green, ed. (Jet Prop. Lab., 1995), pp. 71–74.
22. A. Berk, G. P. Anderson, P. K. Acharya, L. S. Bernstein, L. Muratov, J. Lee, M. Fox, S. M. Adler-Golden, J. H. Chetwynd, M. L. Hoke, R. B. Lockwood, J. A. Gardner, T. W. Cooley, C. C. Borel, and P. E. Lewis, "MODTRAN 5, a reformulated atmospheric band model with auxiliary species and practical multiple scattering options: Update," Proc. SPIE **5806**, 662–667 (2005).
23. L. S. Rothman, I. E. Gordon, and A. Barbe, "The HITRAN 2008 molecular spectroscopic database," J. Quant. Spectrosc. Radiat. Transfer **110**, 533–572 (2009).
24. L. Guanter, R. Richter, and H. Kaufmann, "On the application of the MODTRAN 4 atmospheric radiative transfer code to optical remote sensing," Int. J. Remote Sens. **30**, 1407–1424 (2009).
25. J. C. Lagarias, J. A. Reeds, M. H. Wright, and P. E. Wright, "Convergence properties of the Nelder–Mead simplex method in low dimensions," SIAM J. Optim. **9**, 112–147 (1998).
26. L. Guanter, K. Segl, B. Sang, L. Alonso, H. Kaufmann, and J. Moreno, "Scene-based spectral calibration assessment of high spectral resolution imaging spectrometers," Opt. Express **17**, 11594–11606 (2009).

5 EXPERIMENTAL EVALUATION OF SENTINEL-2 SPECTRAL RESPONSE FUNCTION FOR NDVI TIME-SERIES CONTINUITY

This chapter has been submitted as: D'Odorico, P., Gonsamo, A., Damm, A. and Schaepman, M.E., 2011. Experimental evaluation of Sentinel-2 spectral response function for NDVI time-series continuity. IEEE Transactions on Geoscience and Remote Sensing, submitted.

Experimental Evaluation of Sentinel-2 Spectral Response Functions for NDVI Time-Series Continuity

Petra D'Odorico, Alemu Gonsamo, Alexander Damm and Michael E. Schaepman

***Abstract*—Remote sensing of long-term vegetation monitoring relies on the analysis of multi-sensor and multi-temporal time-series measurements. Cross-sensor calibration is therefore important to prevent artifacts in the temporal signal due to inherent differences in sensors configurations. Variations in Spectral Response Functions (SRFs) are among the major causes of differences in multi-sensor reflectances and products. In this paper, we report on the SRF comparability of the upcoming Sentinel-2 Multispectral Instrument (MSI) sensor with a number of operational sensors (NOAA/AVHRR9, Landsat 7 ETM+, SPOT VEGETATION1, MODIS and MERIS) relevant for vegetation monitoring. SRF cross-sensor calibration methods for the conversion of red and NIR reflectances and Normalized Difference Vegetation Index (NDVI) values of the operational sensors in reference to Sentinel-2 MSI sensor were evaluated. Calibration datasets obtained using the soil-leaf-canopy (SLC) radiative transfer model; a state-of-the-art airborne imaging spectrometer (Airborne Prism EXperiment (APEX)); and univariate and multivariate regression models were considered for SRF cross-sensor calibration. For AVHRR9 and VGT1, reflectances in the red spectral region differed more than 30% from Sentinel-2 reflectances. These differences translated in NDVI deviations of up to 10%. The developed SRF cross-sensor calibration method reduced the differences by factors up to 6, 3, and 7 for red, NIR and NDVI values, respectively. All but AVHRR9 have been found to be cross-calibrated to within 5% differences for reflectances and NDVI values. The present work is considered as part of a broader harmonization effort aimed at preparing for the integration of Sentinel-2 MSI data with existing historical data records and product time-series.**

***Index Terms*— APEX, Cross-calibration, NDVI continuity, Sentinel-2, Spectral response function, vegetation monitoring.**

I. Introduction

THE integration of data from different satellite sensors is necessary in long-term studies of phenomena with time scales exceeding the life span of space missions, e.g., analysis in the context of climate change [1] or dynamic vegetation processes [2]. Multi-sensor data are also important in cross-sensor reflectance calibration exercises (i.e., vicarious calibration) for satellite sensors lacking onboard calibration facilities in the solar spectrum [3]. However, the use of multi-sensor data poses a number of conceptual and technical challenges. The platform and sensor combinations differ in their orbital, spatial, and spectral configurations. In consequence, measured physical values and radiometric attributes of the imagery are affected [4] causing surface-independent deviations among solar reflective data measured by different satellite sensors [5].

In this study, we focus on the instruments' spectral characteristics, in particular the Spectral Response Functions (SRF), contributing to multi-sensor data divergence. SRFs determine the position and width of a spectral band and have been identified as one of the most important sources of uncertainty for continuity and usability of multi-sensor datasets [5, 6]. Differences introduced by varying SRFs on multi-sensor spectral data and remote sensing products were investigated by several studies. The majority of these have done so in the context of vegetation monitoring based on Normalized Difference Vegetation Index (NDVI) time-series [4, 5, 7-15], while others focused on SRF induced variations of spectral albedo [6, 16, 17]. The frequent exploitation of NDVI [18] compared to numerous other vegetation indices (VI) that have been developed to monitor the state of vegetation from spaceborne instruments [19] affirms its importance as the most widely employment VI for global monitoring of vegetation. The Advanced Very High Resolution Radiometer (AVHRR) family of instruments provides the longest running series of NDVI products, dating back to the late seventies. Trishchenko et al. [8] found that even among same-type instruments, the effect of differing SRFs on Top of Canopy (TOC) and Top of Atmosphere (TOA) reflectances and NDVI is sufficiently large to require correction. Differences of the AVHRR/NOAA-9 instrument relative to other AVHRR sensors were found reaching 10-15% for the red and 2-3% for the NIR reflectances. Accordingly, NDVI values of vegetated surfaces were found varying across instruments up to 4-6%. Significant deviations were also identified when AVHRR-based NDVI data series were extended using other sensors, e.g., the Satellite Pour l'Observation de la Terre (SPOT) VEGETATION (VGT) [4, 9], the Moderate Resolution Imaging Spectroradiometer (MODIS) [9, 13-15] or the Medium Resolution Imaging

Manuscript received November 28, 2011.

P. D'Odorico, A. Damm and M. E. Schaepman are with the Remote Sensing Laboratories, Department of Geography, University of Zurich, Winterthurerstr 190, CH-8057 Zurich, Switzerland.

A. Gonsamo is with Department of Geography and Program in Planning, University of Toronto, Sidney Smith Hall, 100 St. George Street, Toronto, Ontario, Canada M5S 3G3.

Spectrometer (MERIS) [12]. The European Space Agency's (ESA) upcoming Sentinel-2 Multi Spectral Instrument (MSI) [20, 21] is considered as the follow-up mission to SPOT and Landsat type of instruments and is intended to provide continuity of remote sensing products. The placement and the number of Sentinel-2 MSI spectral bands are, however, defined to offer an increased performance compared to analogous bands in SPOT and Landsat sensors. These refinements will, hence, cause deviations of NDVI values obtained from the Sentinel-2 MSI sensor compared to existing satellite sensors and will require adjustments to allow extending actual NDVI time series.

Cross-sensor calibration efforts directly based on the comparison of measured satellite imagery face several limitations. Their applicability is limited to sensor combinations for which temporally and spatially overlapping data exist. Moreover, other sources of deviation, e.g., spatial sampling and radiometric resolution, influence the comparison and prevent quantifying the isolated impact of SRF differences in the total uncertainty budget [4, 14, 17]. Cross-sensor calibration strategies incorporating either Radiative Transfer Model (RTM) simulations or airborne and in-situ measurements allow overcoming such restrictions. Other sources of difference, such as those linked with the spectral convolution operation to broadband SRFs, are however inherent to the latter approach. This difference was ignored in previous studies [5, 8], which used airborne measurements for developing SRF cross-sensor calibration models. Further weaknesses of existing cross-sensor SRF calibration approaches arise from the land cover dependency of the SRFs difference effect, which are not accounted for when using radiative transfer modeling [4, 13, 22, 23], and the dependency on data availability when using airborne [5, 8] or in-situ measurements [7, 11, 15]. To the best of our knowledge, none of the past efforts systematically compared strategies for cross-sensor SRF calibration.

The goal of this study is to quantify differences that can be expected in the red, NIR and NDVI time series expansion through Sentinel-2 MSI measurements caused by the isolated impact of spectral sensor properties, i.e., the sensor SRF. Results are considered being one important component of the total uncertainty budget related to the integration of multi-sensor data for establishing continuous time series of earth observation products. We deliberately neglect uncertainties caused by effects of the atmosphere, spatial sampling, or other sources of variability, as they require individual comprehensive analysis. The specific objectives of our analysis are: i) to investigate cross-sensor differences of the frequently used NDVI vegetation index and thus of cross-sensor differences in position and width of the red and the near-infrared (NIR) bands; ii) to propose a simple approach to minimize the effect of land cover on the SRF cross-calibration based on multivariate regression analysis; and iii) to evaluate a number of cross-sensor calibration data sets and the validity of the use of airborne measurement to replicate the satellite observation based on the Airborne Prism EXperiment (APEX) airborne imaging spectrometer.

NDVI time-series derivation is not a primary objective of the Sentinel-2 mission, since it samples the red-edge chlorophyll absorption region with three narrow bands in addition to those used for NDVI computation (Fig. 1). Nonetheless, it is essential to use Sentinel-2 based NDVI data given the high temporal resolution compared to SPOT HRG or Landsat type of instruments and the cross-calibration opportunity it offers for any given large swath sensor. The present work is considered as part of a broader harmonization effort aimed at preparing for the integration of Sentinel-2 MSI data with existing historical data records and product time-series.

II. Data and methods

A. Satellite sensors and their SRFs considered in this study

The upcoming Sentinel-2 MSI [21] was taken as the reference comparison instrument. Sentinel-2 is one of a series of five ESA missions aimed at addressing the operational needs of the Global Monitoring for Environment and Security programme (GMES). The mission is scheduled for launch in 2013 and among its objectives is providing enhanced continuity of data acquisition of SPOT and Landsat types of

TABLE I
SATELLITE SENSORS CHARACTERISTICS CONSIDERED IN THIS STUDY.

ID	Sensor	Operational period	Revisit frequency	Nominal band nr and wvl (nm)		Nominal pixel size
				Red	NIR	
SEN-2	Sentinel-2 MSI	2013−	2-5 days	#4: 640−690	#8: 780−910	10 m
AVHRR9	NOAA/AVHRR9	1989−1994	daily	#1: 580−680	#2: 725−1100	1 km
ETM7	Landsat 7 ETM+	1999−present	16 days	#3: 630−690	#4: 750−900	30 m
VGT1	SPOT5 VGT1	1998−present	daily	#2: 610−680	#3: 780−890	1 km
MER	MERIS	2002−present	3 days	#7: 657−672	#13: 852−877	260m x 300m
MOD	MODIS	1999−present	2 days	#3: 620−670	#4: 841−876	250 m

satellites. The Sentinel-2 local revisit time is close to the Landsat local overpass time and matches SPOT's, allowing the combination of Sentinel-2 MSI data with historical images to build a long-term time series. The optical payload onboard Sentinel-2 includes visible, NIR and shortwave infrared (SWIR) sensors featuring a total of 13 spectral bands (Fig. 1). Four bands image the Earth surface at 10 m, six bands at 20 m and three bands at 60 m spatial resolution [21]. Other spaceborne instruments chosen for the comparison are a representative selection of the most relevant instruments for continued NDVI measurements featuring long historical data records. Key instruments characteristics are summarized in Table 1. Analogous SRFs for the red and NIR regions for each of these sensors are shown in Fig. 1. SRFs were obtained from various sources: for AVHRR9 from NOAA portal (http://www.star.nesdis.noaa.gov/smcd/spb/calibration/avhrr/nrf.html); for MODIS from NASA portal (http://mcst.gsfc.nasa.gov/index.php?section=32); for SPOT VGT, MERIS and Landsat from the CEOS Cal/Val portal (http://calvalportal.ceos.org/cvp/web/guest/instruments); and for Sentinel-2 MSI from personal contact at ESA ESRIN. The SRFs differ in shape, central wavelength position, bandwidth and degree of overlap between the red and NIR channels. These differences become relevant when involving the transition region (red edge region) from strong chlorophyll absorption to strong foliage reflection between 680 and 720 nm. The Sentinel-2 satellites will orbit at a mean altitude of approximately 800 km, having a revisit time of five days at the equator and 2–3 days at mid-latitudes. Given the relatively high temporal resolution of both Sentinel-2 satellites to comparable SPOT HRG and Landsat type satellites, it is also important to compare the SRF with other large swath sensors such as AVHRR, SPOT VEGTATION, MODIS and MERIS, which also have high temporal resolution.

B. Data

Several datasets are used in this study. Measured data include satellite, airborne and in-situ spectral data acquired in the framework of the recent APEX [24, 26] flight campaigns. Modeled data consist of RTM simulations, i.e., spectral reflectances, obtained with the soil-leaf-canopy (SLC) model [25]. Airborne, in-situ and modeled data are convolved with the satellite sensors SRFs to simulate the satellite sensors observations.

Airborne and field spectrometer data

Airborne data used in this study were acquired using APEX, which entered the exploitation phase in 2011. APEX is an airborne dispersive pushbroom imaging spectrometer operating in the solar reflected wavelength domain. APEX is designed to serve as a simulation, validation and calibration sensor for current and future spaceborne missions. A sophisticated calibration concept, including in-flight performance monitoring through onboard characterization equipment [27, 28], makes this airborne system particularly suited for simulation of satellite sensor data. APEX data were acquired in 301 narrow contiguous spectral bands covering the

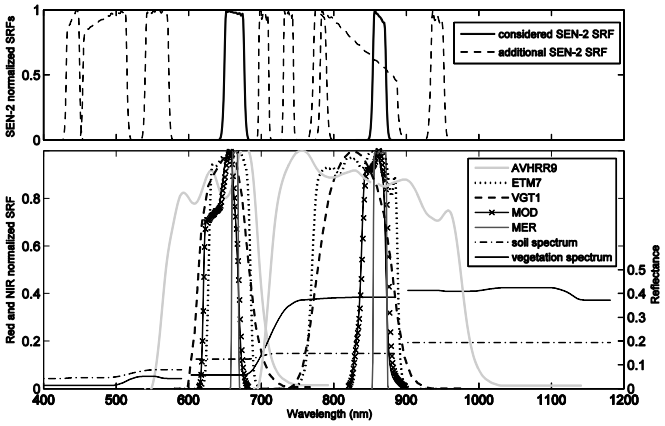

Fig. 1. Spectral Response Functions (SRF) for Sentinel-2 MSI (SEN-2 MSI) in the 400-1200 nm spectral wavelength range (upper plot). Red and near infrared spectral bands for the sensor systems used in this study: Sentinel-2 MSI (SEN-2), NOAA/AVHRR9 (AVHRR9), Landsat 7 ETM+ (ETM7), SPOT VEGETATION1 (VGT1), MODIS (MOD) and MERIS (MER). Sample green vegetation and soil spectra are also plotted.

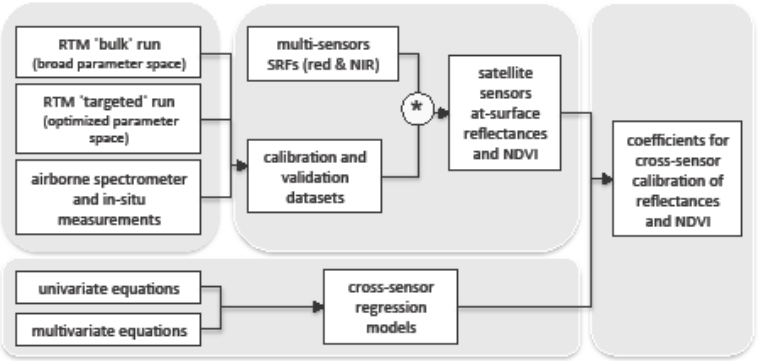

Fig. 2. Flowchart of cross-sensor Spectral Response Function (SRF) calibration approaches used in this study.

400─2500 nm spectral region. An average Spectral Sampling Interval (SSI) of 4 nm and a Full-Width-at-Half-Maximum (FWHM) of 5 nm characterize APEX bands in the red-visible region. In the NIR region, the average SSI and FWHM are 5.5 nm and 6.8 nm, respectively. The two APEX scenes used in this study were acquired over the same test site in two consecutive years, 2009 and 2010. The 2009 scene was acquired on June 17 (10:17:00 UTC), while in 2010 an over-flight took place on June 29 (09:54:00 UTC). The flight height was 5 km above sea level for both years, resulting in a 2 m x 2 m ground pixel size. The study area is located south of the city of Oensingen (47°17′N, 7°43′E) in the northwestern part of Switzerland. It is characterized by heterogeneous land cover, dominated by cultivated crop fields (e.g., corn, winter wheat, pea, sugar beet) and grasslands intermitted by mixed forest stands. The APEX data pre-processing included a spectral, geometric and radiometric calibration, a geo-rectification and an atmospheric correction [29, 30].

Field measurements were taken at the Oensingen study area as part of the APEX 2010 flight campaign. Data were acquired top-of-canopy using a FieldSpec Pro spectroradiometer (Analytical Spectral Devices, Boulder, USA). The instrument allows to measure reflected radiation within the spectral domain of 350─2500 nm with a spectral resolution of 3.0 nm in the red and NIR spectral region and a FOV of 25°. A calibrated SpectralonTM panel served as a white reference to estimate incident irradiance and compute reflectances. Measurements used were limited to agricultural plots (corn, winter wheat, pea, and sugar beet).

Satellite data

A Landsat TM5 scene encompassing the Oensingen test site was acquired on June 29, 2010 (10:07:03 UTC), being 13 minutes later than the APEX acquisition. Pre-processing of the Landsat scene included the conversion from calibrated digital numbers of the Level 1 product to at-sensor spectral radiances. This step required knowledge of the band-specific lower and upper limits of the original rescaling factors, obtained from the corresponding header file (.MTL). Further, the TM5 image was projected to the Hotine Oblique Mercator Azimuth Map Projection and cropped to a region of about 2 km x 10 km to spatially correspond with the APEX scene acquired at the same day. Co-registration with the APEX scene was performed using classical ground control point approaches.

Radiative Transfer Model (RTM)

The soil-leaf-canopy (SLC) model [25, 31] was chosen because it includes canopy structure (i.e., crown shape, forest stand density and canopy heterogeneity), leaf optical properties and background information in the modeling. Its arbitrary inclined leaf approximation best represents the land cover setting of the test site. Based on the four-stream radiative transfer theory, SLC combines a modified Hapke (1981) soil bidirectional reflectance distribution function (BRDF) model, a robust version of the PROSPECT leaf optical properties model [32], and the improved SAIL canopy RTM for forest and heterogeneous vegetation (4SAIL2). 4SAIL2 differs from previous versions of the SAIL-family of models by the inclusion of crown clumping effects relevant for forests.

C. SRF cross-sensor calibration approach

The presentation of SRFs in Fig. 1 shows the different spectral band settings of the sensor systems. To quantify and correct for the effects originating from these differences, numerical experiments were conducted on red and NIR reflectance data and NDVI values. The implementation of this

TABLE II
SLC MODEL PARAMETERS DISTRIBUTIONS FOR THE 'BULK' AND 'TARGETED' RUN, THE LATTER PARAMETERIZED BY THE A PRIORI INFORMATION AND AIRBORNE IMAGERY.

Variable	Definition	Parameters distribution	
		'*bulk*' run	'*targeted*' run
Leaf (PROSAIL)			
Cab (μg.cm-2)	Chlorophyll content	5 -100, step 5	25 random values with normal distribution
Cw (cm)	Water content	0.005, 0.01, 0.02	0.005 0.01 0.02
Cdm (g.cm-2)	Dry matter content	0.003, 0.005	0.003 0.005
Cs	Concentration of brown pigment	0.05	0.05
N	Leaf structure parameter	1.5	1.5
Canopy (4SAIL2)			
LAI (m2.m-2)	Total (green+brown) leaf area index or total crown LAI for clumped vegetation	0 – 8, step 1	25 random values with normal distribution
LIDFa	Leaf Inclination Distribution Function parameter controlling the average leaf slope	spherical	spherical
LIDFb	Leaf Inclination Distribution Function parameter controlling the distribution's bimodality	spherical	spherical
hot	Hot spot size parameter	0.05	0.05
fB	Fraction brown leaf area	0	0
diss	Layer dissociation factor	0	0
Cv	Vertical crown cover percentage	0.6, 1	0.6, 1
ξ	Tree shape factor	0, 0.2, 0.4	0, 0.2, 0.4
Soil	Background reflectance	modeled spectra (Hapke model, 4 soil types)	measured spectra (airborne & field spectrometer)
View-sun geometry			
tts (°)	Sun Zenith angle	45	27.1
tto (°)	Observing zenith angle	0	0, 7, 14
θ (°)	Relative azimuth angle	0	56.4, 123.6

experimental setup can be subdivided into three main steps leading to the estimation of cross-sensor calibration coefficients. As shown in Fig. 2 these steps are: i) the SRF cross-sensor calibration using univariate and multivariate regression models; ii) the generation of calibration and validation datasets used for the cross-sensor calibration exercise, and iii) the convolution of spectral reflectances with the satellite sensors SRFs.

Synthetic rather than measured data are used for the evaluation of SRF differences, on NDVI and reflectance data, for two reasons. Firstly, the Sentinel-2 mission had not been launched at the time of this work and thus, cross-sensor calibration based on satellite imagery was not feasible. Secondly, compared to measured data, synthetic data allows isolating the factor of interest, i.e., SRF variations, from other perturbing effects.

Regression models

Regression models using univariate and multivariate linear equations were used for the SRF cross-sensor calibration of reflectances and NDVI values in reference to Sentinel-2 MSI data. The following sets of equations were tested:

Univariate model:

$$y_{red\ or\ NIR} = \beta_1 x_{red\ or\ NIR} + \varepsilon$$

for red and NIR, and

$$y_{NDVI} = \beta_0 + \beta_1 x_{NDVI} + \varepsilon \quad \text{for NDVI} \qquad (1)$$

Multivariate model:

$$y_{red\ or\ NIR} = \beta_1 x_{red} + \beta_2 x_{NIR} + \beta_3 x_{NDVI} + \beta_4 x_{NDVI^2} + \varepsilon$$

for red and NIR, and

$$y_{NDVI} = \beta_0 + \beta_1 x_{NDVI} + \beta_2 x_{NDVI^2} + \varepsilon \quad \text{for NDVI} \qquad (2)$$

where y and x are the dependent (other sensors) and independent (Sentinel-2 MSI) reflectance or NDVI values, respectively. The β_0 is the intercept and $\beta_1, \ldots, \beta_4$ are the slopes of the different independent variables. The ε term represents the unexplained residual error of the model. To predict red and NIR data, the regression equation is forced to have zero intercept. For NDVI values the intercept is estimated as a parameter from the equation, as an NDVI value of zero in sensor x may correspond to a non-zero value in sensor y. Due to the residual regression model error ε, the regression coefficients of the transfer equation x as $f(y)$ are not the exact inverse of those obtained from y as $f(x)$. Since Sentinel-2 MSI sensor with its improved spatial, spectral and radiometric

TABLE III
PERCENTAGE ROOT-MEAN-SQUARE-ERROR (RMSE) RESULTING FROM SPECTRAL RESPONSE FUNCTION (SRF) DIFFERENCES BETWEEN SENTINEL-2 AND A NUMBER OF OTHER OPERATIONAL SENSORS. RMSE ARE SHOWN FOR ORIGINAL AS WELL AS SRF CROSS-SENSOR CALIBRATED VALIDATION DATA. RMSE (%) FOR MULTIVARIATE(UNIVARIATE) SRF CROSS-SENSOR REGRESSION EQUATIONS AND THREE SETS OF CALIBRATION DATASETS: MODEL ('BULK'), MODEL+AIRBORNE ('TARGETED'), AND AIRBORNE (APEX) ARE PRESENTED.

	Instrument	Original %	'bulk' RTM run multi (uni) variate %	'targeted' RTM multi (uni) variate %	APEX multi (uni) variate %	Gain factor (original/best)
RED	AVHRR9	33.1	9.4 (23.1)	8.5 (23.6)	**7.4** (23.4)	4.5
	ETM7	8.5	3.2 (5.5)	**2.8** (5.8)	3.5 (5.6)	3.0
	VGT1	33.6	10.6 (22.6)	8.1 (22.7)	**5.3** (21.5)	6.3
	MERIS	1.4	0.5 (0.5)	1.0 (0.5)	0.8 (0.8)	2.8
	MODIS	8.2	4.9 (7.5)	5.7 (6.8)	**4.6** (6.9)	1.8
NIR	AVHRR9	7.3	3.1 (3.3)	2.7 (**2.4**)	2.7 (2.8)	3.0
	ETM7	2.3	2.3 (1.5)	**1.5** (1.5)	1.8 (1.9)	1.5
	VGT1	2.4	2.3 (1.5)	**1.5** (1.5)	1.9 (1.9)	1.6
	MERIS	0.0	0.0 (0.0)	0.0 (0.0)	0.0 (0.0)	0.0
	MODIS	0.6	0.8 (0.4)	0.4 (0.4)	**0.4** (0.4)	1.5
NDVI*	AVHRR9	11.3	3.5 (3.0)	2.5 (2.6)	**2.4** (2.5)	4.7
	ETM7	3.1	**0.8** (1.4)	1.3 (1.3)	1.0 (1.1)	3.9
	VGT1	10.1	3.4 (3.6)	3.5 (3.5)	**1.5** (1.5)	6.7
	MERIS	0.4	0.2 (0.2)	**0.1** (0.2)	0.2 (0.2)	4.0
	MODIS	2.4	1.4 (1.1)	**1.0** (1.1)	1.1 (1.3)	2.4
NDVI**	AVHRR9	11.3	3.1 (8.1)	5.4 (8.2)	**2.5** (8.2)	4.5
	ETM7	3.1	1.5 (1.7)	1.7 (1.9)	**1.0** (1.6)	3.1
	VGT1	10.1	3.7 (7.3)	5.1 (7.4)	**1.6** (6.9)	6.3
	MERIS	0.4	0.2 (0.2)	0.3 (0.2)	0.2 (0.2)	2.0
	MODIS	2.4	**1.2** (1.9)	2.3 (1.9)	1.3 (1.9)	2.0

* NDVI values were obtained by applying the NDVI cross-sensor calibration equation whereas NDVI** values are computed based on cross-sensor calibrated red and NIR reflectances.

performances, is the likely choice for expansion of other sensors' data archives, we here present only the regression coefficients needed to correct Sentinel-2 MSI data in relation to other sensors.

The rationale for using a multivariate regression model as of Eq.(2) is based on theoretical considerations and on supportive results by previous studies [3, 8, 14, 23]. These studies demonstrated that SRF cross-sensors differences are land cover dependent. The inclusion of both red and NIR in the regression model to predict SRF cross-sensor red and NIR reflectances provides additional information on land cover type and its effect on the spectral curve. NDVI alone would have provided information about land cover. Nevertheless NDVI values of soils may be similar to NDVI values of sparsely vegetated land cover although both respond differently for varying SRF. Trishchenko *et al.* [8] demonstrated that the variations of red, NIR and NDVI between two pairs of sensors with varying SRF are in the order of $NDVI^2$ while NDVI itself partially explains the magnitude of the SRF effect and the spectral shape of red and NIR bands over vegetated land cover.

The percentage root mean square error (RMSE) (Eq.3) was used as an error metric to quantify multi-sensor reflectances and NDVI differences before and after SRF cross-sensor calibration.

$$RMSE\% = \frac{1}{\mu_{x^{ref}}}\sqrt{\frac{\sum_{n=1}^{n=N}\left(y_n - x_n^{ref}\right)^2}{N}} * 100 \qquad (3)$$

where x_n and y_n are the nth observations of the Sentinel-2 MSI sensor and the compared sensor, respectively. N represents the total number of observations. The RMSE was normalized by the mean of the respective reference signal (Sentinel-2 MSI) to make error magnitudes comparable across red and NIR reflectances and NDVI.

Calibration and validation data sets

Three different approaches were evaluated for the generation of a calibration dataset. The first approach relied exclusively on a 'bulk' RTM run. Information on the study area was not considered in the parameterization of the RTM. The definition of the model parameters was based on literature [25, 31, 33, 34] to represent a broad range of vegetation types. Broad and evenly distributed parameter spaces were defined for the leaf chlorophyll content of green biomass (Cab) and the Leaf Area Index (LAI). Background optical properties were defined by means of Hapke's soil BRDF model. Four soil types were additionally chosen, rock, litter as background

Table IV
SRF CROSS-SENSOR CALIBRATION COEFFICIENTS NEEDED FOR THE CONVERSION OF SENTINEL-2 (X) REFLECTANCES AND NDVI VALUES INTO THOSE OF THE INVESTIGATED SENSORS (Y). COEFFICIENTS WERE OBTAINED BASED ON THE BEST PERFORMING DATA-MODEL COMBINATION PRESENTED IN TABLE 3. COEFFICIENTS ARE USED WITH EQUATIONS 1-2.

Prediction	Instrument	Regression Coefficients				
		intercept	*red*	*NIR*	*NDVI*	$NDVI^2$
RED	N9		0.8618	0.0533	0.0230	-0.0287
	ETM7		0.9786	0.0104	0.0060	-0.0076
	VGT1		0.9185	0.0499	0.0123	-0.0159
	MER		0.9988	-0.0008	-0.0006	0.0008
	MOD		0.9423	0.0137	0.0131	-0.0167
NIR	N9			0.9196		
	ETM7			0.9717		
	VGT1			0.9699		
	MER			1.0000		
	MOD			0.9940		
NDVI	N9	0.1056			0.5847	0.2282
	ETM7	0.0207			0.8678	0.1028
	VGT1	0.0309			0.7962	0.0954
	MER	0.0004			1.0052	-0.0045
	MOD	0.0572			0.8146	0.1215

for meadows, forest understory, and snow. Parameters describing the sun-observation geometry were set to resemble typical values encountered for acquisitions at central European latitudes. The parameter distribution for the RTM 'bulk' run are given in Table 2.

In the second approach, a 'targeted' RTM run was intended to simulate the variety of vegetation properties resembling those of a pre-selected study area, i.e., the Oensingen test site. Model inversion based on a look-up-table (LUT) approach was performed to meet this objective [34, 35]. The 2009 APEX scene was used as an input to the inversion. A total of 10'000 reflectance spectra were selected from the airborne scene, which had been stratified in NDVI classes. Pixels with a NDVI value < 0.3 were excluded, representing non-vegetative surfaces. Random points with NDVI values typical for vegetated surfaces were sampled above this threshold. The LUT spectra were convolved to APEX SRFs before entering the search for the best fit. The background reflectance was approximated by three soil spectra extracted from the APEX scene and the illumination-observation geometry was set according to the airborne acquisition. The view zenith angle was defined for nadir (0°) as well as two off-nadir (7°, 14°) positions to simulate APEX ±14° FOV. The relative azimuth angle was computed for two different view azimuth angles, 90° and 270°, corresponding to the right and left half of the swath, respectively. In a second step, the parameter space resulting from the model inversion was used for a forward simulation aimed at generating the calibration dataset representative of the study site, i.e., a 'targeted' run. The parameter distribution for the RTM 'targeted' run is given in Table 2.

In the third approach, the calibration dataset was directly obtained from the 2009 APEX data. Spectra were selected in the same fashion as described above, i.e., NDVI stratification and random sampling, thus granting representativeness of vegetation dynamics in the dataset.

Two validation datasets were further compiled. The first was obtained by sampling the 2010 APEX scene as previously described, while the second was obtained by compiling field measurements acquired simultaneously with the 2010 airborne campaign.

Convolution and deconvolution of spectral reflectances and radiances

Calibration and validation datasets obtained from RTM simulations, airborne and in-situ measurements, were convolved to satellite sensor spectral response functions for the red and NIR bands. It should be noted that in this study we evaluated the isolated impact of sensor properties and intentionally excluded additional atmospheric effect, which have to be addressed in targeted studies. Spectral convolution was applied as follows:

$$\hat{I}(\lambda) = \frac{\int_{\lambda_{\min}}^{\lambda_{\max}} I(\boldsymbol{\lambda_i}) * \mathbf{SRF}(\boldsymbol{\lambda_i}) d(\boldsymbol{\lambda_i})}{\int_{\lambda_{\min}}^{\lambda_{\max}} \mathbf{SRF}(\boldsymbol{\lambda_i}) d(\boldsymbol{\lambda_i})} \quad (4)$$

where $\hat{I}(\lambda)$ is the convolved spectral reflectance (or radiance) as measured by the satellite sensor, and $I(\lambda_i)$ is the reflectance (or radiance) at high spectral sampling.

The validity of the adopted spectral convolution approach for input spectra sampled below Nyquist frequency was tested in this context. The objective was to determine how well APEX data can be used to reproduce broadband acquisitions, i.e., to assess the impact of in-band averaging and under-sampling effects introduced by APEX SRFs on the broadband convolution. This is also a prerequisite for the use of APEX for SRF cross-sensor calibration. To meet this objective, broadband at-sensor radiances simulated starting from original

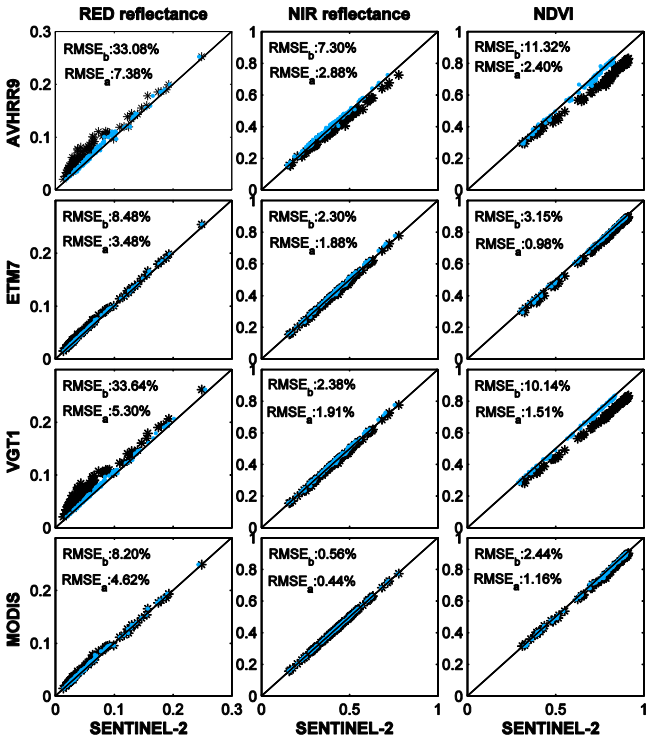

Fig. 3. Scatter plots for the red and NIR reflectances and the NDVI for four sensors compared to Sentinel-2 MSI. Data are plotted for original (black asterisk) and Spectral Response Function (SRF) cross-sensor calibrated (blue dots) data. Data were obtained by convolving 2010 APEX acquisitions with satellite sensors' SRFs. The percentage Root Mean Square Error is given before (RMSEb) and after (RMSEa) applying SRF cross-sensor regression models in Table 3.

and deconvolved APEX data were compared to observed broadband at-sensor radiances. The Landsat-5 Thematic Mapper (TM5) was chosen as the reference instrument given its reputation as a well-calibrated system whose performances have been studied throughout the years [36-38]. The co-registered TM5 and APEX scenes acquired on June 29, 2010, only 13 minutes apart, were resampled to an 120 m x 120 m ground pixel size to mitigate the effect of Point Spread Function (PSF) differences as well as possible co-registration errors. APEX measured radiances (L_A) were propagated to the top of the atmosphere (TOA) based on Eq.(5) [39]. MODTRAN5 was used to calculate the atmospheric spectral upward transmittance (T_U) and path scattered radiance (Lp) from an altitude of 5 km corresponding to the flight height during APEX data acquisition. An illumination correction factor computed as the ratio of the cosine of the solar zenith angles for APEX ($\theta = 30.9$) and Landsat TM5 ($\theta = 29.5$), accounted for the near-simultaneous acquisition times.

$$L_{ATOA} = \frac{\cos(\theta_A)}{\cos(\theta_{TM5})}(L_A T_U + L_p) \quad (5)$$

A similar procedure was applied to APEX spectra that had been deconvolved. The Van Cittert iterative deconvolution technique [40, 41] was used to derive the most accurate approximation of the true radiance, l, by decorrelating the SRFs from the observed radiance, L. It is given as:

$$\hat{l}^{k+1} = \hat{l}^k + (L - \mathrm{SRF} * \hat{l}^k) \quad (6)$$

where $\hat{l}^k$ is the kth estimate of l. The correction factor $(L - \mathrm{SRF} * \hat{l}^k)$ used to adjust the kth estimate of l is interpolated to match the 1 nm sampling step of $\hat{l}^k$. Cubic spline interpolation is used to get the continuous delta spectrum as well as to derive a first estimation, $\hat{l}^0$, of the observed spectrum. For more details on the Van Cittert iterative deconvolution technique we refer to [42].

Eventually, APEX TOA original and deconvolved radiances were convolved with Landsat TM5 SRFs (Eq. (4)).

III. Results and Discussion

A. SRF difference effects

Results of the reflectance and NDVI cross-sensor comparison are reported in Table 3. Results are obtained by applying the regression coefficients on the independent airborne validation dataset and consider the different calibration datasets and regression models.

The first column of Table 3 shows the differences we can expect if no SRF cross-sensor calibration is performed. One should note that the differences only capture discrepancies in nominal instrument spectral responses. This means that performance drifts occurring over time are not considered, assuming an insignificant change of SRFs through the life span of satellite sensors. MERIS is the only instrument for which continuity with Sentinel-2 MSI can be established with differences in reflectances and NDVI below 1.5%. Broadband instruments such as AVHRR9 and VGT1exhibit the highest SRF based differences with RMSEs greater than 33% and 10% for the red band and NDVI, respectively. Similarly, ETM+ and MODIS data differed from Sentinel-2 MSI data in the red visible region with a RMSE greater 8%, whereas for NIR and NDVI the RMSE was around 3% (Table 3). For all sensors, position and shape of the red spectral band was the most critical for sensor cross-comparison subsequently contributing to the NDVI differences. This is in line with findings by [5] which identified the width of the red spectral band having the most significant impact due to the relatively narrow spectral width of the red absorption feature of chlorophyll. The same study found the position of the NIR band less critical provided that the bandwidth (FWHM) is no more than 50 nm and the atmospheric correction is accurate. The latter aspect relates with the significant influence of atmospheric gas absorption, in particular of water vapor, on the spectral region of the near-infrared plateau.

B. SRF cross-sensor regression models

Band-to-band univariate and multivariate regression models were tested for SRF cross-sensor calibration and the choice of the regression model equations was found having an influence on the correction of SRF difference effects. The multivariate regression model showed overall better results. The spectral comparability in the red spectral region improved up to a factor of 4.5 and 6.3, for AVHRR9 and VGT1, respectively. For ETM7 and MODIS, the improvement in the red band compared to the original difference was threefold (6th column Table 3). The observed improvements can be explained with the inclusion of information from the NIR region, in form of NIR reflectance and NDVI values. Both information sources account for the impact of changing land cover and amount of existing biomass on the spectral overlap between visible and NIR bands over the red-edge region (around 700 nm). The NDVI is a good indicator of the shape of surface spectra, explaining its sensitivity to the dependency of cross-calibration accuracy on land cover changes. NIR reflectances are also included in the set of red band cross-sensor calibration because NDVI alone cannot differentiate between land cover types featuring similar NDVI values, e.g., soil and sparse vegetation. For the cross-sensor calibration of the NIR signal, the inclusion of information from the red spectral region in form of red or NDVI was instead found having no benefit. One can thus conclude that the band-to-band SRF cross-sensor calibration in the NIR region can be made effectively using the univariate linear regression model. For NDVI, regression models were either applied directly on NDVI values or the NDVI was derived from the red and NIR for which the SRF cross-sensor calibration was performed. The former gave slightly better results besides being preferable from an operational point of view given that the global products generally do not provide red and NIR reflectances from which NDVI time-series were computed. SRF based differences of NDVI values were improved by a factor 4.7 and 6.7 for AVHRR9 and VGT1, respectively after the applied cross-sensor calibration. A fourfold improvement was reached for ETM7 and MERIS. It can be observed that NDVI multi-sensor differences are only marginally affected by land cover type as the NDVI per se partially compensates this effect. However, NDVI multi-sensor differences can be affected non-linearly by variations in the optical thickness of photosynthetic biomass. This effects can be represented by including NDVI2 (Eq.2; [8]).

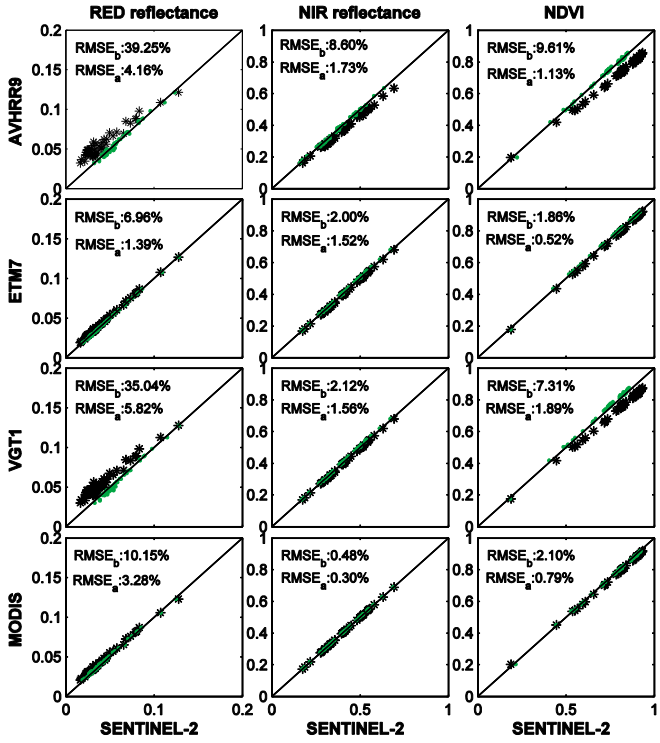

Fig. 4. Scatter plots for the red and NIR reflectances and the NDVI for four sensors compared to Sentinel-2 MSI. Data are plotted for original (black asterisk) and Spectral Response Function (SRF) cross-sensor calibrated (blue dots) data. Data were obtained by convolving in-situ field spectrometer measurements with satellite sensors' SRFs. The percentage Root Mean Square Error is given before (RMSEb) and after (RMSEa) applying SRF cross-sensor regression models in Table 3.

Table 4 provides the regression coefficients associated with the best performing data-model combination presented in Table 3. Scatter plots in Fig. 3-4 show original and converted Sentinel-2 MSI reflectance and NDVI values plotted against those of the sensors to be predicted (MERIS was omitted as original differences were smaller than 3%). Results are given for the two validation datasets: the airborne data (Fig. 3) and the field spectrometer measurements (Fig. 4). For all investigated cases, the slope of the regression line between reflectances or NDVI datasets was much closer to the one-to-one line after cross-sensor correction had been applied. This finding is evidenced by a decreasing RMSE. The validation exercise in this study was based on independent datasets increasing our confidence on the use of the calibration data sets and regression models developed in this study for SRF cross-sensor calibration.

C. SRF cross-sensor calibration data sets

The choice of calibration data sets determines the quality of the cross-sensor calibration. This sensitivity is among others caused by the position and shape of the red spectral band. For

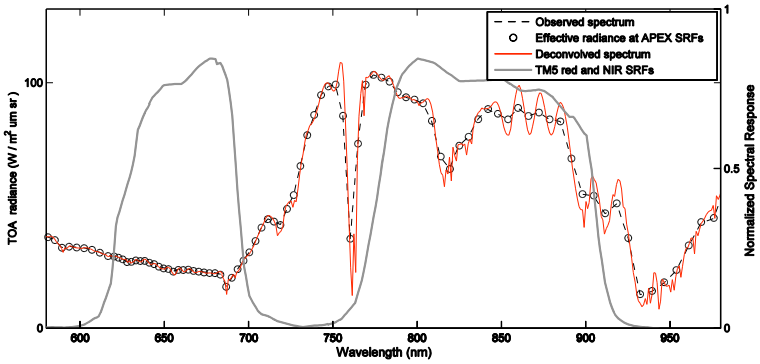

Fig. 5. Deconvolved spectrum compared to the observed APEX spectrum from which it was derived. Landsat TM5 Spectral Response Function (SRF) for red and NIR bands are plotted for reference (TOA is top-of-atmosphere).

sensors with narrower red band, i.e., less contaminated by the elevated reflection in NIR, comparable performances were obtained using either of the three calibration datasets. This was not the case for instruments whose red band covered the red-NIR transition region, e.g., AVHRR and VGT1. For these instruments, a higher knowledge about the spectral content of the scene showed increasingly beneficial in correcting for the SRF difference effects. For AVHRR red band cross-sensor calibration, the RMSE drops from 33.1% to 9.4%, 8.5%, and 7.4% when scene independent ('bulk' RTM run), semi-dependent ('targeted' RTM run) or dependent (airborne scene) calibration datasets are used, respectively. A similar trend is shown for VGT1 red band with RMSEs decreasing from 33.6% to 10.6%, 8.1%, and 5.3% with increasing scene-specific information. The choice of calibration dataset transpires but is far less significant for NIR and NDVI cross-sensor calibration.

D. Convolution of airborne imaging spectrometer data to satellite SRFs

Previous SRF cross-sensor calibration activities have ignored the effects of airborne imaging spectrometer in-band averaging and under-sampling (e.g., [5, 8]) although the recent study by [42] suggested the reconstruction of continuous spectra from operational imaging spectrometers. In this study, we performed a sensitivity analysis to judge the impact of this effect and to judge suitability of APEX data supporting satellite SRF cross-sensor calibration. Continuous APEX radiance spectra were simulated using a deconvolution approach and compared with originally measured APEX spectra. As shown in Fig. 5, the deconvolved APEX measurements resulted in negligible added information in relation to the original one. Information about absorption features not present in the original data and about the real position of these features was not recovered; instead the signature of sharp spectral absorption features was increased as a result. The deconvolved super-resolution spectrum resembled signal noise for most contiguous APEX bands resulting in contrasting offset spectra (Fig. 5).

The use of deconvolved rather than original APEX spectra fitted with TM5 SRF did not improve the relationships with the measured TM5 data (results are not presented for brevity). The noticeable amount of noise added to the spectra by the deconvolution might even trigger the opposite effect, decreasing the accuracy in simulated narrow and low reflective bands.

The comparison between simulated TM5 radiances based on APEX measurements and observed TM5 radiances showed a good agreement, with RMSE values of 11%, 9% and 12% for red, NIR and NDVI, respectively (Fig. 6). All relationships were statistically significant ($p<0.0001$), slopes were unity, and intercepts between simulated and measured radiances and NDVI were consistently below 5%. The residual deviation can be attributed to a number of sources, such as calibration uncertainties [37, 38], scaling issues and adjacency effects, as well as spatial resampling and co-registration errors. In consequence, it can be stated that in-band averaging and under-sampling effects introduced by APEX SRFs on the radiance spectra do not require compensation prior to convolution with TM5 broad bands. The performance of APEX in simulating the TM5 radiances increases our confidence in the use of airborne imaging spectrometers data, and particularly of APEX data, for the cross-sensor calibration

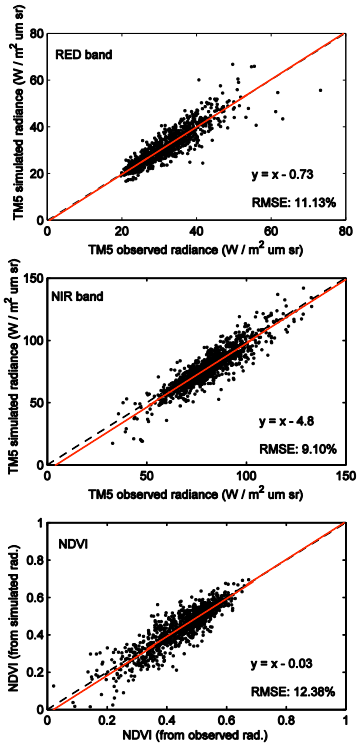

Fig. 6. Comparison between Landsat TM5 observed and simulated Top Of Atmosphere (TOA) radiances and derived NDVI values. Simulated radiances were obtained from APEX data, which were propagated to TOA. The discontinuous line represents the one-to-one line, while the continuous line represents the regression fit.

of operational and upcoming satellite sensors. Nonetheless, additional investigations including narrow band sensors simulations are needed to further strengthen this hypothesis.

IV. Conclusions

As of 2013, ESA's Sentinel-2 mission will start delivering high-resolution optical images on a global scale. To assure that existing satellite based historical data records and product time-series can be complemented and expanded using Sentinel-2 MSI data, uncertainties linked with differences in instrument performances need to be addressed accordingly. In this study we investigated uncertainties originating from differences in position and width of the red and NIR spectral bands and on their implication on NDVI time-series continuity.

Findings showed that differences in SRFs are significant and have to be taken into account to integrate Sentinel-2 NDVI time-series with those of other sensors. Expanding AVHRR NDVI time-series via original Sentinel-2 data is possible with an 11% uncertainty without SRF cross sensor calibration. Similarly, continuing NDVI time-series of the SPOT VGT heritage instrument is related to an uncertainty of 10%. These uncertainties are not acceptable considering the subtle magnitude of natural surface variations we aim at monitoring in vegetation studies. This study demonstrates that compensating for SRF difference effects in the data improves the Sentinel-2 NDVI time series consistency with AVHRR9 and SPOT VGT1 NDVI time series of up to a factor of five and a factor of seven, respectively. The spectral band difference effect was found to be dependent on the surface reflectance spectrum. The inclusion of knowledge about the spectral content of the scene and about the overall shape of the spectrum improved the correction.

The use of multivariate regression improved the SRF cross-sensor calibration, particularly for the red band covering the spectral region with the largest spectral contrast. Multivariate over univariate band-to-band regression improved results by up to a factor six (e.g. Sentinel-2 vs. VGT1 in Table 3). This effect also spreads to the computed NDVI after applying multivariate cross-sensor SRF calibration in the red region, resulting in improved NDVI cross-sensor comparability. We, therefore, recommend an ensemble of regression models for the red and the NIR cross-sensor calibration. In the red region, the use of NIR, NDVI and NDVI2 as multivariate predictor variables improves the comparability of the reflectances between two given sensors. For the NIR region, simple band-to-band SRF cross-sensor calibration suffices the desired level of comparability.

The choice of the calibration data source plays a marginal role in the performance of SRF cross-sensor calibration. Overall, the use of measured airborne data performed best followed by the targeted RTM simulations. However, both airborne measurements and fully parameterized RTMs are often not available for an extended study area. In such cases, the 'bulk' run is the only alternative for cross-sensor SRF calibration, as the parameterization can be performed by a priori guess or by setting large parameter ranges. Our study further indicates that, if the SRF based reflectance differences are below 3%, the cross-sensor calibration is not required or does not necessarily improve the comparability (e.g., Sentinel-2 MSI vs. MERIS in Table 3).

NDVI time series cross-calibration has represented a great challenge within the global climate change community. Once spaceborne, Sentinel-2 will allow for acquisition of comprehensive and extended NDVI time series and can

provide the needed reference tool for cross-calibration of any given large swath sensor. We have demonstrated that – sufficient stability of all other sensor parameters given – substantial improvement can be achieved by using regression models to secure spectral continuity of NDVI time-series.

ACKNOWLEDGMENT

The authors would like to thank J. Timmermans and W. Verhoef for providing and supporting the use of SLC. We acknowledge the support of A. Hüni and M. Jehle of the APEX team.

REFERENCES

[1] S. L. Lewis, P. M. Brando, O. L. Phillips, G. M. F. van der Heijden, and D. Nepstad, "The 2010 Amazon Drought," *Science,* vol. 331, no. 6017, p. 554, Feb. 2011.

[2] R. de Jong, S. de Bruin, A. de Wit, M. E. Schaepman, and D. L. Dent, "Analysis of monotonic greening and browning trends from global NDVI time-series," *Remote Sens. Environ.*, vol. 115, no. 2, pp. 692-702, Feb. 2011.

[3] P. M. Teillet, J. L. Barker, B. L. Markham, R. R. Irish, G. Fedosejevs, and J. C. Storey, "Radiometric cross-calibration of the Landsat-7 ETM+ and Landsat-5 TM sensors based on tandem data sets," *Remote Sens. Environ.*, vol. 78, no.1-2, pp. 39-54, Apr. 2001.

[4] E. Swinnen and F. Veroustraete, "Extending the SPOT-VEGETATION NDVI Time Series (1998-2006) Back in Time With NOAA-AVHRR Data (1985-1998) for Southern Africa," *IEEE Trans. Geosci. Remote Sens.*, vol. 46, no. 2, pp. 558-572, Feb. 2008.

[5] P. M. Teillet, K. Staenz, and D. J. William, "Effects of spectral, spatial, and radiometric characteristics on remote sensing vegetation indices of forested regions," *Remote Sens. Environ.,* vol. 61, no. 1, pp. 139-149, Jul. 1997.

[6] P. M. Teillet, G. Fedosejevs, K. J. Thome, and J. L. Barker, "Impacts of spectral band difference effects on radiometric cross-calibration between satellite sensors in the solar-reflective spectral domain," *Remote Sens. Environ.,* vol. 110, no. 3, pp. 393-409, Oct. 2007.

[7] K. L. Castro-Esau, G. A. Sanchez-Azofeifa, and B. Rivard, "Comparison of spectral indices obtained using multiple spectroradiometers," *Remote Sens. Environ.,* vol. 103, no. 3, pp. 276-288, Aug. 2006.

[8] A. P. Trishchenko, J. Cihlar, and Z. Li, "Effects of spectral response function on surface reflectance and NDVI measured with moderate resolution satellite sensors," *Remote Sens. Environ.,* vol. 81, no. 1, pp. 1-18, Jul. 2002.

[9] A. P. Trishchenko, "Effects of spectral response function on surface reflectance and NDVI measured with moderate resolution satellite sensors: Extension to AVHRR NOAA-17, 18 and METOP-A," *Remote Sens. Environ,* vol. 113, no. 2, pp. 335-341, Feb. 2009.

[10] P. M. Teillet and X. Ren, "Spectral band difference effects on vegetation indices derived from multiple satellite sensor data," *Can. J. Remote Sensing,* vol. 34, no. 3, pp. 159-173, Aug. 2008.

[11] M. D. Steven, T. J. Malthus, F. Baret, H. Xu, and M. J. Chopping, "Intercalibration of vegetation indices from different sensor systems," *Remote Sens. Environ.,* vol. 88, no. 4, pp. 412-422, Dec. 2003.

[12] K. P. Günther and S. W. Maier, "AVHRR compatible vegetation index derived from MERIS data," *Int. J. of Remote Sens.,* vol. 28, no. 3-4, pp. 693-708, Feb. 2007.

[13] W. J. D. van Leeuwen, B. J. Orr, S. E. Marsh, and S. M. Herrmann, "Multi-sensor NDVI data continuity: Uncertainties and implications for vegetation monitoring applications," *Remote Sens. Environ.,* vol. 100, no. 1, pp. 67-81, Jan. 2006.

[14] K. Gallo, L. Ji, B. Reed, J. Eidenshink, and J. Dwyer, "Multi-platform comparison of MODIS and AVHRR normalized difference vegetation index data," *Remote Sens. Environ.,* vol. 99, no. 3, pp. 221-231, Aug. 2005.

[15] A. A. Gitelson and Y. J. Kaufman, "MODIS NDVI Optimization To Fit the AVHRR Data Series − Spectral Considerations," *Remote Sens. Environ.,* vol. 66, no. 3, pp. 343-350, Dec. 1998.

[16] O. Samain, B. Geiger, and J.-L. Roujean, "Spectral Normalization and Fusion of Optical Sensors for the Retrieval of BRDF and Albedo: Application to VEGETATION, MODIS, and MERIS Data Sets," *IEEE Trans. Geosci. Remote Sens.*, vol. 44, no. 11, Nov. 2006.

[17] A. P. Trishchenko, Y. Luo, K. V. Khlopenkov, and S. Wang, "A Method to Derive the Multispectral Surface Albedo Consistent with MODIS from Historical AVHRR and VGT Satellite Data," *J. Appl. Meteor. Climatol.*, vol. 47, no. 4, pp. 1199-1221, Apr. 2008.

[18] C. J. Tucker, "Red and photographic infrared linear combinations for monitoring vegetation," *Remote Sens. Environ.*, vol. 8, no. 2, pp. 127-150, May 1979.

[19] N. Gobron, B. Pinty, M. Verstraete, and J.-L. Widlowski, "Advanced Vegetation Indices Optimized for Up-Coming Sensors: Design, Performance and Applications.," *IEEE Trans. Geosci. Remote Sens.*, vol. 38, no.6, pp. 2489-2505, Nov. 2000.

[20] Z. Malenovský, H. Rott, J. Cihlar, M. E. Schaepman, G. García-Santos, R. Fernandes, and M. Berger, "Sentinels for Science: Potential of Sentinel-1, -2, and -3 missions for scientific observations of ocean, cryosphere, and land.," *Remote Sens. Environ*, accepted Dec. 2011.

[21] M. Drusch, U. Del Bello, S. Carlier, O. Colin, V. Fernandez, F. Gascon, B. Hoersch, C. Isola, P. Laberinti, P. Martimort, A. Meygret, F. Spoto, O. Sy, F. Marchese, and P. Bargellini, "Sentinel -2: ESA's Optical High-Resolution Mission for GMES Operational Services," *Remote Sens. Environ,* accepted Dec. 2011.

[22] A. Prieto-Blanco, P. R. J. North, M. J. Barnsley, and N. Fox, "Satellite-driven modelling of Net Primary Productivity (NPP): Theoretical analysis," *Remote Sens. Environ.,* vol. 113, no. 1, pp. 137-147, Jan. 2009.

[23] A. Gonsamo and J. M. Chen, "Spectral response cross-calibration among 21 satellite sensors for global vegetation monitoring," *IEEE Trans. Geosci. Remote Sens.*, submitted 2011.

[24] M. Jehle, A. Hueni, A. Damm, P. D'Odorico, J. Weyermann, M. Kneubühler, D. Schläpfer, and M. E. Schaepman, "APEX - current status, performance and product generation. ," in *IEEE Sensors 2010 Conference*, Waikoloa (HI), 2010.

[25] W. Verhoef and H. Bach, "Coupled soil-leaf-canopy and atmosphere radiative transfer modeling to simulate hyperspectral multi-angular surface reflectance and TOA radiance data," *Remote Sens. Environ.*, vol. 109, no. 2, pp. 166-182, Jul. 2007.

[26] K. Itten, F. Dell Endice, A. Hueni, M. Kneubuehler, D. Schlaepfer, D. Odermatt, F. Seidel, S. Huber, J. Schopfer, T. Kellenberger, Y. Buehler, P. DOdorico, J. Nieke, E. Alberti, and K. Meuleman, "APEX - the Hyperspectral ESA Airborne Prism Experiment," *Sensors,* vol. 8, no. 10, pp. 6235-6259, Oct. 2008.

[27] P. D'Odorico, E. Alberti, and M. E. Schaepman, "In-flight spectral performance monitoring of the Airborne Prism Experiment.," *Appl. Opt.* , vol. 49, no. 16, pp. 3082-3091, May 2010.

[28] P. D'Odorico, L. Guanter, M. E. Schaepman, and D. Schläpfer, "Performance assessment of onboard and scene-based methods for APEX spectral characterization," *Appl. Opt.,* vol. 50, no. 24, pp. 4755-4764, Aug. 2011.

[29] D. Schläpfer and R. Richter, "Geo-atmospheric processing of airborne imaging spectrometry data. Part 1: Parametric orthorectification," *Int. J. Remote Sens.*, vol. 23, no. 13, pp. 2609-2630, 2002.

[30] R. Richter and D. Schläpfer, "Geo-atmospheric processing of airborne imaging spectrometry data. Part 2: Atmospheric/topographic correction," *Int. J. Remote Sens.*, vol. 23, no. 13, pp. 2631-2649, 2002.

[31] W. Verhoef and H. Bach, "Simulation of hyperspectral and directional radiance images using coupled biophysical and atmospheric radiative transfer models," *Remote Sens. Environ.,* vol. 87, no. 1, pp. 23-41, Sep. 2003.

[32] S. Jacquemoud and F. Baret, "PROSPECT: A model of leaf optical properties spectra," *Remote Sens. Environ.,* vol. 34, no. 2, pp. 75-91, Nov. 1990.

[33] V. Laurent, W. Verhoef, J. Clevers, and M. Schaepman, "Estimating forest variables from top-of-atmosphere radiance satellite measurements using coupled radiative transfer models," *Remote Sens. Environ.,* vol. 115, no. 4, pp. 1043-1052, Apr. 2011.

[34] R. Darvishzadeh, A. Skidmore, M. Schlerf, and C. Atzberger, "Inversion of a radiative transfer model for estimating vegetation LAI and chlorophyll in a heterogeneous grassland," *Remote Sens. Environ.,* vol. 112, no. 5, pp. 2592-2604, May 2008.

[35] M. Schlerf and C. Atzberger, "Inversion of a forest reflectance model to estimate structural canopy variables from hyperspectral remote sensing data," *Remote Sens. Environ.,* vol. 100, no. 3, pp. 281-294, Feb. 2006.

[36] D. L. Helder, B. Markham, K. J. Thome, J. A. Barsi, G. Chander, and R. Malla, "Updated Radiometric Calibration for the Landsat-5 Thematic Mapper Reflective Bands," *IEEE Trans. Geosci. Remote Sens.*, vol. 46, no. 10, Oct. 2008.
[37] G. Chander, B. L. Markham, and D. L. Helder, "Summary of current radiometric calibration coefficients for Landsat MSS, TM, ETM+, and EO-1 ALI sensors," *Remote Sens. Environ.,* vol. 113, no. 5, pp. 893-903, May 2009.
[38] G. Chander, B. Markham, and J. A. Barsi, "Revised Landsat-5 Thematic Mapper Radiometric Calibration," *IEEE Geosci. Remote Sens. Lett.,* vol. 4, no. 3, Jul. 2007.
[39] R. O. Green, B. Pavri, and T. Chrien, "On-Orbit Radiometric and Spectral Calibration Characteristics of EO-1 Hyperion derived with an underflight of AVIRIS and In Situ Measurements at Salar de Arizaro, Argentina," *IEEE Trans. Geosci. Remote Sens.*, vol. 41, no. 6, Jun. 2003.
[40] P. B. Crilly, "A quantitative evaluation of various iterative deconvolution algorithms," *IEEE Trans. Instrum. Meas.*, vol. 40, no. 3, pp. 558-562, Jun. 1991.
[41] P. A. Jansson, *Deconvolution of Images and Spectra*, Second Edition ed.: Academic Press, 1997.
[42] H. Zhao, G. Jia, and N. Li, "Transformation from hyperspectral radiance data to data of other sensors based on spectral superresolution," *IEEE Trans. Geosci. Remote Sens.*, vol. 48, no. 11, Nov. 2010.

Petra D'Odorico received the degree in forestry and environmental technologies from the University of Padua, Italy, in 2004 and the M.Sc. degree in geo-information science from Wageningen University, The Netherlands, in 2006. She is currently working toward the Ph.D. degree at the Department of Geography, Remote Sensing Laboratories, of the University of Zurich, Switzerland.

Since 2008, she has been working on data and instrument calibration and validation, with a focus on the spectral domain. She is part of the scientific team responsible for the calibration of the APEX (Airborne Prism Experiment) imaging spectrometer and she is in charge of the in-flight performance monitoring. Her recent interests include remote sensing of bio-/geophysical and ecological parameters for vegetation monitoring studies.

Alemu Gonsamo studied forestry at Wondo Genet College of Forestry, Debub University, Ethiopia, and graduated in 2002 with a B.Sc. degree (great distinction). He received the M.Sc. degree in geo-information science from Wageningen University, The Netherlands, in 2006, and the Ph.D. degree in geography at the Department of Geography, University of Helsinki, Finland, in 2010.

From 2002 to 2004, he worked as a GRADUATE ASSISTANT and ACADEMIC COORDINATOR. In 2010, he was a Postdoctoral Fellow at the Department of Geography and Geosciences. He is currently a Postdoctoral Fellow with the University of Toronto, Toronto, ON. His recent research interests are in the remote sensing of bio-geophysical parameters, plant canopy radiation modeling, optical satellite sensor cross calibration, remote sensing of plant phenology, and territorial carbon cycle modeling.

Alexander Damm received the Diploma (M.Sc.) and Ph.D. degree in geography from the Humboldt-University Berlin, Germany, in 2004 and 2008, respectively. Since December 2008, he has been as a postdoctoral researcher with the Remote Sensing Laboratories, University of Zurich, Zurich, Switzerland. He currently acts as the responsible project manager for the largest APEX (Airborne Prism Experiment) exploitation programme aiming at supporting advanced product development using spectroscopy based approaches.

His research interests are in earth observation, with particular focus on biosphere-atmosphere interactions using imaging spectroscopy. His recent research is on the quantitative assessment of plant photosynthesis and related ecosystem processes such as GPP by exploiting sun-induced chlorophyll fluorescence at leaf, canopy and regional scale.

Michael E. Schaepman holds MSc (1993) and PhD degrees (1998) in remote sensing from the University of Zurich. Following his PhD, he spent his PostDoc at the Optical Science Center of the University of Arizona (Tucson, AZ, USA). In 2000, he was appointed project manager of the ESA APEX (Airborne Prism Experiment) spectrometer. In 2003, he accepted a position as full chair of geo-information science and remote sensing at Wageningen University (Wageningen, The Netherlands). In 2009 he was appointed full chair of remote sensing at the University of Zurich. Michael's interests are in the computational Earth sciences using remote sensing and physical models. Michael is co-founder and board member of Netcetera Group AG in Zurich. He serves on several national and international boards focusing on the use of Earth Observation instruments and methods.

6 SYNOPSIS

6.1 Main results

The main achievements of this dissertation are structured according to the publications (chapter 3-5) and their respective research questions presented in chapter 1.5. The first publication (chapter 2) gives a general overview of the APEX spectrometer, and is therefore not discussed hereafter.

6.1.1 Feasibility of monitoring in-flight spectral performance of the APEX imaging spectrometer

- Is APEX spectral performance measured during laboratory characterization still valid in an operational environment, if not, which are the causes of deviation?

A series of ground and in-flight experiments carried out starting from 2009 underlined the change of APEX spectral performance when operated in an airborne, or alike, environment. These changes imply that spectral laboratory calibration does not hold during in-flight and that an update of instrument nominal spectral parameters is essential if high-quality APEX data and products should be delivered to the user.

Chapter 3 reported on a series of findings showing how center wavelength positions change up to one spectral pixel during a flight campaign, for both, VNIR and SWIR spectral regions (D'Odorico et al., 2010). Depending on the considered spectral region, the change corresponding to one spectral pixel can range between 3−9 nm and between 6−12 nm for VNIR and SWIR, respectively.

The causes of the APEX spectral performance changes in an operational environment were investigated by means of targeted laboratory experiments. During these experiments, housekeeping data were acquired concurrently with onboard characterization measurements, while the system was exposed to environmental conditions resembling airborne settings. Differential pressure and temperature in the baffle compartment were found to be the housekeeping parameters best explaining APEX's spectral performance changes. The correlation of center wavelengths shifts with one parameter (temperature or pressure) while keeping the other parameters constant, proved to be very robust in the controlled ground settings. Correlation was weaker in the flight setting due to the combined variation of multiple parameters (D'Odorico et al., 2010).

These findings led to an instrument revision aimed at the stabilization of the system for a range of temperature and pressure conditions to be encountered during operation. The revision included the manufacturing of a pressure regulation mechanism for the automatic release or fill-in of nitrogen according to the change in flight altitude. An optimization of the system heating/cooling regulation was further implemented. However, experiments carried out in the following year (2010), revealed that the implemented design revisions did not fully solve the pressure/temperature dependency of the system. As reported in chapter 4, spectral shifts in the range of one spectral pixel were yet again estimated in-flight for both, VNIR and SWIR detectors. A correlating trend between spectral performance change and flight altitude was identified, whereas housekeeping parameters did not show as indicative as prior to the instrument design revision (D'Odorico et al., 2011b).

In summary, APEX spectral performance measured during laboratory characterization cannot be assumed for the operational environment. Causes of deviations are to be sought in the airborne operational environment, the most significant of which are pressure and temperature excursions.

Moreover, changes in instrument spectral performance cannot always be minimized by instrument design, thus onboard characterization measurements must be employed in combination with sophisticated algorithms to detect and compensate for these changes during higher-level processing.

- Is it feasible to monitor and characterize in-flight spectral performance based on the In-Flight Characterization (IFC) facility onboard APEX?

On-ground and in-flight IFC measurements were acquired and successively processed to estimate APEX spectral parameters in-flight. Two approaches were evaluated for this purpose. The first approach, presented in chapter 3, used IFC measurements acquired under controlled laboratory conditions as the reference towards which analogous in-flight IFC measurements were compared. This approach holds the advantage of being completely independent of the nominal parameters (center wavelength and FWHM) estimated during laboratory calibration (D'Odorico et al., 2010), as long as the spectral shift is expressed in units of spectral pixels (i.e., fraction of pixel). In the second approach, described in chapter 4, the reference was given by the transmission spectrum of the NIST Standard Reference Material (SRM) filter, characterized by the NIST standardization laboratory. The NIST filter transmission spectrum was convolved with APEX SRFs to simulate the resolution at which measurements were made (D'Odorico et al., 2011b). An advantage of this approach is that it allows distinguishing between changes affecting center wavelength positions and resolution (i.e., FWHM) as both parameters can be varied in the convolution. The starting values for these parameters are the nominal values as determined during laboratory characterization. Thus a disadvantage of this approach is that estimates will inherit uncertainties linked with the laboratory characterization and subsequent nominal parameters derivation.

The processing of IFC measurements using both approaches resulted in an accurate estimation of center wavelength shifts. The estimation of resolution (i.e., FWHM) changes in addition to center wavelength shifts with the second approach proved more critical. The high inaccuracy associated with the estimation of FWHM suggests that this should only be attempted if an adequate number of spectral bands sampling the absorption features is provided. In line with previous studies (Green et al., 2003; Guanter et al., 2009; Neville et al., 2008) a SSI of 5 nm has been identified as the threshold value above which the number of bands might result insufficient for the estimation of two instrument spectral parameters. It should however be noted that for the same reason, the impact of not updating the nominal FWHM parameter is insignificant for this type of data (Guanter et al., 2009).

A limitation of the APEX IFC based monitoring approach is seen in the number and distribution of IFC spectral filter features to be used for the estimation of APEX spectral parameters. The combination of three bandpass and one NIST SRM filter provides a number of features distributed across the VNIR and SWIR spectral regions. Although most of the available features can be detected at APEX's spectral resolution, insufficient Signal-to-Noise-Ratio (SNR) limits their usability for spectral parameter estimation. A total of four suitable spectral features were identified per detector (for VNIR at: 645 nm, 718 nm, 745 nm, 800 nm; for SWIR at: 1230 nm, 1380 nm, 1545 nm, 1940 nm). The agreement in spectral shift estimated across the different spectral regions proved the representativeness of an estimate derived from one single spectral position for the entire spectral range covered by the spectrometer. This is however not the case when investigating effects caused by non-linear optical aberrations as for instance those causing change in center wavelength position in the across-track detector dimension (i.e., smile). Therefore, multiple features should be used, provided they are available.

In summary, it is feasible to monitor and characterize APEX in-flight spectral performance based on the In-Flight Characterization (IFC) facility. Spectral performance changes are expected to occur as changes in the position of center wavelengths, whereas resolution (i.e.,

FWHM) changes are assumed to be negligible for this particular instrument. The main limitation of the IFC-based monitoring approach is currently seen in the insufficient number and distribution of suitable spectral filter features.

- What are the feasibilities and utilities of employing vicarious approaches to complement onboard methods for the purpose of spectral performance monitoring?

The combination of onboard (IFC) and vicarious (scene-based) approaches was shown to be feasible and beneficial for APEX in-flight spectral performance monitoring. Vicarious approaches, also known as scene-based approaches, rely on the evaluation of absorption features present in the scene and driven by surface and atmospheric constituents. Scene-based approaches are widely used for monitoring airborne spectral performance in-flight (Brazile et al., 2008; Gao et al., 2004; Guanter et al., 2009; Neville et al., 2008). In the study presented in chapter 4, the reference towards which APEX acquired Earth observation spectra are compared is obtained by convolving a MODTRAN 5 (Berk et al., 2005) modeled atmospheric transmission spectrum with APEX nominal SRFs. Comparability of instrument spectral parameters estimated via onboard and vicarious approaches was assessed for those data sets featuring timely proximity and matching flight altitudes between IFC measurements and Earth observation imaging. These requirements originated from the dependency of performance towards environmental parameters trends demonstrated in chapter 3.

The analysis showed good agreement for shifts in center wavelength positions estimated by vicarious and onboard approaches in nearly all investigated analogous spectral regions. Estimates obtained by the oxygen (O_2-A at 760 nm) and the water vapor (H_2O at 1135 nm) features differed in average of 0.3 nm (~0.05 spectral pixels) from estimates obtained by the analogous IFC filter features. Using the CO_2 feature at 2010 nm and analogous IFC filter feature resulted in slightly worse results, with inconsistency up to 2 nm (i.e., 0.2 spectral pixels). The low at-sensor signal within this absorption features and the overlap between water vapor and CO_2 absorption (double feature) is hypothesized to be responsible for the less stable parameter retrieval (D'Odorico et al., 2011b).

This study demonstrated the feasibility to combine onboard and scene-based approaches for APEX in-flight spectral performance monitoring. The agreement between estimates obtained by the two approaches in similar spectral windows suggests they can be used in a complementary fashion so as to exploit the individual advantage each offer. While the method relying on atmospheric features can be applied without the need for dedicated calibration acquisitions, IFC measurements allow assessment at user-selectable wavelength positions by custom filters as well as for the system on-ground. In the future, with the manufacturing of materials providing even sharper absorption features, onboard spectral characterization sources are expected to gain even more importance over scene-based approaches, particularly in the SWIR region (D'Odorico et al., 2011b).

6.1.2 Potential of APEX calibrated data for the simulation, calibration and validation of space missions

- Can APEX calibrated data be used to simulate satellite sensor radiances?

APEX data sets, which have been compensated for the in-flight variations of center wavelength positions, were found suitable to accurately reproduce analogous satellite sensor observations. First findings presented in chapter 5 showed that the correlation between observed Landsat TM5 radiances and simulated radiances obtained using APEX data was altogether satisfactory. Root-mean-square-error (RMSE) values of 11%, 9% and 12% for the red band, the NIR band and NDVI values were found, respectively. All relationships were statistically significant

($p<0.0001$), slopes of unity, and intercepts were consistently below 5% (D'Odorico et al., 2011a). The residual deviations existing between observed TM5 radiances and simulated using APEX can be attributed to a number of sources. Radiometric calibration uncertainty for both sensors represents a known issue (Chander et al., 2007; Chander et al., 2009; Jehle et al., 2010). Spatial effects, such as scaling issues, adjacency effects, spatial resampling and co-registration errors, are further hypothetical causes requiring targeted investigations. Spectral effects introduced by APEX performance could as well affect the broadband convolution to satellite sensor SRFs. However, this is considered unlikely, as the in-flight monitoring and consequent update of APEX spectral performance guarantees the accuracy of the data in terms of spectral integrity. Initial tests presented in chapter 5 have confirmed this hypothesis (D'Odorico et al., 2011a).

- Can APEX calibrated data be used for the spectral cross-calibration and validation of satellite observations?

The study in chapter 5 further reports on the use of calibrated APEX data for the cross-calibration of satellite sensors SRFs in the red and NIR region and in their combination in the form of NDVI values. Sensor cross-calibration directly based on the comparison of measured satellite imagery is limited to sensor combinations for which temporally and spatially overlapping data exist (Gallo et al., 2005; Swinnen et al., 2008). Alternatively, airborne data (Teillet et al., 1997; Trishchenko et al., 2002) or radiative transfer model (RTM) simulations (Prieto-Blanco et al., 2009; van Leeuwen et al., 2006) are used to simulate the satellite sensors observations and derive cross-calibration coefficients. Results presented in chapter 5 showed that in overall APEX data performed better as compared to RTM simulations for multi-sensor SRF cross-calibration. These findings were supported by previous studies (Teillet et al., 2007; Teillet et al., 2008; Trishchenko, 2009; Trishchenko et al., 2002), which identified land cover variation and thus the spectral content of the scene having an impact on cross-sensor SRF difference effects.

Generally speaking, it was concluded that data from airborne imaging spectrometers and in particular from the APEX instrument, when available, are the preferred choice for the cross-calibration and validation of operational and upcoming satellite sensors spectral performances.

6.2 Conclusions and outlooks

Remote sensing is today perhaps the most important source of data to obtain a quantitative understanding on how the Earth systems works and evolved to its current state as well as predicting its future (ESA 2006). Remote Sensing data time series represent fundamental climate data records; processing and assimilation of these data allow the generation of products, which can be used as change indicators. An example of change indicators largely dependent on satellite observations are the Essential Climate Variables (ECVs) defined by the Global Climate Observing System (GCOS) for the monitoring of long term changes in the atmospheric, oceanic and terrestrial domains (GCOS, 2009). The central role of remote sensing places severe demands on the instrumentation used, which needs to ensure accurate physical measurements. To allow reliable judgments to be made decades apart, measurements need to be consistent across sensors as well as in time and must therefore be traceable to recognized reference standards. A framework monitoring the fulfillment of these conditions and providing key guidelines derived from best practices is thus highly desirable. The establishment in 2008 of the Quality Assurance Framework for Earth Observation (QA4EO) represents one major step in this direction.

Imaging spectroscopy data hold an increased potential for information retrieval from the Earth

system. Spectrometers mounted on airborne or spaceborne platforms are characterized by finer and better-defined bands as well as contiguous spectral sampling, enabling the extraction of subtle differences in spectral signatures (Schaepman et al., 2009). However, spectroscopy measurements are known to be one of the least reliable of all physical measurements (Kostkowski, 1997). Under ideal laboratory conditions, measurement errors can reach up to a few percent while higher errors are expected in operational environments (Gege et al., 2009; Green, 1998; Nieke et al., 2008). It is understood that even the slightest measurement error can compromise the detection of the already subtle natural variability interesting the observed target or phenomenon. The most important source of error in spectroscopic measurements can be sought in the instability of the measuring sensor. The rigors of the instrument operational environment are for the most part to be held responsible for this instability. Effects of temperature, pressure, mechanical vibration, significantly add to the natural performance degradation caused by system aging (Neville et al., 2008).

The evaluation of spectral performance stability of an imaging spectrometer deployed on an airborne platform was the central theme of this dissertation. The APEX instrument was chosen for the envisaged investigation allowing the exploitation of an unprecedented large amount of calibration data acquired throughout the various steps of instrument operation. The sophisticated calibration concept designed around this instrument allowed data to be collected from a multitude of sources: i) laboratory characterization and targeted ground experiments (e.g., climate chamber) taking place at different times (i.e., before and after the flight campaign); ii) onboard IFC measurements acquired on-ground and in-flight; iii) Earth observation images (for vicarious assessments); and iv) housekeeping data, co-registered with the Earth observation imaging and with the IFC measurements, reflecting the environmental conditions to which the sensor is exposed.

This dissertation has proved the feasibility and the benefit of combining laboratory, onboard and scene-based data for monitoring spectral performance of the APEX airborne imaging spectrometer in flight. Correction algorithms allowing compensating for the in-flight variations of spectral parameters during post-processing were developed based on these calibration datasets and applied to APEX data. Eventually, calibrated APEX data were successfully used for the simulation and cross-calibration of operational and upcoming satellite sensors spectral performances. APEX represents one of the best examples on how airborne instruments can effectively provide the missing link between on ground reference standards and instrument performance in space.

In future, to optimize even further the usage of the information available to the APEX calibration we recommend exploiting data assimilation methods. An assimilation model should allow combining multiple calibration data sources more effectively. The estimation of APEX spectral parameters could then occur also where calibration measurements are missing or for prediction purposes, based on their past and current values. Moreover, it should allow adjustable and iterative weighting of contributions by different data sources based on their reliability. This in turn implies the development of error propagation models quantifying the uncertainty conveyed by each individual calibration data source to the final parameter estimation. Data assimilation and error models, embedded in APEX' Processing and Archiving Facility (PAF) (Hüni et al., 2009), will lead to better accuracies of calibrated data sets. This in turn will benefit higher-level product generation and the deployment of APEX for satellite mission calibration and validation.

The main focus of this dissertation rested on the spectral dimension of the measuring problem. Although substantial contribution in the understanding and correction of the instrument-derived measurement error was achieved, it is acknowledged that the inclusion of other error dimensions is essential for a comprehensive picture. The error affecting the measurement of the radiometric quantity is known to originate from spectral, temporal, spatial, and radiometric factors (Böttger et al., 2006; Mouroulis et al., 2000; Nieke et al., 2008). The

multidimensionality of the problem of spectroscopic measurements needs therefore to be considered in the development of instrument performance monitoring and calibration strategies (Kostkowski, 1997).

Last but not least, the scarce dissemination of the principles and techniques used for monitoring instrument performances and eliminating or minimizing the instrument-induced measurement errors is seen as a critical reason for errors in spectroscopy measurements (Kostkowski, 1997). The work presented in this dissertation will contribute to fill this information gap.

6.3 References

Berk, A., Anderson, G.P., Acharya, P.K., Bernstein, L.S., Muratov, L., Lee, J., Fox, M., Adler-Golden, S.M., Chetwynd, J.H., Hoke, M.L., Lockwood, R.B., Gardner, J.A., Cooley, T.W., Borel, C.C. and Lewis, P.E., 2005. MODTRAN 5, a reformulated atmospheric band model with auxiliary species and practical multiple scattering options. Proceeding of SPIE, 5806: 662-667.

Böttger, U., Nieke, J. and Schläpfer, D., 2006. Assessing polarization effects for the Airborne imaging spectrometer APEX. Advances in Radio Science, 4: 323-328.

Brazile, J., Neville, R.A., Staenz, K., Schläpfer, D., Sun, L. and Itten, K., 2008. Towards scene-based retrieval of spectral response functions for hyperspectral imagers using Frauenhofer features. Canadian Journal of Remote Sensing, 34(1): S43-S58.

Chander, G., Markham, B. and Barsi, J.A., 2007. Revised Landsat-5 Thematic Mapper radiometric calibration. IEEE Geoscience and Remote Sensing Letters, 4(3): 490 - 494.

Chander, G., Markham, B.L. and Helder, D.L., 2009. Summary of current radiometric calibration coefficients for Landsat MSS, TM, ETM+, and EO-1 ALI sensors. Remote Sensing of Environment, 113(5): 893-903.

D'Odorico, P., Alberti, E. and Schaepman, M.E., 2010. In-flight spectral performance monitoring of the Airborne Prism Experiment,. Applied Optics 49(16): 3082-3091

D'Odorico, P., Gonsamo, A., Damm, A. and Schaepman, M.E., 2011a. Experimental evaluation of Sentinel-2 spectral response function for NDVI time-series continuity. IEEE Transactions on Geoscience and Remote Sensing, submitted.

D'Odorico, P., Guanter, L., Schaepman, M.E. and Schläpfer, D., 2011b. Performance assessment of onboard and scene-based methods for Airborne Prism Experiment spectral characterization. Applied Optics, 50(23): 4755-4764.

ESA, 2006. The Changing Earth. SP-1304:84.

Gallo, K., Ji, L., Reed, B., Eidenshink, J. and Dwyer, J., 2005. Multi-platform comparison of MODIS and AVHRR normalized difference vegetation index data. Remote Sensing of Environment, 99(3): 221-231.

Gao, B.C., Montes, M. and Davis, C., 2004. Refinement of wavelength calibrations of hyperspectral imaging data using a spectrum-matching technique. Remote Sensing of Environment, 90(4): 424-433.

GCOS, 2009. Guidelines for the generation of satellite-based datasets and products meeting GCOS requirements. GCOS-128 (WMO/TD No. 1488), World Meteorological Organization (WMO).

Gege, P., Fries, J., Haschberger, P., Schoetz, P., Schwarzer, H., Strobl, P., Suhr, B., Ulbrich, G. and Jan Vreeling, W., 2009. Calibration facility for airborne imaging spectrometers. ISPRS Journal of Photogrammetry and Remote Sensing, 64(4): 387-397.

Green, R., 1998. Spectral calibration requirements for Earth-looking imaging spectrometers in the solar-reflected spectrum. Applied Optics, 37(4): 683-690.

Green, R.O., Pavri, B. and Chrien, T., 2003. On-orbit radiometric and spectral calibration characteristics of EO-1 Hyperion derived with an underflight of AVIRIS and in situ measurements at Salar de Arizaro, Argentina. IEEE Transactions on Geoscience and Remote Sensing, 41(6): 1194 - 1203.

Guanter, L., Segl, K., Sang, B., Alonso, L., Kaufmann, H. and Moreno, J., 2009. Scene-based spectral calibration assessment of high spectral resolution imaging spectrometers. Optics Express, 17(14): 11594-11606.

Hüni, A., Biesemans, J., Meuleman, K., Dell'Endice, F., Schläpfer, D., Adriaensen, S.,

Kempenaers, S., Odermatt, D., Kneubühler, M. and Nieke, J., 2009. Structure, components and interfaces of the Airborne Prism Experiment (APEX) Processing and Archiving Facility. IEEE Transactions on Geoscience and Remote Sensing, 47(1): 1-4.

Jehle, M., Hueni, A., Damm, A., D'Odorico, P., Weyermann, J., Kneubühler, M., Schläpfer, D. and Schaepman, M.E., 2010. APEX - current status, performance and product generation. IEEE Sensors 2010, Waikoloa (HI), pp. 533 - 537.

Kostkowski, H.J., 1997. Reliable Spectroradiometry. Spectroradiometry Consulting, Maryland, 605 p.

Mouroulis, P., Green, R. and Chrien, T., 2000. Design of pushbroom imaging spectrometer for optimum recovery of spectroscopic and spatial information. Applied Optics, 39(13): 2210-2220.

Neville, R.A., Sun, L. and Staenz, K., 2008. Spectral calibration of imaging spectrometers by atmospheric absorption feature matching. Canadian Journal of Remote Sensing, 34(1): S29–S42.

Nieke, J., Schlaepfer, D., Dell'Endice, F., Brazile, J. and Itten, K.I., 2008. Uniformity of imaging spectrometry data products. IEEE Transactions on Geoscience and Remote Sensing, 46(10): 3326-3336.

Prieto-Blanco, A., North, P.R.J., Barnsley, M.J. and Fox, N., 2009. Satellite-driven modelling of Net Primary Productivity (NPP): Theoretical analysis. Remote Sensing of Environment, 113(1): 137-147.

Schaepman, M.E., Ustin, S.L., Plaza, A.J., Painter, T.H., Verrelst, J. and Liang, S., 2009. Earth system science related imaging spectroscopy - An assessment. Remote Sensing of Environment 113(1): S123-S137.

Swinnen, E. and Veroustraete, F., 2008. Extending the SPOT-VEGETATION NDVI time series (1998-2006) back in time with NOAA-AVHRR data (1985-1998) for southern Africa. IEEE Transactions on Geoscience and Remote Sensing, 46(2): 558-572.

Teillet, P.M., Fedosejevs, G., Thome, K.J. and Barker, J.L., 2007. Impacts of spectral band difference effects on radiometric cross-calibration between satellite sensors in the solar-reflective spectral domain. Remote Sensing of Environment, 110(3): 393-409.

Teillet, P.M. and Ren, X., 2008. Spectral band difference effects on vegetation indices derived from multiple satellite sensor data. Canadian Journal of Remote Sensing, 34(3): 159-173.

Teillet, P.M., Staenz, K. and William, D.J., 1997. Effects of spectral, spatial, and radiometric characteristics on remote sensing vegetation indices of forested regions. Remote Sensing of Environment, 61(1): 139-149.

Trishchenko, A.P., 2009. Effects of spectral response function on surface reflectance and NDVI measured with moderate resolution satellite sensors: Extension to AVHRR NOAA-17, 18 and METOP-A. Remote Sensing of Environment, 113(2): 335-341.

Trishchenko, A.P., Cihlar, J. and Li, Z., 2002. Effects of spectral response function on surface reflectance and NDVI measured with moderate resolution satellite sensors. Remote Sensing of Environment, 81(1): 1-18.

van Leeuwen, W.J.D., Orr, B.J., Marsh, S.E. and Herrmann, S.M., 2006. Multi-sensor NDVI data continuity: Uncertainties and implications for vegetation monitoring applications. Remote Sensing of Environment, 100(1): 67-81.

CURRICULUM VITAE

Education

2008－2012 **Ph.D.** University of Zurich (Switzerland), Department of Geography, Remote Sensing Laboratories (RSL). Thesis: Monitoring the Spectral Performance of the APEX Imaging Spectrometer for Inter-Calibration of Satellite Missions.

2004－2006 **MSc** Geo-Information Sciences, Wageningen University (The Netherlands). Thesis: Land Cover Monitoring by means of Medium Resolution Satellite Imagery.

2000－2004 **BSc** Forestry and Environmental Technologies, University of Padua (Italy), Department of Agriculture. Thesis: Correction for Topographic Effects on Satellite Images.

1996－2000 **European Baccalaureate**, European School of Munich (Germany).

Professional experience

2008－2012 **Research assistant and APEX CalVal Team Scientist,** University of Zurich, Department of Geography, Remote Sensing Laboratories (RSL), Zurich, Switzerland.

2007－2008 **Visiting Scientist**, Kayser Threde GmbH, Munich, Germany.

2007－2007 **GIS technician**, GAF AG, Munich, Germany.

2006－2006 **Internship,** Global Land Cover 2000 (GLC 2000) Project, Global Environment Monitoring (GEM) unit, Joint Research Centre (JRC), European Commission (EC), Ispra, Italy.

Competitive grants

2012－2013 EMRP EURAMET Researcher Excellence Grant (REG) in Earth Observation Metrology (calibration and validation of sensors and products).

2007－2010 Early Stage Researcher (ESR) Marie Curie Fellowship, Hyperspectral Imaging Network (HYPER-I-NET).

2002－2003 Erasmus mobility grant, Department of Remote Sensing and Landscape Information Systems (FeLis), University of Freiburg, Germany.

Graduate courses and professional training

- IDL programming
- Matlab programming
- Scientific Writing
- Graduate Seminar I & II
- Hyper-I-Net summer schools (Caceres, Spain, 2008; Pavia, Italy, 2009)
- ESA summer school (Frascati, Italy, 2010)

Poster and oral contributions:

- EARSeL SIG workshop imaging spectroscopy (Tel Aviv, Israel, 2009)
- IGARSS conference (Cape Town, South Africa, 2009)
- ESA hyperspectral workshop (Frascati, Italy, 2010)
- Swiss Geo Science meeting (Zurich, Switzerland, 2011)

Publications

Peer-reviewed publications

D'Odorico, P., Gonsamo, A., Damm, A. and Schaepman, M.E., 2011. Experimental evaluation of Sentinel-2 spectral response function for NDVI time-series continuity. IEEE Transactions on Geoscience and Remote Sensing, submitted.

D'Odorico, P., Guanter, L., Schaepman, M.E. and Schläpfer, D., 2011. Performance assessment of onboard and scene-based methods for Airborne Prism Experiment spectral characterization. Applied Optics, 50(23): 4755-4764.

D'Odorico, P., Alberti, E. and Schaepman, M.E., 2010. In-flight spectral performance monitoring of the Airborne Prism Experiment. Applied Optics, 49(16): 3082-3091.

Itten, K., Dell Endice, F., Hueni, A., Kneubuehler, M., Schlaepfer, D., Odermatt, D., Seidel, F., Huber, S., Schopfer, J., Kellenberger, T., Buehler, Y., **D'Odorico, P.**, Nieke, J., Alberti, E. and Meuleman, K., 2008. APEX - the Hyperspectral ESA Airborne Prism Experiment. Sensors, 8(10): 6235-6259.

Other scientific publications

Jehle, M., Hueni, A., Damm, A., **D'Odorico, P.**, Weyermann, J., Kneubühler, M., Schläpfer, D. and Schaepman, M. E., 2010. APEX - current status, performance and product generation. IEEE Sensors 2010, Waikoloa (HI), pp. 533 - 537.

Alberti, E., Dell'Endice, F., **D'Odorico, P.**, Hueni, A., Schaepman, M. E., Schläpfer, D., Meuleman, K., Bomans, B., Raymaeckers, D., Vreys, K., Kempenaers, S., Sterckx, S., Knaeps, E., Damm, A., Kneubuehler, M., Rezaei, Y., Malenovsky, Z., Weyermann, J. and Seidel, F., 2010. APEX status Pt.1: Instrument development and performance. ESA Hyperspectral Workshop, Frascati, Italy.

Meuleman, K., Bomans, B., Vreys, K., Kempenaers, S., Deroose, T., Biesemans, J., Hueni, A., Alberti, E., Dell'Endice, F., **D'Odorico, P.**, Schaepman, M. and Schläpfer, D., 2010. APEX status part 2: Operations and product generation. ESA Hyperspectral Workshop, Frascati, Italy.

D'Odorico, P., Alberti, E., Dell'Endice F., Hüni A. and Schaepman, M., 2009. Spectral stability monitoring of an imaging spectrometer by means of onboard sources. IEEE International Geoscience & Remote Sensing Symposium, Cape Town, pp. I-72 - I-75.

D'Odorico, P., Alberti, E., Dell'Endice, F., Hüni, A. and Itten, K., 2009. An algorithm for tracking APEX spectral stability by means of the In-Flight Characterizarion facility (IFC). 6th EARSeL SIG IS workshop on Imaging Spectroscopy, Tel Aviv, Israel.

Itten, K., Meuleman, K., Schaepman, M., Alberti, E., Bomans, B., Dell'Endice, F., **D'Odorico, P.**, Hueni, A., Nieke, J., Schläpfer, D. and Ulbrich, G., 2009. First test results of the airborne dispersive pushbroom imaging spectrometer APEX. EARSeL SIG IS workshop on Imaging Spectroscopy, Tel Aviv, Israel.

ACKNOWLEDGEMENTS

A major part of the research relevant for the presented dissertation was funded by the Hyperspectral Imaging Network (HYPER-I-NET), an FP6 Marie Curie Research Training Network of the European Commission. A special thanks goes to the network coordinator Prof. Antonio Plaza (University of Extremadura) for allowing me to modify my scholarly visits according to my research interests. Thanks for taking all the administrative burdens on you!

I greatly appreciate the willingness of Dr. Nigel Fox (National Physical Laboratory) to review the present dissertation. I would also like to thank the members of my dissertation committee who supervised and contributed in various ways to this dissertation.

I would like to thank Prof. Klaus Itten and Dr. Jens Nieke for giving me the opportunity to start working at RSL.

I would like to extend my gratitude to Prof. Michael Schaepman for providing the guidance and at the same time the freedom to pursue my research interests. Thanks for making RSL an interesting place to be! A special thanks goes to the SpectroLab leader Dr. Mathias Kneubühler for his availability and for always clearing my way of problems that could distract from my work.

My appreciation further goes to my colleagues of the RSL APEX team (Edo, Andy, Francesco, Yousef, Michael) for sharing their knowledge, challenges and achievements. I particularly would like to express my sincere gratitude to Edo and Andy for their patience and enthusiasm, for never feeling tired to discuss a new result or a new problem, for all the hours spent writing on blackboards. I enjoyed working with you guys! I also owe my gratitude to Andy and Daniel for the highly valued support in programming, which essentially contributed to the efficiency of my work. A big thanks goes to Damien, our enthusiastic technician, and to the IT staff for their support in dealing with software and hardware adversities.

I am thankful to all of my co-authors and reviewers for the constructive criticism and comments. I am also grateful for the stimulating discussions I shared with collaborators and fellow scientists on different occasions. Special thanks go to: Dr. Valery Mogulsky (Kayser Threde GmbH), Dr. Daniel Schläpfer (ReSe) and Dr. Luis Guanter (University of Berlin).

I really appreciated the friendly working atmosphere created by RSL and GIUZ administrative and scientific staffs, students and visiting scholars. I will be forever thankful for the beautiful friendships I developed during these years in Zurich. I will miss my office with Lucia, Valérie, Lucie, Charity (visiting), Parviz (visiting) and Hossein.

Last but not least, my heart felt thanks goes to my family and in particular to my parents, Anna and Sandro, and my sister Sara, for their irreplaceable support and love. I further owe my loving thanks to Alemu for so many reasons. Discussing my research with you motivated and encouraged me each time anew. Thanks for being such an inspiration, for the brilliance and generosity you put in every step.

To those that I have forgotten here, please take it as a flaw of the mind and not as one of the heart.

ISBN Nr. 978-3-03703-029-5